Mechanisms of DNA Organization Unraveled with Novel Single-Molecule Methods

Noom, M.C.

2008

document version
Publisher's PDF, also known as Version of record

Mechanisms of DNA Organization Unraveled with Novel Single-Molecule Methods

This thesis was reviewed by:

prof.dr. C.J. Dorman	Trinity College, Dublin, Ireland
prof.dr. J.T. Liphardt	University of California, Berkeley, U.S.A.
prof.dr. W. Ubachs	Vrije Universiteit, Amsterdam, the Netherlands
dr.ir. E.J.G. Peterman	Vrije Universiteit, Amsterdam, the Netherlands
dr. P.A. Wiggins	Whitehead Institute, Cambridge, U.S.A.
dr. N.H. Dekker	Delft University of Technology, Delft, the Netherlands

Printed in the Netherlands by PrintPartners Ipskamp, Enschede, http://www.ppi.nl.

Cover: Artist's rendition of the 'dual DNA' assay. Two DNA molecules (green and yellow) attached to beads (blue) are manipulated by optical tweezers (red cones) in a laminar flow cell with multiple buffer solutions running parallel to each other. Adapted from the cover Figure of *Nature Methods*, volume 4, issue 12, 2007.

A digital version of this thesis can be obtained at
http://www.ubvu.vu.nl/dissertations

This work is financially supported by the 'Nederlandse Organisatie voor Wetenschappelijk Onderzoek (NWO)'. The research was performed in the section 'Physics of Complex Systems' at the Vrije Universiteit.

vrije Universiteit *amsterdam*

VRIJE UNIVERSITEIT

Mechanisms of DNA Organization Unraveled with Novel Single-Molecule Methods

ACADEMISCH PROEFSCHRIFT

ter verkrijging van de graad Doctor aan
de Vrije Universiteit Amsterdam,
op gezag van de rector magnificus
prof.dr. L.M. Bouter,
in het openbaar te verdedigen
ten overstaan van de promotiecommissie
van de faculteit der Exacte Wetenschappen
op maandag 16 juni 2008 om 13.45 uur
in de aula van de universiteit,
De Boelelaan 1105

door

Maarten Cornelis Noom

geboren te Heiloo

promotor: prof.dr. F.C. MacKintosh
copromotor: dr.ir. G.J.L. Wuite

Contents

Preface

In this thesis I describe experiments that were performed to gain more insight in the organization of bacterial DNA. We have done this by using so-called '*single-molecule methods*'. These methods allow for manipulating a single DNA molecule. Even though DNA is a very important information carrier in a cell, we have sometimes been working with DNA as if it were just a micro-rope. More then once, we grabbed a piece of actual rope to figure out what was happening under the microscope. When, sometimes only hours later, I was sailing to clear my mind after a day waisted on what seemed like impossible experiments, I couldn't help noticing the resemblance between the organization of DNA inside a bacterial cell and the organization of the rigging aboard a ship. In both cases, DNA and rigging, it is essential to keep it well-organized, accessible and in good condition at all times. Where poor DNA organization can lead to cell-death, aboard a ship a big accidental knot in a line or a big pile of chaotic ropes can lead to catastrophe, such as capsizing of the ship. In order to give the reader a new, albeit a very mechanistic, perspective on the contents of the chapter, I have tried to capture the principal message of the chapter in a photograph of a nautical analogue.

Maarten Noom
Amsterdam, April 2008

Chapter 1

The rigging aboard a ship comprises all lines present on the ship. Without rigging, a ship would be lost. No sail could be hoisted, no mast would stay upright.

Introduction

The title of this thesis is: "Mechanisms of DNA Organization Unraveled with Novel Single-Molecule Methods" and it covers (some) of the work I did as a PhD-student at the Vrije Universiteit in the field of biophysics. In order to give the reader some framework for the subjects covered in this thesis, this introduction contains a brief overview of cell biology (first part) and some biophysics techniques used in this thesis (second part). It was meant to be written in such a way that it requires hardly any prior knowledge of the reader about these subjects. At the end of the chapter the reader will find a synopsis of all the other chapters.

1.1 The building block of life

It's not exactly known when and how life on earth started to emerge but we do know that it exists for more than 3 billion years. And even though modern science has been documenting species for hundreds of years, still new species are being discovered. The diversity among all known life is incredible yet, strikingly, all living organisms: bacteria, plants and all animals, have the same functional and structural unit, the cell, often called '*the building block of life*'. Some organisms consist of only a single cell, for example, bacteria, but others consist of many cells. Still, every single cell has its own tasks and, depending on the organism, they are to some extent self-maintaining: they can absorb nutrients, convert these to energy and reproduce. In uni-cellular organisms, all these functions must be performed by this single cell. In more complex, multi-cellular organisms, different cells carry out specialized functions and therefore these cells can have different shapes or sub cellular components, *organelles*. However, the basic machinery needed to keep the cell alive and functioning is very much the same for all cells. The most important feature is that cells carry their hereditary or genetic information and this information forms the basis for the machinery of the cell.

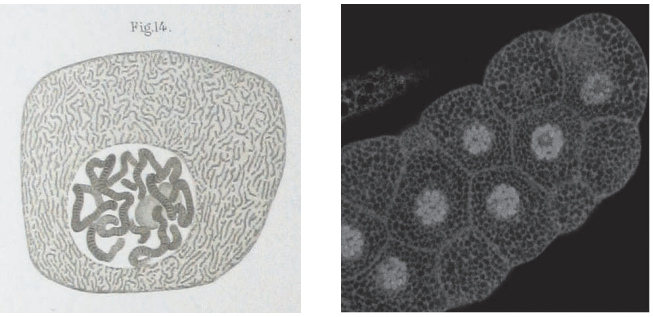

Figure 1.1: Saliva cells. On the left an observation of a Chironimus salivary gland cell drawn by Walter Flemming in 1881. On the right a fluorescence microscopy image of Drosophila salivary gland cells made by Sarah Smolik [160]. In both pictures the genetic material of the cell can clearly be identified.

In a very simple yet elegant way, all this information is stored in a linear code based on only four different units. The sequence of these units is called deoxyribonucleic acid (DNA) and basically the DNA of a cell can be compared to the blueprint of a building; it contains instructions needed to construct many other components of the cell, such as proteins, and replicate the cell.

1.1.1 History and structure of DNA

In 1831, around the same time the discovery was made that plants and animals both consist of cells, botanist Robert Brown (1773 – 1858) gave a detailed description, in words, of a nucleus present in saliva cells of insects [26] (see Fig. 1.1). Although Matthias Schleiden (1804 – 1881) suggested [149] that the nucleus plays a role in the generation of new cells in 1838, only in the beginning of the 20th century, when cell division was well described, the chromosome theory of heredity was developed. Since then, the structure of DNA has been, even today, the subject of research and several models have been suggested, varying from one to three helices and even more complex structures. In 1953, X-ray technology allowed researchers to finally unravel the structure of DNA. James Watson (1928) and Francis Crick (1916 – 2004) interpreted the data taken by Rosalind Franklin (1920 – 1958) and came up with an accurate model of two helical chains coiled around each other [193]. The chains are long polymers and consist of building blocks called *nucleotides*. And even though there is such a large diversity among organisms in nature, there are only four different nucleotides or bases that make up the code in DNA, *adenine* (A), *guanine* (G), *thymine* (T) and *cytosine* (C). Bases on opposite positions of the two helices form only two different kinds of base pairs. Adenine always pairs with thymine and guanine always pairs with cytosine joining the helices together and forming complementary base pairs. The re-

sulting sequence of bases (e.g. ATGAAATACCG) is what makes the genetic code that functions as a blueprint for the synthesis of proteins. A 'simple' single celled organism like a bacterium has a few million bases. For comparison, the human genetic code contains three billion bases.

The two helical polynucleotide chains both have a backbone built from deoxyribose units and held together by phosphate groups, which are located on the outside of the chain whereas the bases are on the inside of the helix. These phosphate and deoxyribose units are linked together with phosphodiester bonds which give each helix a 'direction'. This direction of the DNA is very important, as soon will become clear that GCT is very different from TCG. The diameter of a DNA molecule is 20 Ångstroms, or 2 nm, and the structure repeats itself at intervals of 34 Ångstroms, every 10 basepairs. This corresponds with a rotation angle of 36 degrees per base (see Fig. 1.2). As a consequence of the a-symmetry in the DNA double helix, there are two different grooves in the helical structure, the major- and the minor groove and the major groove is twice the size of the minor groove. Because at the major groove the bases of the DNA are more accessible, this is a popular interaction point for DNA interacting proteins.

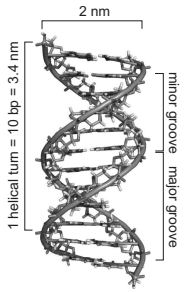

Figure 1.2: Structure of DNA. The double helical structure of DNA with the two backbones coiling around each other and bases on each backbone forming base pairs. Indicated are the dimensions and the major- and minor groove.

1.1.2 DNA replication and protein synthesis

In their article [193], published in 1953, Watson and Crick noted, with a sense of understatement, that the specific pairing of the base pairs on the double helical structure suggested a possible mechanism to copy the genetic material. Proven by Meselson and Stahl [124], indeed DNA is copied by *semi-conservative replication*. This means that when a copy of the DNA is needed, for instance when a cell divides, the double helix is separated into two single helices which are then used as template for the addition of complementary nucleotides. As a consequence, a newly replicated DNA molecule only consists of one new helix and one old helix.

As indicated above, DNA forms the blueprint for the synthesis of proteins used in the cells of the organism. The (simplified) mechanism for the synthesis of protein is as follows; first a *gene*, the code for one protein, is *transcribed* by *RNA polymerase*. RNA polymerase reads the DNA template in the direction $3' \rightarrow 5$' and catalyses the synthesis of a single stranded copy called *messenger RNA*. The sequence of the *mRNA*

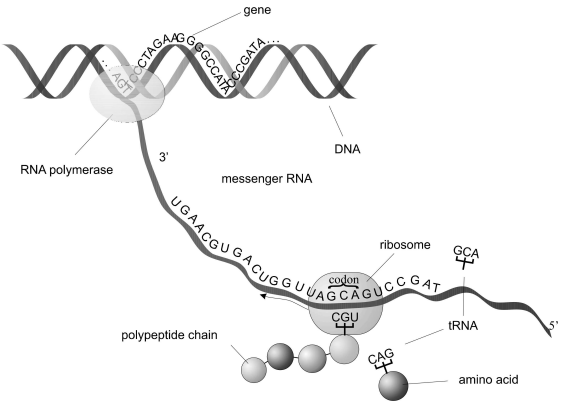

Figure 1.3: Protein synthesis. A schematic representation of protein synthesis. RNA-polymerase copies a gene on the DNA into mRNA. The mRNA then gets converted into a polypeptide chain in a ribosome.

then forms the template for the synthesis of proteins. The sequence is 'grouped' in units of three bases that form a *codon*. A codon specifies a specific *amino acid*, the building block of proteins. The aforementioned direction is very important here because 'ACG' codes for a very different amino acid than 'GCA'. Subsequently, *transfer RNA* then converts the codon sequence to a sequence of amino acids, a *polypeptide chain*, in the *ribosome*. This forms the basic structure of a protein (see Fig. 1.3).

1.1.3 Regulation of gene expression

In a multicellular organism, the DNA in cells with a completely different function and a very different set of proteins, is exactly the same. The production of proteins, both the amount and which protein, can be regulated by controlling the genes that code for the proteins. There are several mechanisms that play a role in the regulation of genes, each targeting a different step of gene expression. Two of these mechanisms that play a role in this thesis are:

1. structural changes in the organization of DNA; in the cell, DNA is not present as a long linear polymer, typically the DNA is compacted and organized in such a way that some parts, i.e. genes, are more accessible than others (for example due to compaction caused by *supercoiling*, see Fig. 1.4).

2. regulatory proteins; these are proteins that can bind to a regulatory binding site, influencing the transcription machinery that read the gene. This way these proteins can switch a gene on, then they are called *activators*, or to shut off a gene, then they are called *repressors*.

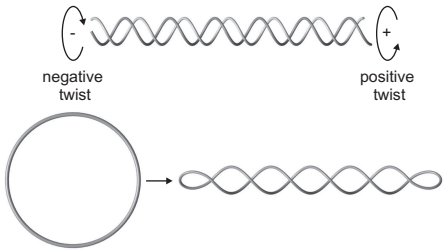

Figure 1.4: Supercoiling of DNA. The DNA double helix can be twisted by rotation around its axis, either anticlockwise (positive twist) or clockwise (negative twist)(top). The torsional stress of twisting results in *supercoiled* structures such as a supercoiled circular plasmid molecule (bottom).

In unicellular organisms, the regulation of gene expression usually has consequences for a single cell only. In more complex organisms cells have to cooperate, and therefore the regulation of genes becomes more sophisticated. The next section explains the main differences between unicellular and multi-cellular organisms.

1.2 The three domains of life

It is common belief that all animal life on earth originates from the same ancestor, small single cell organisms. In evolution, diversity eventually started to occur and certain groups of organisms began to differ substantially from others. This has resulted in a great variety in life as we know it, and still discover, as new species are still discovered. There are many ways to categorize all the organisms but one common way is to distinguish three domains of life based on their genomic characteristics: eukaryotic organisms, prokaryotic organisms and archaea (see Fig. 1.5). Whereas among eukaryotic organisms there are very complex, multi-cellular organisms like humans (a human body is estimated to have 10^{12}-10^{14} cells), most of the prokaryotes and archaea are unicellular organisms, for example bacteria. Another important difference is that the cells of both prokaryotic and archaea are much smaller than eukaryotes, as shown in Figure 1.6. Looking a little closer, we find that some cellular components are also slightly different, the most important of which has to do with the organization of their genetic material. This aspect is covered in the next subsections.

1.2.1 Eukaryotic DNA organization

Eukaryotic organisms have their DNA, which can be over 18000 times longer than the size of the cell, organized into one or more chromosomes and compacted into a nucleus [61] (see Fig. 1.6). The cells in a human body contain approximately 1.8 m of DNA per nucleus which has a diameter of 5 μm; This requires the DNA to be immensely compacted in order to fit inside the nucleus that holds the genetic information, and still the DNA has to be readily accessible and untangled. In order to achieve such a compact chromosome, there are several orders of compaction [100, 120, 197]. Initially, the

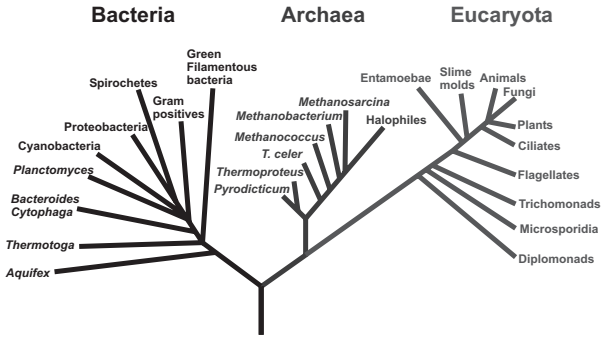

Figure 1.5: The phylogenetic tree of life. The phylogenetic tree of life was first proposed by Dr. Woese when working at NASA [202] and shows the differences between bacteria, eukaryotic organisms and Archaea based on RNA.

DNA is wrapped 1.7 times around a protein complex called a *histone* forming a *nucleosome* (see Fig. 1.7). The resulting structure, which looks like 'beads on a string' is called *'the 11 nm fiber'* and at this point the DNA is compacted a factor of six. The next step is to coil the 11 nm fiber into a higher order structure called *'the 30 nm fiber'*. The DNA is now again compacted with a factor of six. These 30 nm fibers are then packed into looped domains by interacting with a protein matrix (see Fig. 1.7). The looped domains consist of approximately 300.000 bp and contain approximately 10 genes. The looped domain structure interacts with a protein matrix. The looped domain structure is then further compacted into the final chromosome form to reach to required order of compaction.

1.2.2 Prokaryotic DNA organization

Bacterial chromosomal DNA is not confined to an envelope-enclosed organelle such as the nucleus in eukaryotes; it is present in a microscopically visible structure called the nucleoid, comparable to noodles in a bowl of soup (see left). The 1.6 mm long chromosomal DNA molecule of *Escherichia coli* is contained within a cell that is only 2 μm long and 1 μm wide, so it is much less compacted than the DNA in eukaryotic cells. An unconstrained DNA molecule of this size would form a random coil with a volume of approximately 200 μm^3 i.e. about 400 times the volume of an *E. coli* nucleoid ($\sim$0.5 μm^3). There are several mechanisms that compact the chromosomal DNA sufficiently to fit inside the cell [38, 93, 178]. These mechanisms include macromolecular crowding and DNA supercoiling.

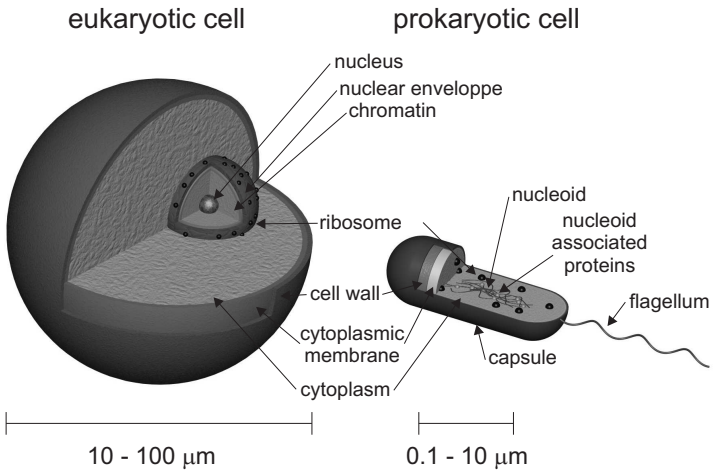

Figure 1.6: Eukaryotic and prokaryotic cell. This cartoon displays general similarities and differences between eukaryote and prokaryote cells. Organelles such as ribosomes are present in both types of cells but in eukaryotes the genetic material is confined in the nucleus whereas in prokaryotes the genome is not confined. Note the big difference in size indicated by the scale bars.

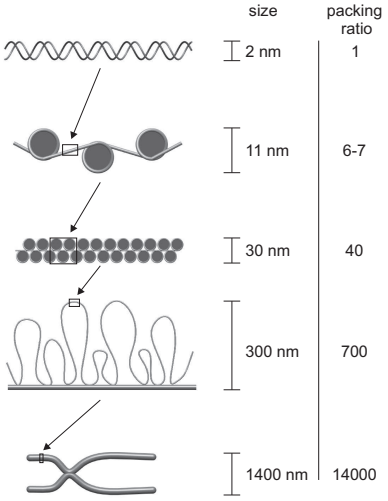

Figure 1.7: Eukaryotic DNA organization. A cartoon of chromosome structure. The DNA double helix is wound around histones to form nucleosomes, each of which contains 147 bp (8 per turn). These nucleosomes are then wound to form the 30 nm fiber. The 30 nm fiber forms long DNA loops, each containing about 60,000 bp, which are attached at their base to the *nuclear matrix* indicated by the grey bar. The looped structure is then further compacted into the final, well known, chromosome form.

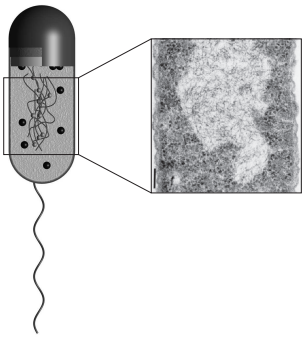

Figure 1.8: Prokaryotic DNA organization. Cartoon of a bacterium with its genome 'floating' in the middle of the cell (left). On the right a cross section taken by transmission electron microscopy [55]. The genome is visible as the white structure in the middle.

The bacterial chromosome consists of 50 – 400 negatively supercoiled DNA loops that are on average about 10,000 bases in size [76, 93]. The nucleoid is a dynamic structure and the boundaries of these topological DNA loops distributed in an apparently random manner throughout the genome (see Fig. 1.8). The organization of the nucleoid into numerous small supercoiled loops significantly compacts the genome. Small proteins that associate with the chromosomal DNA cause it to fold into an even more compact structure and stabilize half of the free supercoils [137]. This group of proteins is often referred to as histone-like proteins based on superficial similarities with eukaryotic histone proteins. However, they are more appropriately referred to as nucleoid-associated proteins (NAPs), since there is no structural resemblance with histones. Besides functioning in chromatin organization and compaction, these proteins play roles in a variety of DNA transacting processes (e.g. recombination, DNA repair, replication and transcription). The combination of structural and regulatory roles suggests that the global genome functions of the nucleoid are tightly linked to its organization.

Open questions on this subject, addressed in this thesis, are:

- What is the interplay between the different NAP's in organizing the bacterial nucleoid?
- How can the bacterial genome be compacted by proteins and still be dynamically accessible?
- What is the nature of the topological domain barriers in the organization of the bacterial nucleoid?

1.2.3 DNA organization in Archaea

The phylogenetic tree in Figure 1.5 illustrates that the divergence between prokaryotes, archaea and eukaryotes is reflected in their genetic material, in that case RNA. In general, archaea combine traits of both eukaryotes and bacteria and the mechanisms

for the packaging of DNA in archaea appears to be no exception. For example, many archaea do possess histones, which are homologous to their eukaryotic counterparts and form nucleosomes. But in many archaeal species at least one type of DNA bending protein has been identified, similar to prokaryotic DNA organization. A good example of this is the protein Alba, which occurs abundantly in archaea, but is also conserved in both prokaryotic and eukaryotic cells. Another interesting aspect of archaeal DNA organization is that the requirements are very different. Compacting the genome to fit it inside the cell is still a primary requirement, but a second requirement is given by the habitat of many archaea. Numerous archaea are *extremophiles*. They live and thrive at locations with an environment that can be far too extreme for other species to live. For example: environments with a exceptionally high (80°C) or low (-45°C) temperatures or very high pressures and a very acidic environment. All these circumstances require an effective protection of the precious genetic material. These aspects make archaea a very fascinating organisms. One particulary interesting protein that is involved in the organization of the archaeal genome is Alba. This protein is present in most archaea but it can also be found in eukaryotes and prokaryotes. Some questions about this protein that are still open, addressed in this thesis, are:

- What are the molecular details of the Alba-DNA interaction?
- Can Alba protein bridge DNA duplexes together and if so, how?
- Can Alba protein provide some method of protection for the DNA?

1.2.4 Condensation of DNA

Besides the different means of compaction introduced in the sections above, there are other means of compacting DNA to fit it inside a small volume and not always proteins are necessary or available. Since the backbone of DNA itself is negatively charged, strongly positively charged *polyamines* like spermine (4+) and spermidine (3+) can induce the DNA to collapse onto itself [114]. In this process, DNA molecules aggregate into highly ordered structures, generally with toroidal or rod-like shapes [198, 85, 34] (see Fig. 1.9), consisting of many circumferentially wound DNA strands. Toroidal DNA condensates are of particular interest because of their striking similarity with the morphology of compacted DNA found in viruses and sperm cells.

This phenomenon has been the subject of numerous (single-molecule) studies; however, there are still many open questions, a few of which are addressed in this thesis:

- What are the dynamics of toroid formation and the stability of such condensates?

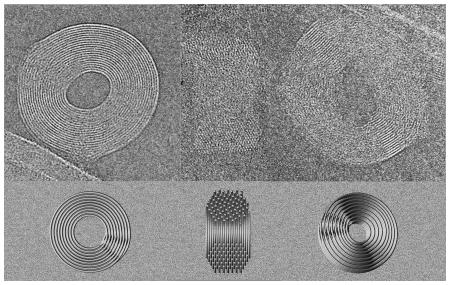

Figure 1.9: DNA toroids. The figure shows three electron microscope images of DNA toroids (top) and computer simulations of toroids in corresponding orientations. Below each electron microscopy image is a view of a solid model oriented to match the toroid [85].

- Do the DNA molecules condense directly into a single structure or are there intermediates?

1.3 Experimental techniques

1.3.1 Visualizing and Manipulating Single Molecules

In 1657 Antonie van Leeuwenhoek put a raindrop from his rainwater tank under his microscope and he was amazed when he saw "very small living creatures". Ever since, the field of microscopy has been developing new techniques and stronger microscopes to lower the limit of what can still be made visible. Recent improvements in the instrumentation used in biophysics allow for, instead of studying reactions on the level of ensembles of molecules, looking at the behavior of single molecules. Moreover, some of these techniques can do more than just *look* at single molecules; several techniques allow for mechanical *manipulation* of single molecules. An excellent example of such a technique is the application of the *optical tweezers* or *optical trapping*. The further development of this technique has been a substantial part of the experimental work described in this thesis. For example, chapters 2 and 3 describe a novel addition to an optical trapping apparatus to manipulate multiple DNA molecules independently.

1.3.2 Optical trapping

Nowadays widely used as a tool in large variety of experiments, the principle of optical trapping was discovered by Arthur Ashkin in 1970 [5]. He discovered that a laser beam with a power of 1 Watt exerts enough force on a particle, with a radius comparable to the wavelength of the laser light, to displace the particle. In 1987, Ashkin first showed this principle to work with living bacteria [6], trapping them one at the time

with 100 mW of light (and subsequently killing them due to photo damage). Later that year he showed that, by using laser light with a wavelength of 1064 nm, he could trap cells and keep them alive [7]. Together with one of his collaborators on these projects, Steve Chu, he also utilized an optical trap to cool atoms [35] and for this, Steve Chu won the 1997 Physics Nobel Prize.

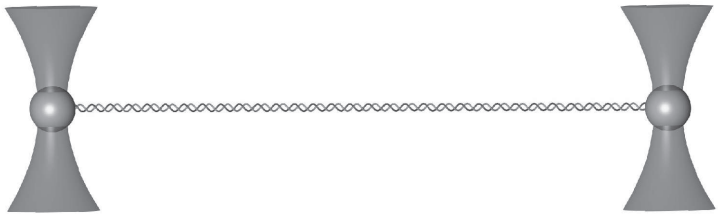

Figure 1.10: Single DNA molecule manipulation. A schematic picture of a single DNA molecule suspended between two beads, each held in optical tweezers.

Using optical tweezers, small neutral particles can be manipulated by lasers using the *radiation pressure*. By focusing the beam with a very powerful lens, a lens with a high *numerical aperture*, a particle can be trapped in three dimensions. In the experiments described in this thesis, optical tweezers are used to trap small spherical polystyrene spheres or 'beads'. Because these beads can be made to stick, to for instance proteins or DNA, the beads can act as 'handles' in single molecule experiments [167] (see Fig. 1.10).

The principle of a single beam optical trap is based on transfer of momentum from light to a particle, in this case a bead. To create a stable three-dimensional trap for a bead, a three dimensional balance of forces is needed. How this can be obtained is schematically depicted in Figure 1.11. Displacement of the bead away from the focus results in a restoring force, forcing the bead back to the focus. In the non-axial direction (or the direction of the light) this is the gradient force, caused by the inhomogeneous intensity profile of the laser (Fig. 1.11a). In the axial direction the scattering force and the force generated by the high incident angle rays keep the bead positioned in the focus of the beam.

Since the bead is forced to be in the centre of the optical trap, beads can be used as 'handles' attached to for instance DNA. By moving the optical trap and thus the bead caught in it, force can be exerted to single DNA molecules. In order to measure the force on the bead (and henceforth the DNA), the movement of the trapped beads can be analyzed. When the beads are 'free' in solution, they move in a random manner caused by the continuous collision with water molecules from all directions. This effect, first described by Robert Brown (the botanist mentioned before), is called Brownian motion [25]. The amplitude of this characteristic movement decreases sig-

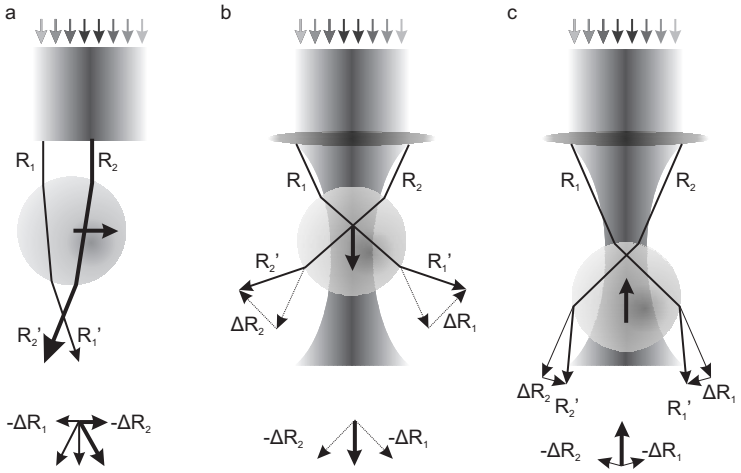

Figure 1.11: Principles of optical trapping. Optical trapping in a ray-optics representation. Panel a shows the results of using a Gaussian beam. This causes a lateral gradient force, which pushes the particle towards the center of the beam. Panels b and c show the axial forces to the center of the focus of the trapping light. In each figure, the arrow in the bead shows the resultant force towards the center of the trap.

nificantly when this bead is caught with optical tweezers. The suppressed Brownian motion can be measured by detecting the laser light that scatters of the trapped bead with a sensitive detector. By analyzing the resulting signal from the detector, forces smaller than a pico Newton can be measured [2, 15].

1.3.3 Multi channel flow system

Experiments on biological materials such as proteins and DNA often require very specific circumstances. Therefore, it is of great importance that the circumstances of

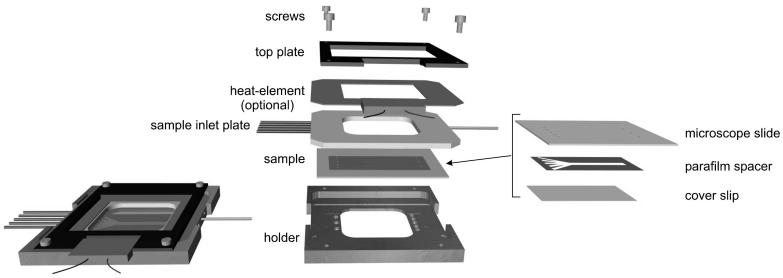

Figure 1.12: Flow cell. Cartoon of the flow cell assembly.

the experiment can be well controlled. Moreover, since every experiment on a single molecule will typically yield one data point, in order to achieve a statistically valid result, high throughput is very important. To resolve these issues, a flow-chamber was custom developed and built (Fig. 1.12). The basic concept is that multiple channels of solutions are flowing parallel to each other. Mixing of these channels occurs through diffusion (a process related to Brownian motion), but since this is a very slow process over large enough distances, as used in the flow chamber, and the solutions thus remain relatively pure and well separated. These multiple flows of solution close to each other allow for extremely rapid exchange of solution and thus a rapid change of environment of the experiment. For example, an optical trap can catch a bead in a channel containing a solution with beads, then move to a channel containing DNA molecules. Here a DNA molecule can be attached to the bead and subsequently this construct can be moved into a channel containing a protein that might interact with the DNA (see Figure 1.13). When the concentrations of the solutions are optimized, a construct as described can be assembled in less than one minute allowing for high throughput.

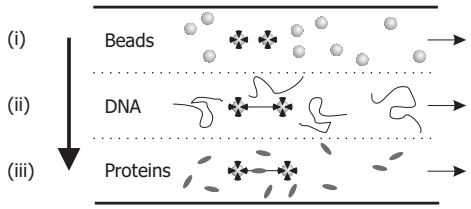

Figure 1.13: Laminar flows of solution. First, two beads are caught by optical tweezers in the bead channel (i). Then a DNA molecule is caught between the beads in a channel containing DNA molecules with sticky ends (ii). Finally, the bead-DNA construct is placed in a solution containing proteins (iii).

1.3.4 Dual-DNA manipulation

Experiments with single DNA molecules have revealed many intrinsic properties of DNA and associated proteins. In these experiments, the precise control of a single DNA molecule allows studying properties of, and interactions between DNA and proteins difficult to assess in conventional biochemical experiments. However, biological processes that require the involvement of multiple DNA tracts are still hard to explore with single DNA molecule experiments. For example, various DNA recombination proteins, restriction endonucleases and bridging nucleoid-associated proteins interact simultaneously with two separate DNA regions. The relative angle between, and tensions on such regions can not be controlled when handling a single DNA molecule. Using four moveable optical traps in combination with the laminar flow system, both described above, provides a powerful means to study biological processes governed by proteins interacting with multiple DNA sites [44, 73, 101, 182].

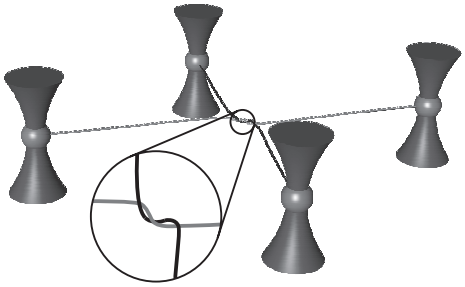

Figure 1.14: Dual-DNA manipulation assay. Cartoon of two DNA molecules suspended between polystyrene beads held with optical tweezers. In this particular case, one of the two DNA molecules is wound around the other.

1.3.5 Single-molecule fluorescence

When manipulating a single DNA molecule with optical tweezers, the DNA can only indirectly be 'visualized'; when exerting force on a bead on one end of the DNA, the bead on the other end moves along accordingly. With the recent development of sensitive cameras, single molecules can now be directly imaged by attaching a fluorescent dye to it. By combining single molecule fluorescent imaging with optical tweezers, single DNA molecules (Fig. 1.15) and even single proteins on DNA can be imaged (van Mameren *et al.*, manuscript in preparation) in solution and away from any surface. By analyzing the images obtained from the camera, the force-dependent conformation of a DNA molecule over time or the kinetics and even the movement of single proteins can be followed in time. However, attaching a fluorescent dye to either DNA or a protein might change the structure or the kinetics of the molecule under investigation and this has to be taken into account.

Figure 1.15: Single fluorescent DNA molecule.

1.3.6 Tethered Particle Motion

Optical traps allow for the *manipulation* of one or more DNA molecules, but in some experiments this is not necessary. By tracking the (Brownian) motion of tethered particles (see Fig. 1.16), protein induced changes in the conformation of a DNA molecule can be monitored, without interference such as the forces exerted by an optical trap. With this method, one end of a DNA molecule is fixed to the bottom of a sample chamber whereas the other end is attached to a small (500 nm) bead. This bead moves in a Brownian fashion, however, the length of the DNA determines the volume the bead can move in (see Fig. 1.16). As soon as a protein stabilizes a loop in the DNA molecule, the DNA effectively becomes shorter and hence this volume decreases. This

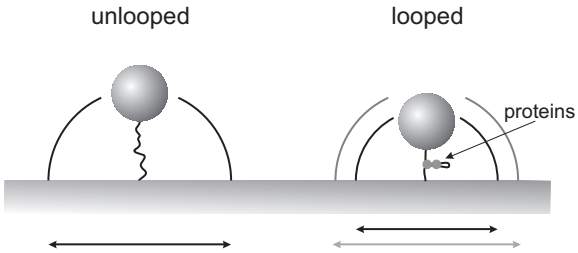

Figure 1.16: Tethered particle motion. Schematic representation of the effect of protein induced changes in the conformation of the DNA, in this case looping of DNA. When a tethered DNA molecule (see left panel) is looped, the DNA is effectively shortened compared to the unlooped state (see right panel) and as a result, the bead can only make excursion in a smaller volume (indicated by the arrows on the bottom of the panel).

can be visualized using simple video microscopy and tracking the movement of the beads attached to DNA tethers. The great advantage of this technique that many (tens to hundreds) DNA molecules can be monitored in parallel, resulting rapidly in a statistical sound result whereas by manipulating single molecules with optical tweezers this takes much longer.

1.3.7 Scanning Force Microscopy

An established technique that is capable of imaging [106] and manipulating single molecules [63] is Scanning Force Microscopy (SFM). With SFM, deviations of a scanning tip are used to generate a topographic image, very much like a pick-up music player 'reads' the grooves of a record. A tiny needle ($\sim$ 30 nm) on the tip of a cantilever is scanning over a surface and the deflection of the needle is detected. The movement of the tip is tracked by a laser with high precision by detecting the reflection of the laser on the cantilever with a sensitive photodetector (see Fig. 1.17). Typically, an SFM will scan many lines to create a topographic image of a surface. Where for instance DNA is too small to see under a normal light microscope, with an SFM single DNA molecules can be imaged (shown in Fig. 1.17). Moreover, using functionalized SFM tips, receptor-ligand binding forces can be studied [123], e.g. the interaction of a DNA-binding protein and DNA. The downside of this technique is that in order to visualize objects, they have to be bound to a (charged) surface, possibly affecting the interaction between proteins and DNA.

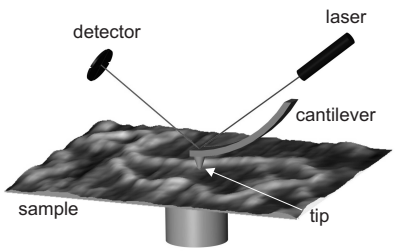

Figure 1.17: Scanning Force Microscope. Cartoon of an scanning force microscope. A tip is scanned across a surface. Any deflections of the tip caused by objects present on the surface are detected by a detector that measures deflections of a laser beam aimed at the edge of the cantilever holding the tip.

1.4 Outline of this thesis

This thesis describes the scientific work I did during my PhD-period at the Vrije Universiteit on the subjects described in the first half of this chapter using techniques described in the second half of this chapter. Chapters 2, 3, 4, and 5 are published in scientific journals and chapters 6 and 7 are manuscripts in preparation.

Chapter two is a description of the apparatus I have designed and built to do the experiments described in the other chapters. The apparatus allows for the simultaneous but independent manipulation of multiple DNA molecules. In this chapter we demonstrate the full control over the orientation it provides in the manipulation of two DNA molecules. As if it were micro-ropes, we used one of the DNA molecules to make a tight loop around another. Next, we pulled this loop carefully along this DNA molecule. Any obstacle this loop finds on its way along the DNA causes the required pulling force to increase briefly. In this way we can detect at which locations specific proteins bind to DNA. Moreover, when the loop is pulled tighter we can even wipe bound proteins off.

Chapter three reviews the proteins that play an important role in the organization of the prokaryotic genome. Moreover, it introduces a new classification of the major nucleoid associated proteins according to their structural effect on DNA (e.g. bridging or bending), which we believe is key to understanding the interplay between these proteins.

Chapter four utilizes the setup described in chapter two to study a key player in prokaryotic DNA organization: the protein H-NS. The instrumental advance described in chapter two opens up the possibility of investigating proteins that interact with multiple DNA duplexes. By applying this new experimental approach we describe numerous important aspects of H-NS-DNA interactions such as the energy landscape, interaction kinetics, the nature of the cooperative binding and organization of H-NS bridged regions. With these results we can for the first time appreciate the interplay between DNA compaction *in vivo* and DNA tracking enzymes such as RNA polymerase. Moreover, our findings reveal how bacterial chromatin can be effectively organized and compacted, but at the same time remain dynamic in nature.

In **chapter five** we combine a new analysis of the results obtained by another group, William Navarre and co-workers, and the results obtained in chapter four. By combining the data from these studies we demonstrate that the nucleoid associated protein H-NS is responsible for looped domain formation. With this approach we can show for the first time that the large majority of loops *in vivo* are protein-induced. The fact that H-NS binds to defined sites implies that the bacterial genome is much more ordered than generally believed and that there is limited cell-to-cell variation in basal genome organization. The observations in this chapter also have direct implications for how chromosomes are temporarily remodeled and how such remodeling is exploited for global gene regulation.

In **chapter six** we present the results obtained with experiments on Alba 1, an archaeal DNA architectural protein. Alba has been suggested to play an important role in DNA organization and regulation in Archaea. However, very little is known about the structural role of Alba in DNA-organization. Based on previous work it was suggested that Alba might be capable of dsDNA bridging as part of its organizational role. Using optical tweezers we show that under saturating conditions nucleoprotein filaments form when Alba interacts with DNA, stiffening the DNA up to three-fold with respect to bare DNA. Upon lowering the concentration, the persistence length quickly reverses to that of bare DNA in an apparently cooperative process. In addition, dual DNA experiments using quadruple optical tweezers, SFM experiments and tethered-particle-motion experiments provide the first experimental evidence in the DNA cross-linking ability of this protein.

Chapter seven describes the results of an experiment in which for the first time the formation of DNA condensates is directly imaged with high resolution, integrating optical manipulation techniques with fluorescence. Using this combination, we describe the formation and unraveling of DNA condensates with very high temporal, spatial and force resolution. These data provide important new insights in the understanding of the formation of DNA condensates. In this manuscript we demonstrate these insights and put forward a new mechanism for the formation of DNA condensates.

Chapter 2

All knots, bends, hitches and splices, are made out of only a few basic line configurations, such as a winding, loop, elbow or bright.

Visualizing single DNA-bound proteins using DNA as a scanning probe

Abstract – Many biological processes involve enzymes moving along DNA. Such motion might be impeded by DNA-bound proteins or supercoils. Current techniques are incapable of directly measuring forces such 'roadblocks' might impose. We have constructed a setup with four independently moveable optical traps, enabling us to manipulate two DNA molecules held between beads. By tightly wrapping one DNA around the other, we create a probe that can be scanned along the contour of the second DNA. Here we show that friction between the two polymers remains below 1 pN. Upon encountering DNA-bound proteins substantial friction forces are measured, allowing for accurate localization of protein positions. Furthermore, we show that these proteins remain associated at low probe tensions but can be driven off using forces that exceed 20 pN. Finally, the orientational control of two DNA molecules opens a wide range of experiments on proteins interacting with multiple DNA regions.

2.1 Introduction

Experiments with single DNA molecules have revealed many intrinsic properties of DNA and associated proteins. In these experiments, the precise control of a single DNA molecule allows studying properties of, and interactions between DNA and proteins difficult to assess in conventional biochemical experiments. However, biological processes that require the involvement of multiple DNA tracts are still hard to explore with single DNA molecule experiments. For example various DNA recombination proteins [194, 180, 183], restriction endonucleases [182] and bridging nucleoid-associated proteins [110] interact simultaneously with two separate DNA regions. The relative angle between, and tensions on such regions can not be controlled when handling a single DNA molecule. Here we describe a method which allows us to manipulate two DNA molecules independently. This technique enables us to study proteins interacting with multiple DNA binding sites as mentioned [40]. To demonstrate the capabilities of this technique, we utilize the two DNA molecules as a novel scanning probe technique to detect and manipulate DNA-bound proteins. Many biological processes on DNA involve either ATP-driven or 1D-diffusive motion along the DNA contour [14, 68, 190]. Bound proteins or DNA supercoils might act as roadblocks [57], impeding such motion. With this new scanning technique, one DNA molecule is wrapped around the other molecule (Fig. 2.1) and then employed as a mechanical probe to scan along the contour of the first DNA molecule. With this scanning mode, we apply forces on single DNA-bound proteins in a direction along the DNA contour. Consequently, we are capable of directly exploring removal of these roadblocks similar to when they are encountered *in vivo* by motor proteins translocating along the DNA contour.

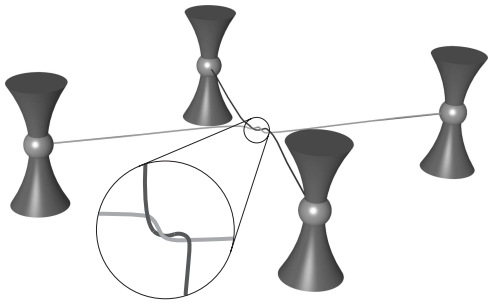

Figure 2.1: Dual DNA manipulation assay. Two λ-DNA molecules suspended between four optically trapped polystyrene beads and wound around each other.

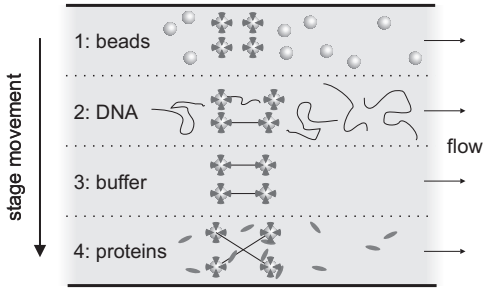

Figure 2.2: Laminar flow cell. The dual-DNA experiment is conducted in a multi-channel flow cell exhibiting non-mixing laminar flows: **1**, bead channel: four beads are trapped with optical traps. **2**, DNA channel: two λ-DNA molecules are caught between the beads. **3**, buffer channel: here, a number of DNA windings is imposed. **4**, protein channel: the DNA is incubated in protein solution. Scanning can be performed either in the protein or buffer channel.

2.2 Results

We have designed and built an optical-tweezers instrument that enables the manipulation of two DNA molecules in three dimensions simultaneously and independently. This is done by trapping micron-sized polystyrene beads attached to the ends of the DNA molecules. As schematically depicted in Figure 2.1, four optical traps are generated by first splitting a laser beam in two orthogonally polarized beams. One of these beams generates a continuous trap; the other beam is time-shared over three trap positions using acousto-optic deflectors. Forces acting on the bead in the continuous trap can be detected with sub-picoNewton resolution using back-focal-plane interferometry [2, 64]. In order to attach DNA between the four beads held in the optical traps, we designed and constructed a flow chamber with multiple laminar flows of solution running parallel to each other [22] (see Methods for details). By moving the chamber relative to the optical traps, the four trapped beads can be moved into different solutions. In this way, the ends of two DNA molecules can be attached to the four beads (Fig. 2.2). After catching two λ-DNA molecules, they are moved into a channel containing only buffer. Using force-extension analysis we ensure that every pair of beads only holds one DNA molecule (Fig. 2.3). The four traps can be freely moved with respect to each other in the sample plane, giving us full control over the relative orientation of the two DNA molecules as well as the tension on both molecules. In addition, moving the continuous trap in the third dimension enables us to wind one DNA molecule around the other.

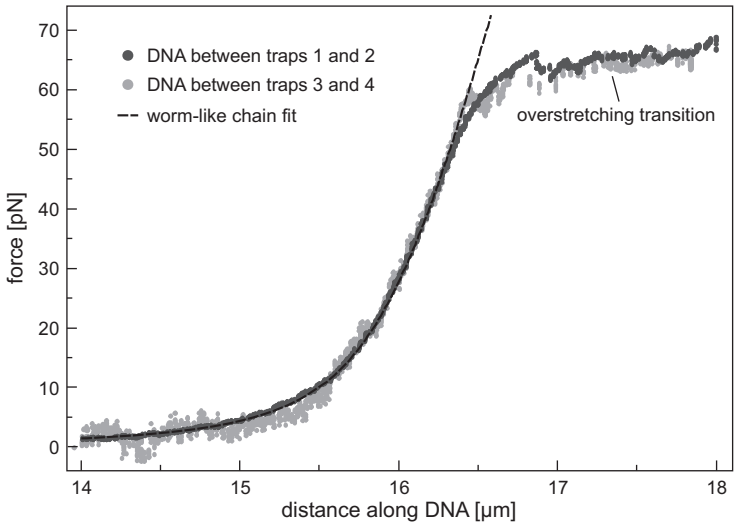

Figure 2.3: Force-extension analysis of two DNA molecules. Two force-extension curves of two λ-DNA molecules, taken simultaneously. The scanned DNA molecule is suspended between two beads, one in the continuous trap and one in a time-shared trap. The probing DNA is suspended between two beads caught in time-shared traps and a separate detection laser is used for detection on one of these beads. The black trace shows the worm-like chain behavior with which the DNA can be modeled.

2.2.1 Using DNA as a scanning probe.

In order to scan one DNA duplex (the *scanned* DNA) using the second one as probe (the *probing* DNA), we positioned the beads such that the two DNA molecules are in a crossed configuration. Next, the probing DNA is wrapped around the scanned DNA one or multiple time(s), creating a tight loop (Fig. 2.1) and a Supplementary Movie (to be found at www.nat.vu.nl/compl/dualdna). We stretch both DNA molecules to a pre-set tension, (typically 5–20 pN) to create a tight DNA loop. For a circular DNA loop, the diameter D depends on the tension S and the persistence length l_p as [4] $D \approx \sqrt{2 l_p k_b T / S}$, approximately 5–10 nm for the tensions mentioned above. This is an upper limit of the actual probe size, since in our experiments the DNA loop does not have a circular, but a twisted or supercoil-like structure (Fig. 2.1). By moving both beads that hold the probing DNA (beads 3 and 4 in Fig. 2.4a) simultaneously parallel to the scanned DNA, we utilize the DNA loop to probe the contour of the scanned DNA (Fig. 2.4a). If due to an obstacle or friction on the scanned DNA this loop DNA stalls, we measure an increase in force on the bead in the continuous trap.

Figure 2.4b displays a typical scanning trace of λ-DNA in the presence of 5 mM Ca^{2+}. The feature visible on the left side of the measured reference scan (grey) in Figure 2.4b is due to the collinear alignment of the time-shared optical traps 3 and 4 with the (continuous) trap 1, used for force detection [186]. In the black trace and all subsequent traces this is corrected for (See Fig. 2.5 for details). The left edge of a scanning trace is marked by the probing DNA pushing against bead 1, resulting in a negative force. Similarly, at the right edge of the trace, the probing DNA pushes against bead 2 resulting in a positive force measured at bead 1. The difference in slopes originates from additional stretching of the scanned DNA.

What is most notable about this curve is that the friction force between the tightly pulled DNA loop and the scanned DNA remains well below 1 pN (s.d. of friction signal: 0.3 pN around the base line). Similar results were obtained when scanning in the presence of 150 mM Na^+ (s.d.: 0.2 pN) and even in DNA condensing conditions [67], 200 μM spermine, (s.d.: 0.4 pN). Scans at various speeds (∼200–2000 bp s^{-1}) and with various tensions on both DNA molecules, with single and multiple DNA windings yielded similar results as well. Thus, even though in DNA condensing conditions the repulsion between the negatively charged DNA molecules is practically neutralized, very little frictional interaction is present when the two tightly wrapped DNA molecules are moved past each other.

To further demonstrate the localization and manipulation capabilities of our technique, we incubated the scanned λ-DNA with Type IIP restriction enzymes in non-cleaving conditions. These restriction enzymes bind specifically to their recognition sequence. Because the locations of these recognition sequences are known, these enzymes function as a convenient site-specific marker in these experiments. Figure 2.6a

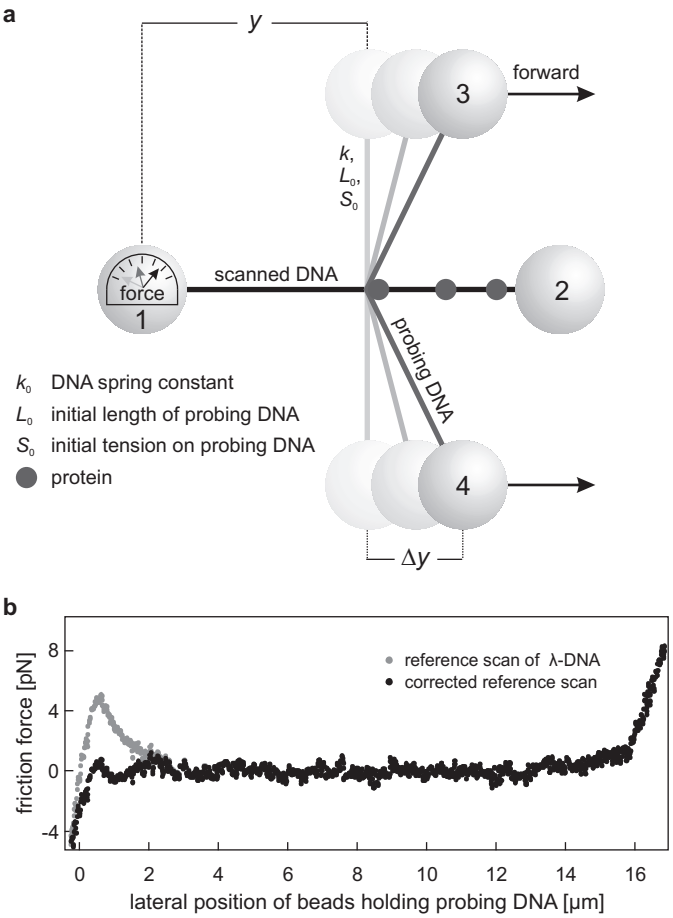

Figure 2.4: DNA scanning scheme and reference scan. **a**, To detect DNA-bound proteins, the probing DNA (held between beads 3 and 4) is moved along the scanned DNA. Upon encountering a protein bound to the scanned DNA, the measured force on bead 1 scales with distance y. **b**, Typical scanning trace of λ-DNA without proteins (grey) using a probing force of 10 pN. The black trace shows the same data, corrected for interference between time-shared traps holding beads 3 and 4 and the continuous trap holding bead 1 (see Fig. 2.5).

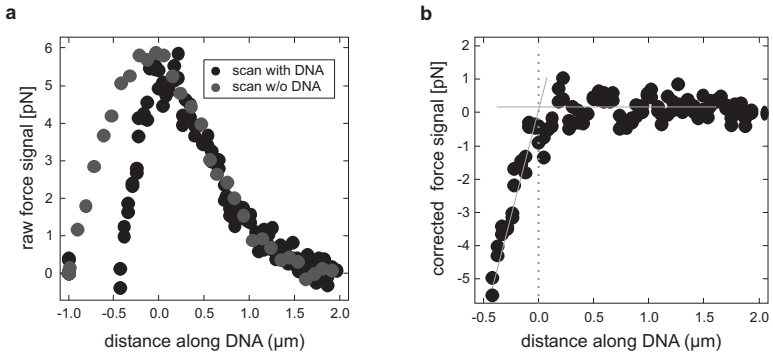

Figure 2.5: Correction of interference between traps. **a**, Scan with and without DNA present between the beads. At the beginning of a scan, when time-shared traps 3 and 4 are in a collinear geometry with trap 1, the rapid time-sharing between traps 3 and 4 causes interference on the optical trap holding bead 1, as seen in the scan without DNA. The deviation of DNA scan from this reference scan is caused by the pushing of the probing DNA on bead 1. **b**, The same scan (with DNA) corrected for this interference effect by subtracting the scan without DNA. This correction allows for marking the beginning of the scanned DNA.

displays three consecutive scans in forward and backward directions along the same λ-DNA molecule with *Eco*RI restriction enzymes associated to it. In these traces, force peaks are measured at four locations that match with the expected specific target sites of *Eco*RI, immediately revealing the orientation of the DNA. Besides peaks at these specific sites, we occasionally observe additional (smaller) peaks at other locations. Presumably this is a signature of non-specific or non-cognate binding of *Eco*RI to sites that are similar (e.g. 1 base pair mismatch) to the specific binding sequence (over 250 of such sites are present on λ-DNA). At every bound protein that is encountered by the DNA probe the measured force on bead 1 increases with similar inclination, after which it 'snaps back' to a zero friction force. The distribution of measured peak forces for both non-specific and specific events from the scan displayed in Figure 2.6 shows that forces measured at non-specific sites, 2 ± 1 pN ($n = 7$, s.e.m.) with a typical duration of 3 ± 1 s, are substantially lower than at specific sites, 5 ± 1 pN ($n = 11$, s.e.m.) with a duration of 7 ± 2 s. The distinctly different forces measured at specific and non-specific sites imply that the nature of the events is different. The fact that peak forces at non-specific sites are lower may indicate that the probe triggers such a protein to dissociate, whereas a specifically bound protein may either dissociate (at a higher peak force) or stay bound with the probe slipping over it. Below we demonstrate that for low probe tensions the latter is the case.

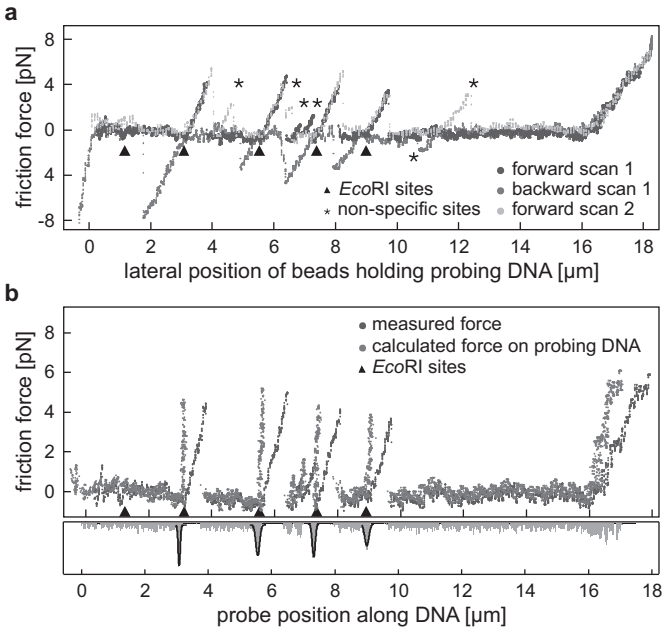

Figure 2.6: Detection of individual DNA-bound restriction enzymes. a, Three consecutive scans along λ-DNA in forward and backward directions, with 0.1 units l^{-1} (∼1 nM) *Eco*RI restriction enzyme bound to the DNA using a probe tension of 10 pN. An additional friction force is measured when the probing DNA loop stalls behind DNA-bound *Eco*RI proteins (sites indicated with black triangles). Less substantial peaks presumably indicate non-specific scanned DNA–*Eco*RI interactions (indicated with black asterisks). The x–axis depicts the location of the beads holding the probing DNA. **b**, During each event, the traveled distance by the probing DNA y, can be corrected by modeling the lateral stretching of the probing DNA and the bead displacement out of the optical traps (see the Appendix). Corrected data of the probing DNA scanning loop (light grey), calculated from the *Eco*RI forward scan (dark grey). The x-axis now depicts the location of the scanning loop. At four peaks the distribution is fit with Gaussians (lower graph) to determine the location of specifically bound proteins with ∼120 bp resolution.

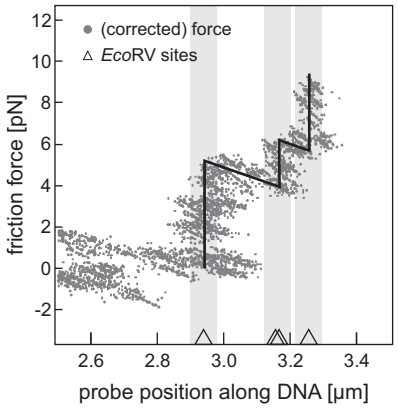

Figure 2.7: Resolution of protein localization. Detail of a scan along a λ-DNA molecule incubated with EcoRV restriction enzymes using a probe tension of 25 pN. The scan shows the presence of three proteins on the DNA whereas there are four known binding sites, demonstrating the resolution of the method. The grey boxes indicate the spatial resolution of the localization. The dark line is drawn to guide the eye.

2.2.2 Resolution and accuracy

To determine the accuracy and resolution of our scanning technique, we corrected our data to compensate for lateral stretching of the scanning DNA molecule and bead displacement out of the optical traps (see Appendix). Figure 2.6b displays a corrected force-distance trace for the *Eco*RI forward curve (Fig. 2.6a), where the *x*-axis now represents the actual position of the probing loop and the force increases vertically at every encountered protein. The accuracy of localization of the DNA-bound proteins is assessed by evaluating a dwell time histogram of the corrected data (Fig. 2.6b lower graph). From the standard deviations of Gaussian fits to the observed peaks, we determine the *spatial resolution* to be ∼120 bp. Comparison with the known locations of the specific binding sequences on λ-DNA yields a *relative position accuracy* of ∼50 bp. In Figure 2.7 we focus on a part of the DNA that contains four *Eco*RV restriction sites, three of which can be unambiguously distinguished. The fourth site cannot be distinguished since it is only separated 35 bp from the adjacent site, demonstrating the resolution of the technique.

The (un)binding of DNA-associated proteins can be probed with a repetition rate equal to the scan time, typically 100 seconds for the complete λ-DNA at a scanning speed of 500 bp s^{-1}. The temporal resolution can be greatly improved by scanning only part of the DNA or by increasing the scanning speed. However, high scanning speeds will result in larger loading rates acting on the enzyme-DNA bond, possibly activating dissociation. Moreover, the stretch correction fails where the DNA elasticity starts to deviate from the worm-like chain (WLC), at ∼50 pN total force. Finally, the nature of the DNA itself sets an upper limit to the force that can be applied since at 65 pN the DNA double helix starts to overstretch, making it difficult to interpret the signal.

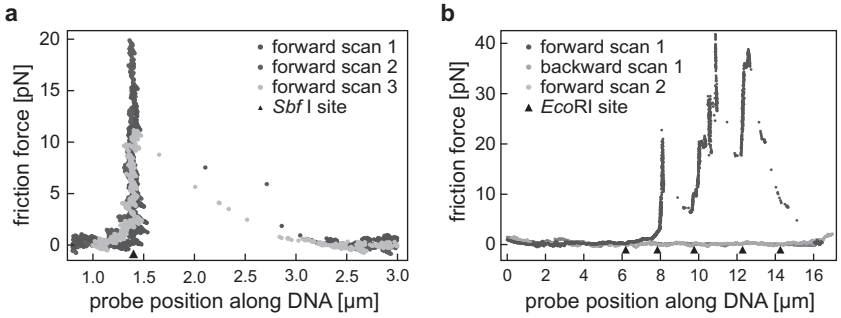

Figure 2.8: (Non-)destructive imaging. **a**, Three consecutive scans (in forward direction and corrected for lateral stretching of the probing DNA) acquired in a buffer solution without proteins, after loading of the DNA construct with *Sbf*I. All detected proteins stay bound when scanned with a low probe tension (5-10 pN). **b**, Destructive imaging. A larger tension on the probing DNA (35-40 pN) yields a smaller loop-size. Consecutive traces show that this results in a DNA molecule with no proteins associated to it. The two peaks right after the third specific site are attributed to non-specifically bound proteins, briefly interacting (∼3 sec) with the scanning probe before dissociating.

2.2.3 Detection efficiency

We determined the detection efficiency using Type IIP restriction enzymes that have well-known (and well-separated) locations of their binding sites on λ–DNA. This allows for distinguishing false positives (probe sticking at locations where no protein is bound) from specifically bound proteins. We did not observe such events when scanning DNA in the absence of proteins. Since it is known that restriction enzymes can bind DNA in a non-specific manner [154], we do not regard events in the presence of proteins at non-specific sites as false positives.

On λ-DNA there are five recognition sites for *Eco*RI whereas in Figure 2.6a we detect four specifically bound proteins. The fact that we neither detect a protein at this particular location in the second and third scan (while the other four are consequently detected) makes it unlikely that there is actually a protein bound at this location, probably due to the close proximity of the bead. When we repeatedly scan other constructs we observe similar results and therefore we argue that hardly any proteins are missed with this method. Apparently, the absence of proteins at specific binding locations is limited by the biochemical binding probability of proteins [177] or irregularities on the DNA.

2.2.4 (Non)-destructive imaging

Do the specifically bound proteins stay bound when the scanning loop encounters them or are they pulled off their binding site and subsequently replaced by others

present in the surrounding solution? To examine this, we first "loaded" the DNA construct with *Sbf*I restriction enzyme (under conditions where generally k_{off} ∼1hr) [78] by briefly moving it into a flow channel containing the proteins. We then moved the DNA into a channel with identical buffer conditions but without proteins to ensure that no more proteins could bind to the DNA. Hereafter, we scanned the DNA repeatedly at a probe tension of ∼10 pN. Figure 2.8a shows the friction force of a part of a λ–DNA molecule with a protein bound to the single *Sbf*I-site that is present in this region, which is scanned three times in succession. The scans show that the SbfI stays bound, demonstrating that the protein binding is undisturbed by the DNA scanning. Apparently, the DNA loop that exerts lateral force on the bound protein slips over it when some critical force is reached (in this case ∼10–20 pN).

Increasing the tension on the probing DNA results in a tighter DNA loop, potentially preventing it from slipping over the protein. When this probe tension is increased to 25–40 pN, the observed force peaks are in fact higher: 20–40 pN (Fig. 2.8b). In subsequent scans no more force peaks appear, indicating that proteins are indeed pushed off by the application of high lateral forces.

2.3 Discussion

An alternative technique capable of manipulating multiple DNA molecules is to attach two DNA molecules between a surface and a single paramagnetic bead manipulated by magnetic tweezers [33]. By rotating the magnetic bead braids can be induced. Unlike our approach, this technique yields very limited control over the relative orientation of the DNA molecules and lacks the ability to exert different forces on them.

An established scanning probe technique is scanning force microscopy (SFM) [17]. With SFM, deviations of a scanning tip are used to generate a topographic image. DNA can be visualized and associated proteins may be observed [106] and manipulated [63]. In contrast to SFM experiments, the technique introduced here is performed far away from any (charged) surfaces that potentially affect protein-DNA interactions [97, 185]. Additionally, we exert and measure forces on the proteins *in the direction* of the DNA contour, as is expected for a roadblock encounter *in vivo*.

Recently, the development of a technique combining a scanning probe and optical tweezers was reported [88]. A micropipette is used as a probe to scan along the contour of a DNA molecule suspended between optical tweezers. The technique, however, has not yet been shown to enable detection of proteins bound to DNA. Since the micropipette scans the DNA on one side only and does not enclose it as in our case, it might miss bound proteins due to the finite torsional compliance of the DNA. Finally, a technique in which mechanical separation of the two strands of the DNA double helix provides information about the location of associated proteins and bind-

ing strengths has been described [99]. Contrary to our capability to visualize individual DNA-associated proteins repeatedly without affecting the binding, unzipping the double helix leads to destruction of the protein recognition site.

2.4 Outlook

We have described the design and application of a dual DNA manipulation technique. The realization of four moveable optical traps in combination with the laminar flow system provides a powerful means to study biological processes governed by proteins interacting with multiple DNA sites [101, 44, 73, 182]. The involvement of multiple DNA-binding domains complicates studying their interactions with conventional single-molecule approaches. With our dual-DNA manipulation technique, such interactions can now be explored in detail [40]. The scanning probe technique introduced here, where DNA itself is utilized as a scanning probe, is indicative of the topological freedom this dual DNA assay offers.

2.5 Acknowledgements

The authors thank E.J.G. Peterman and R.T. Dame for useful discussions. We acknowledge D.A. Hiller and J.J. Perona for the kind gift of *Eco*RV. This research was supported by the Netherlands Organization for Scientific Research (NWO) through an NWO-Vernieuwingsimpuls grant, a FOM-projectruimte grant and a grant from ALW-NWO.

2.6 Materials and methods

2.6.1 DNA and proteins

To allow specific binding to streptavidin-coated beads (1.87 μm diameter, Spherotech Inc., IL), we biotinylated lambda phage dsDNA (Roche) on both ends, as described previously [181]. *Eco*RI was purchased from New England Biolabs (Ipswich, MA) and used without further purification. EcoRV, a gift of D.A. Hiller and J.J. Perona, was recovered from ammonium sulfate precipitates, dialyzed into 10% (v/v) glycerol, 20 mM Tris-HCl (pH 7.5), 1 M NaCl, 10 mM 2-mercaptoethanol, 1 mM EDTA and filtered through 0.2 μm syringe filters. Aliquots (59 μM) were flash-frozen and stored at -80° C. We performed all protein scanning experiments in 10 mM Tris-HCl (pH 7.5), 100 mM NaCl, 5 mM $CaCl_2$ and 1 mM DTT, with protein concentrations of ∼1–5 nM.

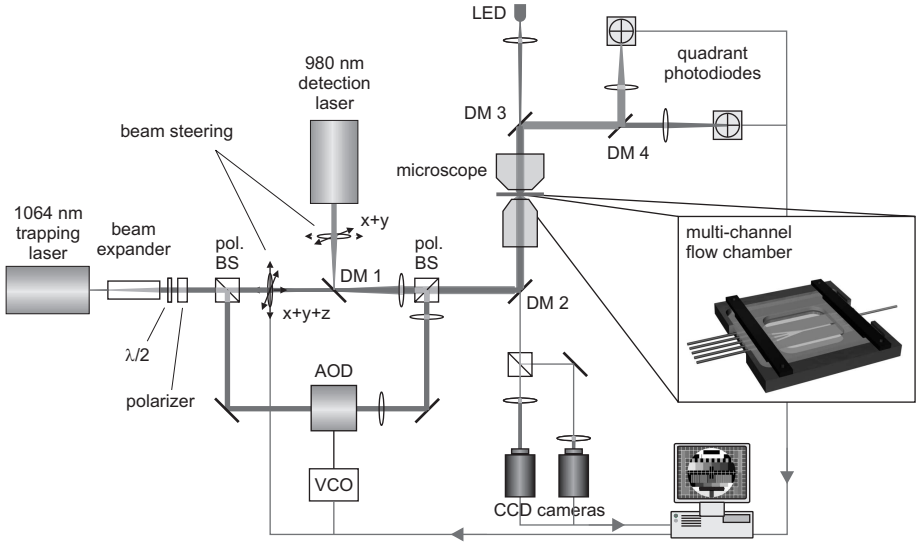

Figure 2.9: Schematic representation of the experimental setup. The inset shows an impression of the multi-channel flow cell.

2.6.2 Experimental setup

We performed the experiments using a custom-built inverted microscope as shown in Figure 2.9. To generate the optical traps we used a Nd:YVO_4 laser (1064 nm 10 W cw, Millennia IR, Spectra Physics, Mountain View, CA), isolated against back-reflections by a Faraday isolator (IO-3-λ-VHP, Optics For Research, Caldwell, NJ) and expanded by a beam expander (2–8x, Linos Photonics GmbH, Göttingen, Germany). We split this laser beam into two beams by a polarizing beam splitter cube (PBS-1064, CVI, Albuquerque, NM). In both beam paths, we implemented a 1:1 telescope system ($f = 150$ mm) allowing beam steering in the sample [167]. In one path (which we refer to as the 'continuous' path), the first telescope lens could be displaced laterally using two computer-controlled actuators (T-LA28, Zaber Technologies Inc., Richmond, British Columbia, Canada). In the other 'time-shared' path, we placed two orthogonal acousto-optic deflectors (AODs, DTD 276HD6, IntraAction, Bellwood, IL) directly in front of the telescope. We then coupled first-order deflected beam via a dichroic mirror (1020dclp, Chroma Tech Corp., Rockingham, VT) into a 60x water-immersion objective (Plan Apochromat 60, NA = 1.20, Nikon) to form the other laser traps.

A third computer-controlled actuator moves the first telescope lens in the continuous path in the direction of the laser light, thereby changing the depth of the laser focus with respect to the traps from the time-shared path. Doing so, we can wind two DNA molecules around one another.

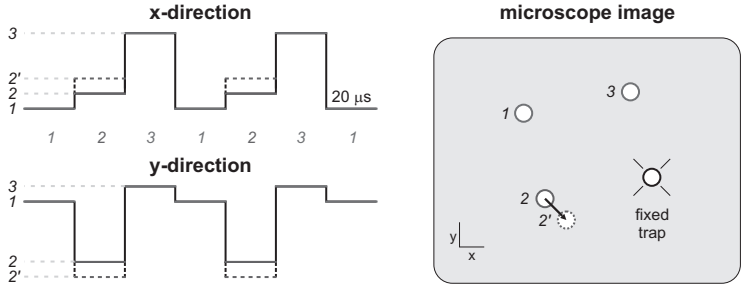

Figure 2.10: Input signal for time-shared trap generation and corresponding trap position. Example of multi-level square-wave voltage signal serving as input for the VCOs. The DC-offset of the voltage that is input to the VCO determines the frequency deviation of the synthesized RF signals that drive the AODs. Altering one of the DC levels, for instance level 2→ 2'), changes the position of one of the traps in the sample. These levels were output at a typical refresh rate of 20 kHz. Since this rate greatly exceeds the cut-off frequencies of the (suppressed) Brownian motion (∼1.5 kHz) that the beads perform in the traps, the beads are trapped stably enough to allow for DNA stretching up to and beyond the overstretching plateau at 65 pN (see figure 2.3).

For displacement detection of the continuous trap, we imaged the intensity profile in the back focal plane of the condenser (Achromat/Aplanat, NA = 1.4, Nikon) onto a quadrant photodiode (QPD, SPOT-9DMI, UDT Sensors, Hawthorne, CA) [64]. We likewise measured displacements in one of the AOD-generated traps using a separate (non-trapping) detection laser (980 nm IQ2C140/6018, Power Technology Inc.), overlaid on the trap and imaged onto a separate QPD. To generate multiple traps, the AODs were driven by voltage-controlled oscillators (VCO's) (DE-272H Deflector Driver, IntraAction, Bellwood, IL) as RF synthesizers (see below). A bright-field image of the trapped beads, illuminated by a blue LED (LXHL-NB98 Luxeon Star/O, LumiLeds) was imaged onto a CCD camera (902B, Watec).

2.6.3 Quadruple Trap Implementation

We used AODs to generate three independent, time-shared traps by modulating the VCOs that synthesize the RF signal with analog voltages generated by a multifunction data acquisition PC board (NI PCI-6221, National Instruments, Austin, TX). Using two orthogonally placed AODs, traps can be generated and steered in both directions in the sample plane. The DC-offset of the voltage that is input to the VCO determines the frequency deviation of the synthesized RF signals (typically 27 MHz) that drive the AODs. Therefore, VCO-input signals consisting of repeated patterns with a number of DC levels yield a corresponding number of successively scanned, independent laser deviations (see Fig. 2.10).

2.6.4 Microfluidic Flow Cell

To enable swift exchange of buffers and to have fine control over the process of catching the DNA molecules between beads, we used a custom-built microfluidic flow chamber (figures 2.2 and 2.9). The central part of this flow chamber consists of four channels cut manually out of a spacer (Parafilm), as indicated in Figure 2.2, sandwiched between a 24 x 60 mm #1 cover slip and a 50 x 75 x 1 mm microscope slide. The slide contains 1 mm-diameter holes which connect to the input channels. By using a pattern with merging channels, a region exists in the flow chamber where juxtaposed buffers exhibit laminar flow. At the locus of the experiment in the flow chamber the channels are well-separated, facilitating rigorous sub-second buffer exchange by simply translating the microscope stage in a direction perpendicular to the flow. A custom-made, sealed pressure chamber holds a reservoir for different solutions (containing beads, DNA, restriction enzymes or buffer). Contents of each channel are input to the channels through PEEK^{TM} tubing (Upchurch Scientific Inc., Oak Harbor, WA) and can be altered using selection valves (V-241, Upchurch Scientific Inc.). We control the flow speed through adjustment of the air pressure in the pressure chamber, thereby pushing the buffers through the flow chamber [204]. Fine control of pressure is attained by using solenoid valves (ES-2T-6, Clippard Europe S.A., Louvain-la-Neuve-Sud, Belgium) to in- or decrease the pressure, while monitoring the pressure using a differential pressure meter (CTE8005GY0, Sensortechnics GmbH, Puchheim, Germany). This approach yields smoother flow (transitions) than when using a stepper motor syringe pump [181]. Typical working flow speeds are on the order of 100 $\mu m\,s^{-1}$, achieved at 50–100 mbar overpressure. To diminish any effects of flow on the measured force, we turned off the buffer flow during actual measurements. To ensure that the solution in which the experiments are performed remain uncontaminated, the measurements are typically done in a channel before it merges with the others in the laminar flow chamber.

2.6.5 Data acquisition and analysis

For two traps, we recorded bead displacements within the traps in *x*- and *y*-directions using two quadrant photodiodes and a data acquisition board (AD16 module on a ChicoPlus PCI board, max. sampling rate 195 kHz, Innovative Integration, Simi Valley, CA) [186, 64]. We calibrated voltages to forces using power spectrum analysis [65]. For concurrent force and extension recordings of the captured DNA molecules, we measured the distances between pairs of beads on-line using pattern matching on a digitized microscope image (IMAQ PCI-1409, National Instruments).

2.7 Appendix

Derivation of lateral spring constant of the probing DNA

The increasing force signal measured upon the encounter with a bound protein is most likely due to the lateral stretching of the probing DNA. To correct the force scan traces for this effect, we devised a model to calculate the position of the scanning 'loop' based on the force and measured position along the contour length. The probing DNA has initial contour length L_0 and initial tension S_0. The center of the probing DNA is deflected by a distance Δy. This causes the tension on it to increase to S and the contour length stretch to length L. These parameters relate to their initial values by:

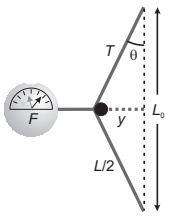

Figure 2.11: Schematic introducing the variables used in the scan correction model.

$$\begin{aligned} L &= \sqrt{L_0^2 + 4\Delta y^2} \\ S &= S_0 + k\left(L - L_0\right), \end{aligned} \tag{2.1}$$

where k is the intrinsic spring constant of the DNA. To correct for the position of the probe, the deflection Δy as a function of force F, we need to calculate the effective spring constant of the probing DNA perpendicular to its axis. Using Figure 2.11, the applied force can be described by

$$F = 2S\sin\theta = \frac{4S\Delta y}{L}. \tag{2.2}$$

This means the perpendicular spring constant $k_\perp$ can be modeled by

$$k_\perp = \frac{F}{\Delta y} = \frac{4S}{L}. \tag{2.3}$$

If we assume that the deflection Δy of the probing DNA is much less then the length L_0 of the probing DNA equations can be approximated as:

$$\begin{aligned} L &\approx L_0 + \frac{2\Delta y^2}{L_0}, \\ S &\approx S_0 + \frac{2k\Delta y^2}{L_0}. \end{aligned} \tag{2.4}$$

The perpendicular spring constant (Equation 2.3) now becomes:

$$k_\perp = \frac{4S}{L} \approx \frac{4S_0 + 8k\Delta y^2/L_0}{L_0 + 2\Delta y^2/L_0} \approx \frac{4}{L_0}\left[S_0 + \frac{2k\Delta y^2}{L_0}\right]. \tag{2.5}$$

The intrinsic spring constant of the probing DNA can be estimated by approximating the behavior of DNA with the worm-like chain interpolation formula [28, 115]:

$$F = \frac{k_B T}{l_p}\left[\frac{1}{4\left(1-\frac{x}{L_0}\right)^2} + \frac{x}{L_0} - \frac{1}{4}\right], \tag{2.6}$$

where F is the applied force, l_p is the persistence length, x is the end-to-end distance, k_B is the Boltzmann constant, T is the temperature and L_0 is the contour length. The intrinsic spring constant k_{DNA} can now be determined as [204]:

$$k_{DNA} = \left(\frac{\partial F}{\partial x}\right)_{x\approx L} = \frac{4F^{3/2}}{L_0}\sqrt{\frac{l_p}{k_B T}}. \tag{2.7}$$

Inserting Equation 2.7 into Equation 2.5, where the force F is equal to tension S, yields:

$$k_\perp = \frac{4}{L_0}\left[S_0 + \frac{8S^{3/2}\Delta y^2}{L_0^2}\sqrt{\frac{l_p}{k_B T}}\right]. \tag{2.8}$$

Chapter 3

The rigging of a ship is vital to its functioning. Keeping lines in order and without knots can make the difference in a hazardous situation.

The role of NAPs in the organization of bacterial chromatin

The architectural role of nucleoid-associated proteins in the organization of bacterial chromatin: a molecular perspective

Abstract – The bacterial genome is folded into a compact structure called the nucleoid. Considerable compaction of the DNA molecule is required in order to reduce its volume below that of the cell. Several mechanisms, such as molecular crowding and DNA supercoiling contribute to the compactness of the nucleoid. Besides these mechanisms, a number of architectural proteins associate with the chromosomal DNA and cause it to fold into a compact structure by bridging, bending or wrapping DNA. In this review, we provide an overview of the major nucleoid-associated proteins from a structural perspective and we discuss their possible roles in dynamically shaping the bacterial nucleoid.

3.1 Introduction

Bacterial chromosomal DNA is not confined to an envelope-enclosed organelle such as the nucleus in eukaryotes, it is present in a microscopically visible structure called the nucleoid. The ~1.6 mm long chromosomal DNA molecule of *Escherichia coli* is contained within a cell that is only 2 μm long and 1 μm wide. An unconstrained DNA molecule of this size would form a random coil with a volume of approximately 200 μm^3 i.e. about 400 times the volume of an *E. coli* nucleoid (~0.5 μm^3). Several mechanisms operate to compact the chromosomal DNA sufficiently to fit inside the cell [178, 93, 38]. These mechanisms include macromolecular crowding and DNA supercoiling. The bacterial chromosome consists of 50-400 negatively supercoiled DNA loops that are on average about 10 kb in size [77, 93]. These DNA loops are discrete chromosomal territories that are topologically independent. The nucleoid is a dynamic structure and the boundaries of these topological domains are distributed in an apparently random manner throughout the genome. The presence of boundaries between different domains preserves the overall superhelicity of the genome when one of the domains becomes more relaxed due to active DNA metabolism [178]. About half of the supercoils in the domains is present as branched intertwined structures (plectonemes). The organization of the nucleoid into numerous small supercoiled topological domains significantly contributes to its overall compactness [93]. Small proteins that associate with the chromosomal DNA cause it to fold into a more compact structure and stabilize the remaining half of the free supercoils [137]. This group of proteins is often referred to as histone-like proteins based on superficial similarities with eukaryotic histone proteins (basicity, abundance, DNA binding properties and low molecular weight). These proteins are more appropriately referred to as nucleoid-associated proteins (NAPs), since there is no structural resemblance with histones. Besides functioning in chromatin organization and compaction, these proteins play roles in a variety of DNA transacting processes (e.g. recombination, DNA repair, replication and transcription). The combination of structural and regulatory roles suggests that the global genome functions of the nucleoid are tightly linked to its organization.

In this review we provide an overview of the structurally and functionally best-characterized NAPs. Each of these proteins is believed to contribute to the organization of the genomic information into an accessible, dynamic and versatile nucleoid that is sufficiently compact to fit inside the bacterial cell. In addition, we introduce a classification of the major NAPs according to their structural effect on DNA (i.e. bridging or bending), which we believe is key to understanding the interplay between these proteins.

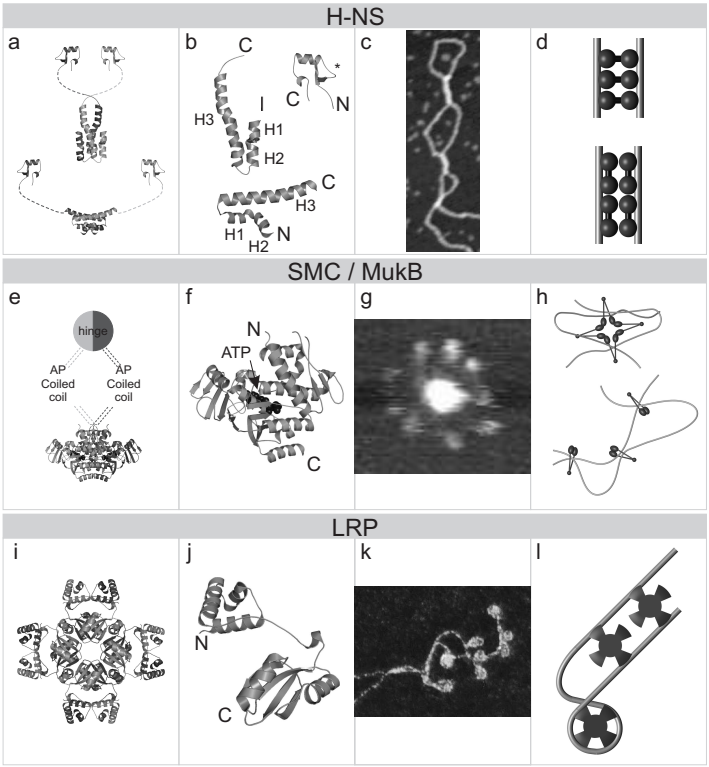

Figure 3.1: Architectural properties of nucleoid-associated proteins: DNA-bridging proteins. **a-d** - H-NS **a**, High-resolution models of dimeric H-NS based on the structure of the *Escherichia coli* H-NS C-terminal DNA-binding domain (PDB: 1HNR - residues 80-136) [156] and two different structures of the N-terminal dimerization domain (PDB: 1NI8 - residues 1-46 (*Escherichia coli*) [18] and 1LR1 - residues 1-57 (*Salmonella typhimurium*) [58]). **b**, Close-up of the monomeric constituents of the H-NS dimer. The positively charged surface (amino acids A80-K96 and T110-T117) [157] of the C-terminal domain is indicated by an asterisk. **c**, SFM image of a DNA loop formed as a consequence of DNA-duplex bridging. Image size: 110 x 340 nm. **d**, Low resolution models for DNA duplex bridging mediated by H-NS. **e-h** - SMC/MukB **e**, High-resolution model of closed dimeric SMC based on the structure of the *Pyrococcus furiosus* SMC interacting isolated head domains (PDB: 1XEX) [103]. **f**, Close-up of the monomeric SMC head domain. **g**, SFM image of *Bacillus subtilis* SMC that forms a rosette-like structure presumably by joining the head domains (courtesy of Peter Graumann) [118]. Image size: 170 x 150 nm. **h**, Low-resolution models for DNA duplex linking due to gathering or trapping by SMC. **i-l** - Lrp **i**, Structure of octameric Lrp from *Pyrococcus furiosus* (PDB: 1I1G) [104]. **j**, Close-up of a monomeric Lrp subunit (within an Lrp octameric context) **k**, EM image of the *Bacillus subtilis* LrpC-DNA complex (courtesy of Eric Le Cam) [12]. Image size: 160 x 120 nm. **l**, Low resolution model for DNA-duplex bridging and wrapping mediated by Lrp.

3.2 DNA-bridging proteins

3.2.1 H-NS

The histone-like nucleoid structuring protein (H-NS) is a 15.4 kDa protein conserved among Gram-negative bacteria. H-NS contains two functionally different domains separated by a flexible linker (see Fig. 3.1a). The C-terminal domain is involved in DNA binding, while the N-terminal domain is required for oligomerization. The active form of H-NS is believed to be dimeric, although larger oligomers have been detected in solution [60, 161]. Dimerization of H-NS monomers requires the first 64 N-terminal amino acids and the formation of larger oligomers involves amino acids 65 to 91. The N-terminal domain consists of one large α-helix (H3 - residues 22-49) and two smaller α-helices (H1 residues 2-7 and H2 - residues 10-16). The H3 helices of two H-NS monomers adopt a negatively charged coiled-coil structure flanked by the H1 and H2 helices, which fold back onto the coiled-coil (see Fig. 3.1b). The precise structure of dimeric H-NS is unknown since the structure of the full-length H-NS protein has not been resolved. The alignment of the H3 helices that form the coiled-coil and thus the orientation of the H-NS oligomerization domain is still unclear, since both parallel and anti-parallel alignments have been suggested (see Fig. 3.1a) [18, 58]. The DNA-binding domain, which lacks a prototypical DNA binding motif, consists of an α-helix and two anti-parallel β-sheets linked by short regions. The regions close to the more N terminal β-sheet (amino acids A80 to K96) and between the second β-sheet and the α-helix (amino acids T110 to A117), are located close together and form a positively charged surface (see Fig. 3.1b, asterisk), which presumably interacts with the major groove [156, 157].

A characteristic feature of dimeric H-NS is the presence of two DNA-binding domains that can potentially interact with two DNA duplexes simultaneously. Indeed scanning force microscopy images of H-NS-DNA complexes show that binding of H-NS results in bridges between adjacent DNA duplexes (Fig 3.1c) [39, 43]. The simplest model to explain these observations is that H-NS dimers are packed side-by-side between two adjacent DNA duplexes. The DNA-binding domains of each dimer extend in opposite directions, which allows simultaneous contacts between both DNA duplexes (i.e. bridging) (Fig. 3.1d). In an alternative model, H-NS dimers bind simultaneously to one and the same tract of DNA. The bridging of tracts coated with H-NS then stems from interactions between the flexible linker regions in H-NS (Fig. 3.1d) [8, 52]. H-NS binds DNA without any obvious sequence specificity but displays preferential binding to DNA that is curved and/or more flexible than random DNA [44, 94]. The duplex tracts around the center of a curved or flexible region are on average spatially close together. This locally increased DNA concentration effect might eplain the preferential binding by an increased probability that DNA-bound H-NS dimers form a bridge between two

such tracts. This then provides a structural basis for the specific repressive role of H-NS [44].

In exponentially growing cells there is approximately 1 H-NS dimer per 1400 bp of DNA [170]. Assuming a binding site of 15 bp, there is sufficient H-NS to cover approximately 1% of the genome (assuming 3 chromosome equivalents during exponential growth). Although this degree of coverage might appear low, bridging distant DNA segments (which are only partially covered by H-NS) is expected to have a large impact on the overall organization and compactness of the nucleoid. *In vivo* evidence for an important architectural role of H-NS stems from studies in which over-expression of H-NS results in highly compacted nucleoids [163].

3.2.2 SMC complexes

Structural maintenance of chromosomes (SMC) complexes are large V-shaped homodimeric molecules [127]. If compared to other NAPs, bacterial SMC proteins have a high molecular weight (∼150-200 kDa) [122]. *E. coli* MukB and the *B. subtilis* SMC-complex (BsSMC) have been extensively studied. The bacterial SMC monomeric structure entails two long stretches of anti-parallel coiled coils joining the N-terminus (containing a Walker A motif) and C-terminus (containing a Walker B motif) of the same protamer (Fig. 3.1e, f) [80]. This results in a globular domain referred to as the "head" containing both motifs to form an ATP binding cassette. The apex region of the anti-parallel coiled coils of two monomers can associate into a hinge domain resulting in a V-shaped dimer. The flexible hinge enables angular orientations between 0 and 180 degrees allowing the heads to come together. The engagement (yielding a ring-like structure) and disengagement of the heads is believed to be dependent on ATP binding and hydrolysis in the heads respectively [81, 71, 71]. The stability of this ring-like structure can be enhanced by protein co-factors [79, 189, 205]. The head domains are also involved in joining dimers, which can give rise to end-joined (sometimes rosette-like (Fig. 3.1g) [118]) multimeric structures [165].

SMC-complexes are believed to act by enclosing multiple DNA duplexes either as a dimer, switching from the open V-shape to a closed conformation, or in rosette-like structures. Ring-closure of both the dimeric SMC-complexes and the rosette-like structures might be stabilized by the binding of co-factors other than ATP (MukE, MukF for MukB and ScpA, ScpB for BsSMC). Direct interaction with DNA is possibly mediated by three consecutive lysine residues located in the hinge-domain [80]. The formation of multimeric structures might be relevant for the organization of chromosomal DNA and is likely to involve 'trapping' and/or gathering of DNA (Fig. 3.1h) [80, 165].

BsSMC and MukBEF are uniformly distributed throughout the nucleoid, although local enrichment has been observed in *B. subtilis* [24, 46]. The activity of BsSMC and MukBEF affects the topological state of the DNA thus indirectly contributing to chro-

matin organization and compaction [105]. Bacterial SMC proteins have also been implicated in the separation of newly replicated chromosomes, attributed to its DNA condensing activity [165, 71].

3.2.3 Lrp

Leucine-responsive regulatory protein (Lrp) is a 15 kDa protein that functionally responds to changes in leucine concentration. Members of the Lrp/AsnC family are present in both Gram-positiveand Gram-negative bacteria. The functional oligomeric state of *E. coli* Lrp is an octamer (Fig. 3.1i) that can self-associate into a hexadecamer. The N-terminus consists of three α-helices that adopt a helix-turn-helix motif (residues 21-45), believed to be responsible for interaction with DNA. The N-terminus is connected via a hinge to the C-terminus, the leucine responsive part of the protein. The C-terminus consists of a four-stranded anti-parallel β-sheet flanked on one face by two α-helices and a short C-terminal β-strand (Fig. 3.1j). An octamer composed of four dimers is formed through equivalent dimer-dimer contacts (mediated by the C-terminus). The result is a 'disk-like' complex with multiple DNA binding sites. The binding of leucine may trigger dissociation of hexadecameric Lrp into two octamers, affecting its DNA binding properties [29, 23].

Although the functional oligomeric state of Lrp is an octamer or hexadecamer, the interaction with DNA is mediated by individual homo-dimers and thus multiple DNA-binding domains are present. The DNA-binding domain recognizes the consensus sequence 'AGAATTTTATTCT' [37], but Lrp is believed to bind cooperatively to DNA with high affinity via multiple suboptimal binding sites. The presence of multiple DNA binding sites in the Lrp structure pointed towards the capability of bridging DNA duplexes. Indeed, DNA-duplex bridging was recently demonstrated for *B. subtilis* LrpC by electron microscopy. A second mode of binding involves the wrapping of a DNA duplex around an Lrp core (Fig. 3.1k, l) [12, 89, 173]. The 'disk-like' structure of Lrp enables it to wrap DNA, which occurs in a right handed superhelix constraining positively supercoils and effectively compacting DNA. Both positive and negative supercoiling increase the affinity of Lrp for DNA, presumably because bridging and wrapping is promoted by the presence of loops [12]. Despite the relatively low amounts of Lrp (~3000 dimers) it probably has a significant impact on overall bacterial chromatin organization, since about 10 % of all genes is affected by Lrp (without the need for a specific binding site).

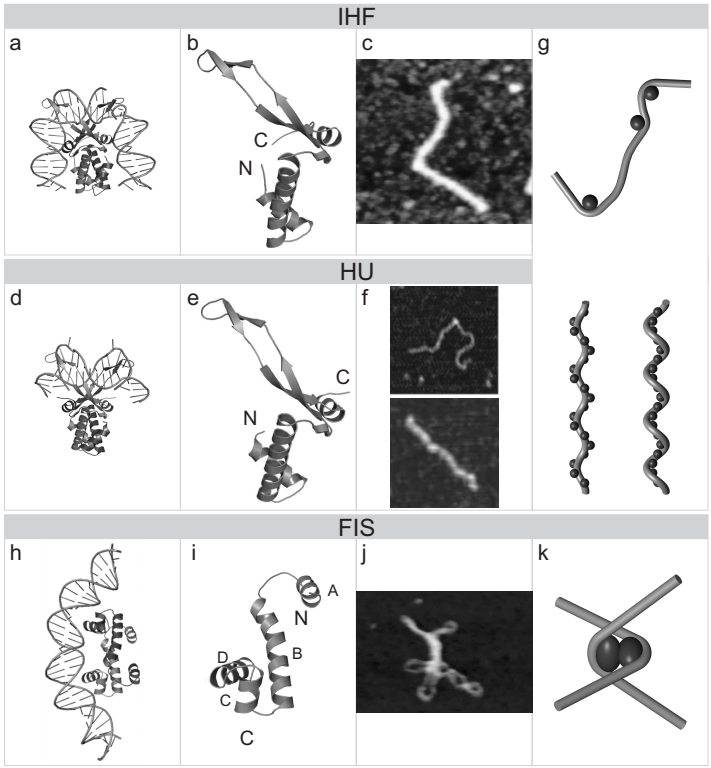

Figure 3.2: Architectural properties of nucleoid-associated proteins: DNA-bending proteins. a-g - IHF/HU **a**, Structure of an IHF-DNA from *Escherichia coli* IHF (PDB: 1IHF) [142]. **b**, Close-up of a monomeric IHF subunit. **c**, SFM image of an IHF-DNA complex. **d**, Structure of an HU-DNA complex from *Escherichia coli* HU (PDB: 1P51) [168]. It should be noted that the DNA substrate used for the HU-DNA co-crystals was pre-distorted and that the observed bend does not necessarily reflect the extent of bending induced in native DNA. **e**, Close-up of a monomeric HU subunit. **f**, SFM images of HU-DNA complexes. HU, from *Escherichia coli*, bends (top) DNA at low concentrations and induces the formation of rigid filaments (bottom) at high HU concentrations [184]. Image size: 200 x 200 nm (top) / 70 x 70 nm (bottom) **g**, Low resolution model for DNA compaction by the binding of multiple HU/IHF molecules and for the formation of HU-DNA filaments. A filamentous structure of this kind has also been proposed to occur at high IHF/DNA ratio [38]. **h-k** - Fis **h**, High resolution model of a Fis-DNA complex from *Escherichia coli* [133] (courtesy of Reid Johnson). **i**, Close-up of a monomeric Fis subunit. **j**, SFM image of Fis-DNA complexes with Fis from *Escherichia coli* bound at the nodes of supercoiled pUC18 plasmids (courtesy of Georgi Muskhelishvili) [150]. Image size: 700 x 500 nm. **k**, Low resolution model for node formation due to Fis-Fis interactions.

3.3 DNA-bending proteins

3.3.1 IHF

Integration host factor (IHF) is composed of two subunits that share about 25% homology. The α-subunit is approximately 11 kDa and the β-subunit about 9.5 kDa in size. The structure of the hetero-dimeric protein has been resolved and can be described as a body with protruding flexible arms [142]. The compact body of IHF is made of intertwined α-helices from both IHF subunits. This compact body is capped by β-sheets that extend into two flexible β-ribbon arms and can be inserted into the minor groove of DNA (Fig. 3.2a, b) [142, 169].

A typical specific IHF-binding site on DNA is approximately 30 bp. The 3' region is conserved (matching the consensus (A/T)ATCAANNNNTT(A/G))(where N = any nucleotide)), whereas the 5' region is not conserved, although commonly A/T rich [66]. At the tip of each β-ribbon arm that is inserted into the minor groove upon binding is a highly conserved proline. This residue intercalates between adjacent base pairs and induces or stabilizes DNA bending. The insertion of the two proline residues (one from each β-ribbon arm) results in extensive hydrophobic interactions with the DNA bases, which leads to an unusual narrow minor groove. This in turn leads to two sharp kinks at the sites were the β-arms are inserted (9 bp apart), which results in sharp bending (up to 180°) (Fig. 3.2a, c) [41, 49, 107, 142]. The DNA bend is stabilized by interactions between the negatively charged DNA sugar-phosphate backbone and positively charged residues along the body of IHF [169]. IHF is an abundant protein with a limited number of high affinity sites (∼1000 binding sites) on the *E. coli* genome. Single-molecule micromanipulation experiments revealed that binding of IHF to DNA can result in up to 30% length reduction (attributed to bending - Fig. 3.2g) [1]. Since this effect can be reversed by adding competitor DNA, compaction must primarily be the result of non-specific DNA binding. As a vast majority of IHF *in vivo* is bound to DNA [56, 206], non-specific binding is frequent and probably important. Expression of IHF is maximal during stationary growth (1 IHF/335 bp) of DNA [170], which is sufficient to cover around 9% of the bacterial chromosome. The observation that non-specific binding and bending leads to effective compaction *in vitro* suggests that IHF contributes significantly to the compact form of the nucleoid *in vivo*, in particular during early stationary growth before Dps (see below) predominates.

3.3.2 HU

The histone-like protein from *E. coli* strain U93 (HU) [53] is closely related to IHF. Most bacteria have a homodimeric HU that either consists of two HUα or two HUβ subunits. Enteric bacteria have a heterodimeric HU(αβ) that consists of two 9.5 kDa subunits that share 70% homology. HU and IHF have a similar structure consisting

of a globular body from which two β-ribbon arms protrude (Fig. 3.2d, e) and share about 30-40% homology [168].

HU binds non-specifically to DNA, but has a higher affinity for supercoiled DNA and distorted DNA structures. Like IHF, HU employs the intercalation of two conserved proline residues that are inserted into the minor groove 9 bp apart and induce or stabilize DNA bending (Fig. 3.2d). The two kinks induced by HU are not co-planar, which results in underwinding of the DNA double helix (i.e. negative supercoiling close to 3° per bp DNA) [168]. HU can stabilize or constrain negative supercoiling, which reduces writhe and thus prevents the formation of plectonemes. The HU-induced bend is not rigid as IHF-induced bends but better considered as a flexible hinge and it seems that HU can induce and stabilize a range of different bend angles similar to high mobility group (HMG) proteins in eukaryotes [134, 168, 169]. Random, non-specific binding of HU results in many flexible bends [146]. (with bend angles up to about 180°) along the DNA and a reduction in length of up to 50% (Fig. 3.2f, g) [184]. Besides bending, HU can (at higher concentrations *in vitro*) form rigid superhelical filaments in which HU and DNA spiral around each other (Fig. 3.2f, g) [184]. This 'rigidification' mode involves close side-by-side binding of HU dimers which could be cooperative due to protein-protein interactions [38]. The minimal HU binding site is smaller compared to that of IHF (~30 bp at a specific site) and is about 9 bp. HU is believed to primarily promote DNA compaction by bending. HU has also been suggested to induce negative supercoiling [145, 171] either directly due to non-co-planar DNA bending, or indirectly by stimulation of DNA gyrase [169]. These two mechanisms are likely to contribute to the compaction of the nucleoid especially during exponential growth when HU expression reaches its optimum (1 HU/550 bp) [170]. Rigidification of DNA by HU - if relevant *in vivo* - would counteract compaction [45, 184]. However, this type of binding is likely to occur only locally and would therefore have limited impact on overall compaction [38].

3.3.3 Fis

The factor for inversion stimulation (Fis) is a 22 kDa homodimeric protein [92]. Fis has an ellipsoidal structure and each monomer is made of 4 α-helices (A,B,C and D) connected by β-turns and 2 β-hairpins. The hydrophobic core of the Fis dimer is formed by the A, A' and B, B' helices of two Fis monomers. The helices C and D adopt a helix-turn-helix motif which is involved in DNA binding (Fig. 3.2h, i) [133, 93].

Although Fis is often described as a sequence-specific DNA binding protein (binding to the degenerate 15 bp consensus sequence (G/T)NN(C/T)(A/G)NN(A/T)NN-(C/T)(A/G)NN(C/A) (where N is any nucleotide) [133], it binds non-specifically to DNA with relatively high affinity. A Fis-DNA co-crystal structure is not available. However, insertion of both recognition helices (CD and C'D') would require bending of the DNA

close to 50°, since the two CD helices are spaced 2.5 nm apart, while two adjacent major grooves of the DNA are 3.4 nm apart. Additional curvature of the DNA is generated by interactions between the DNA flanking the Fis binding site and the sides of the Fis dimer. Altogether, Fis binding results in DNA bending between 50° and 90° (Fig. 3.2h) [133]. Strong binding sites are located upstream of many stable RNA operons on which Fis acts as transcriptional activator. The Fis binding sites at these locations are often helically phased. If multiple Fis molecules bind and bend the DNA in the same plane, this yields a small co-planar loop in which the DNA can be bent up to 160° [178]. Fis is the most abundant NAP in early exponentially growing cells (1 Fis/450 bp) [170]. The expression of Fis strongly decreases after early exponential phase and Fis is completely absent during stationary growth. There are approximately 6000 sites in the genome that match the consensus sequence, which leaves the majority of Fis (during early exponential growth) to bind non-specifically to DNA. Fis seems to be a sensor for DNA supercoiling, since it inhibits the expression of DNA gyrase in a DNA topology dependent manner [151]. An increase in negative supercoiling leads to larger amounts of Fis, which, in turn, down-regulates the expression of DNA gyrase. Analysis of Fis-DNA complexes by scanning force microscopy revealed binding of Fis to sites where two DNA segments cross (branch points) (Fig. 3.2j). Higher Fis concentrations resulted in complete coating of DNA and significant DNA compaction [150]. Similarly, DNA micromanipulation experiments showed that Fis binding results in severe DNA compaction. At low Fis concentrations this appears due to non-specific binding and bending of DNA. At higher concentrations, Fis binding results in the formation and stabilization of DNA loops [158], presumably due to interactions between DNA-bound Fis dimers (giving rise to branch points, similar to those observed by SFM) (Fig. 3.2j, k). It is thus likely that Fis significantly contributes to nucleoid compaction (in particular in early exponential phase) both by non-specific binding and bending of DNA and by forming and stabilizing DNA loops.

3.4 Alternative mechanisms of organization and compaction

3.4.1 Dps

The DNA protection during starvation protein (Dps) becomes abundant upon entering the stationary phase. The 19 kDa protein is considered a member of the ferritin/bacterioferritin superfamily, based on structural homology [136]. For instance, the Dps monomer has a four helix bundle core (Fig. 3.3a, b) resembling the monomer core of bacterioferritin. Like (bacterio) ferritin, Dps forms oligomers (dodecamers) resulting in a large (90 Å) hollow ball (Fig. 3.3a) with a negatively charged inner

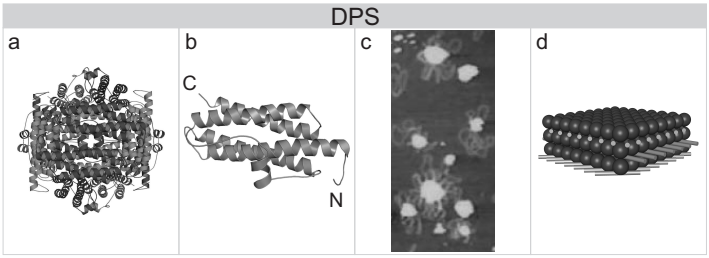

Figure 3.3: Architectural properties of nucleoid-associated proteins: alternative mechanisms of organization and compaction. Dps **a**, Structure of dodecameric Escherichia coli Dps (PDB: 1DPS) [70]. **b**, Close-up of a monomeric Dps subunit (within a Dps dodecameric context) **c**, SFM image of Dps-DNA complexes [31]. Image size: 600 x 1300 nm. **d**, Low resolution model of three-dimensional hexagonal Dps-DNA arrays.

surface. The outer surface (which is also negatively charged) exposes no prototypical DNA-binding domain [70].

Dps binds to DNA without any sequence specificity. The exact way in which this occurs remains to be elucidated. From electron microscopy it is clear that the Dps-DNA complex *in vitro* forms hexagonally packed 2-dimensional arrays [62]. Since the surface of the dodecamer -the functional unit- is negatively charged it is not likely to interact with DNA. A non-typical binding mode has been proposed that implicates the pores present in the hexagonal arrays formed by the dodecamers and DNA. These pores contain three neighboring disordered N-termini from different dodecamers, each containing three lysine residues providing a positively charged patch that allows for interaction with DNA [70]. DNA binding has been proposed to promote dodecamer-dodecamer interactions (possibly reflected in SFM images of Dps-DNA complexes (Fig. 3.3c) [31]), which results in the formation of sheets of dodecamers with the DNA as a structural framework. In such a complex the pores would be aligned to accommodate the next layer of DNA resulting in sheets of Dps with DNA threaded through the pores. Such hexagonally packed 3-dimensional arrays (Fig. 3.3d) would yield significant compaction of DNA. *In vivo*, the effects of Dps on chromatin structure are very obvious; in 24h starved bacteria, a toroidal Dps-DNA structure is observed whereas after 48h tightly packed Dps-DNA co-crystals become prominent [62]. By co-crystallizing with DNA, it protects DNA from oxidative cleavage or redox-stress, thermal shock and UV-light [125].

3.5 Discussion

3.5.1 Global compaction

The degree to which NAPs contribute to global nucleoid compaction is still unclear. Certainly none of these proteins is solely responsible for DNA compaction, in contrast to eukaryotes where protein-mediated compaction is attributed exclusively to histones. *In vitro* all NAPs clearly have the ability to compact DNA, whereas *in vivo* the contribution of most proteins individually appears modest. Bacterial cells deficient in one of the NAPs usually have subtle phenotypes, which indicates that (some of) the roles of one NAP can be fulfilled by another. For example, HU and IHF single mutants are viable while HU/IHF double mutants have compromised growth and survival [95]. Bacterial cells without functional HU have a severe phenotype including larger decondensed nucleoids. This phenotype is even more severe in HU/Fis double mutants [135]. Similarly, MukB mutants have more decondensed nucleoids and HU/MukB double mutants are lethal [71]. This suggests that indeed all four proteins play a role in DNA compaction. Expression of an eukaryotic HMG protein in HU/Fis deficient cells, largely complements the phenotype of these cells [135], underlining that the contribution of these proteins to nucleoid compaction is due to non-specific binding and bending of DNA. Over-expression of H-NS and Dps results in significant compaction of the nucleoid [125, 163], demonstrating that these proteins significantly contribute to nucleoid compactness *in vivo*. Expression of a mutant HU (selected by its ability to stabilize a DNA loop more effectively than wtHU) results in severe nucleoid compaction and altered morphology of bacterial cells [96]. The global transcription profile is also dramatically altered in this mutant, which illustrates the link between global nucleoid structure and local transcriptional activity. Interestingly, expression of mutant HU induces activation of a subset of genes that is normally silenced by H-NS [96]. This illustrates the ability of HU to effectively antagonize H-NS [45].

3.5.2 Local organization and compaction

Although it is not clear to what degree NAPs contribute to the overall degree of compaction, this group of architectural proteins certainly has important local effects on nucleoid structure. The nucleoid is organized in topologically independent loops [77], which are in the order of 10 kb in size [138]. The loop structure of the nucleoid is, in part, dictated by the binding of proteins that cross-link the DNA. NAPs that bridge DNA, such as H-NS [74], Lrp and SMC proteins are thus likely to play a role in loop formation. Proteins such as SMC might be involved in directly setting domain boundaries. DNA-bridging proteins, such as H-NS, might then primarily stabilize DNA loops by forming patches of bridged DNA segments along the DNA loop (Fig. 3.4a) [38].

DNA-bending proteins do not only contribute directly to overall compactness, but

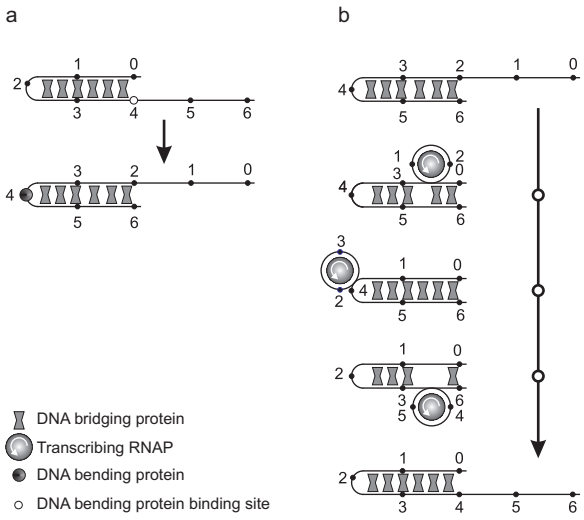

Figure 3.4: Hypothetical mechanisms of DNA loop remodeling by DNA bending nucleoid-associated proteins (a) or transcriptional activity (b). a, Binding of a DNA bending protein at position 4 results in translocation of this position to the apex of the loop. **b**, Transcription involves wrapping of DNA around RNA polymerase. The amount of DNA wrapped around RNA polymerase is translocated through the loop. Numbers 1-6 are used to indicate the rearrangements occurring within the loops. It should be noted that, in addition, transcription is known to affect DNA topology [203].

are in addition potential 'bacterial chromatin remodellers'. Bends tend to localize at the apex of supercoiled loops (Fig. 3.4a, and see Dame 2005 [38] for a more detailed discussion) and by dictating the location of the apex, DNA-bending proteins could affect the arrangement of the nucleoid in loops and thereby modulate the global transcription profile. We expect the specific binding of NAPs to regulatory sequences (e.g. IHF and Fis) to have a more profound effect on local structuring of DNA loops compared to non-specific binding to DNA (e.g. HU, but also IHF and Fis binding to non-specific sites). Besides roles for architectural proteins in modulating the organization of loops, transcriptional activity within a loop would also be expected to affect its organization. During transcription, close to 70 bp of DNA is completely wrapped around the surface of RNA polymerase (RNAP) [144]. For instance, in a loop stabilized by H-NS, elongation by RNAP transiently disrupts H-NS-bridged regions. As RNAP continues to elongate and wrap DNA around itself, there is significant remodeling of the DNA loop. The newly formed loop structures are likely to be stabilized by H-NS-induced bridges after RNAP has passed. This would result in a shift in the relative orientation of the loop by at least 70 bp and up to twice this distance if RNAP elongates through the entire loop (Fig. 3.4b). Eventually, the configuration of a loop will be determined by a combination of factors, i.e. the occurrence of transcription, the number and orientation of genes within the loop [48] and the binding of DNA bending proteins. Therefore, we expect the local effect of transcription to have limited impact on global nucleoid organization.

3.5.3 Growth phase dependent expression

Above we described how DNA-bending proteins (IHF, HU, Fis) may locally antagonize the effects of DNA-bridging proteins (such as H-NS or Lrp). It is interesting to note that during each different growth phase at least one of the DNA-bending proteins is maximally expressed (Fig. 3.5). Fis expression is optimal during early exponential phase (1 Fis/460 bp) [170], after which HU is maximally expressed during exponential phase (1 HU/550 bp) [170]. In early stationary phase, IHF reaches its optimal expression (1 IHF/335 bp) [170]. Thus, at any given time there is a DNA bending protein (antagonizing the action of DNA bridging proteins) to modulate the loop structure of the nucleoid. This could be an effective way to ensure an 'open', transcriptionally active nucleoid structure during phases of relatively fast growth. Dps becomes the most abundant protein in (late) stationary cells (1 Dps dodecamer/300 bp) [170]. This protein forms crystal-like structures with DNA and, as a result, transforms the dynamic nucleoid into a static - transcriptionally inactive - structure that is effectively protected against damage.

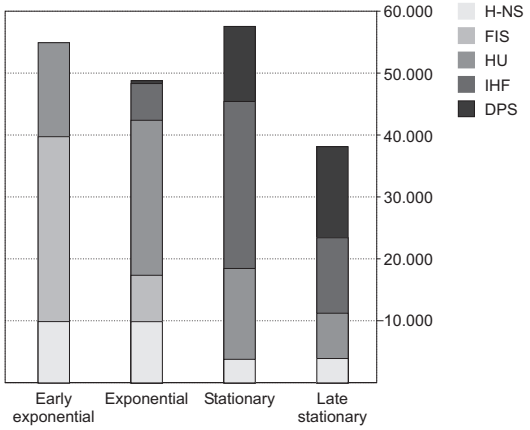

Figure 3.5: Normalized amounts (expressed in functional units) of nucleoid-associated proteins during different growth phases. H-NS, HU, IHF and Fis are dimers. Dps is a dodecamer. Based on data taken from Talukder *et al.* [170]. The calculations in the text (functional binding form i.e. dimer or dodecamer per bp DNA) are based on three, two and one chromosome equivalent in (early) exponential, stationary and late stationary respectively. The given values are approximate because of the assumptions used in the calculations.

3.6 Concluding remarks

Organization and compaction of DNA serves several goals. On one hand reducing the effective volume of the bacterial chromosome is required to fit it in a cell. On the other hand it provides a framework for the global regulation of transcription. It is becoming increasingly clear that the dynamic reprogramming of global transcription profiles in response to environmental stimuli is in large part mediated by the action of NAPs. The first mechanistic clues from studies on selected genes point at these proteins either acting alone, joining forces (and forming repressive multi-protein assemblies) or counteracting each other. An important challenge is to define in molecular detail how this occurs locally, and to expand regulatory studies to the bacterial chromosome as a whole. Integration of knowledge from micro-array studies on different NAP mutants and overexpressing strains will reveal regulatory connections at the global scale *in vivo*. The regulatory impact of individual NAPs could be linked to global structural rearrangements (e.g. changes in nucleoid volume) observed using microscopy techniques. Finally, regulatory effects of NAPs may be correlated with large-scale effects of these proteins in biochemical or biophysical assays, bridging the gap between *in vivo* and *in vitro* data. Joining forces between disciplines, we will gain comprehensive insight into the role of NAPs as essential structural and regulatory components of the nucleoid.

3.7 Acknowledgements

Current research of the authors is supported through various grants from the Netherlands Organization for Scientific Research. We apologize to those colleagues whose interesting work we have not been able to cite due to size restrictions. We thank Reid Johnson for providing the molecular Fis-DNA model, and Eric Le Cam, Peter Graumann, Georgi Muskhelishvili and Claudio Rivetti for EM/SFM images of proteins and protein - DNA complexes. We thank Roel van Driel and Tanneke den Blaauwen for critical reading of the manuscript.

Chapter 4

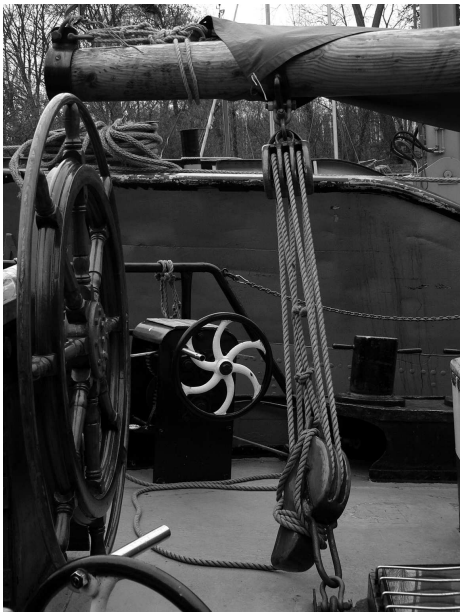

A line often forms the connection between two parts of a ship. In order to allow this connection to very dynamic, a system of pulleys can be used. This makes changing the distance between two parts very easy and divides the strain over the number of loops in the system of pulleys.

Bacterial chromatin organization by H-NS protein unraveled

A dual DNA manipulation experiment

Abstract – DNA-bridging proteins with regulatory and/or architectural function are common and found both among prokaryotic and eukaryotic organisms. The molecular and mechanical details of such proteins are hard to obtain, in particular if they involve non-specific interactions. The bacterial nucleoid consists of hundreds of DNA loops, shaped in part by non-specific DNA-bridging proteins such as H-NS, Lrp and SMC. We have developed an optical tweezers instrument capable of independently handling two DNA molecules, which allows the systematic investigation of protein-mediated DNA-DNA interactions. Here we employ this setup to investigate the abundant non-specific nucleoid-associated protein H-NS, and show that H-NS is dynamically organized between two DNA molecules in register with their helical pitch. Dynamic force spectroscopy on non-specific DNA binding proteins is also accessible with this instrument and allows us to determine an energy landscape for the H-NS-DNA interaction. Our results on H-NS explain how the bacterial nucleoid can be effectively compacted and organized, yet be dynamic in nature and amiable to DNA-tracking motor enzymes. Finally, our experimental approach is widely applicable to other DNA-bridging proteins, as well as to complex DNA transactions involving multiple DNA molecules.

4.1 Introduction

The chromosomal DNA of bacteria is not confined to an envelope-enclosed organelle such as the nucleus in eukaryotes. Instead, it is folded into a compact nucleoid body attributed in part to interactions with abundant nucleoid-associated proteins (NAPs) [38, 93]. The binding of NAPs to DNA is apparently compatible with DNA-tracking motor proteins such as RNA polymerase (RNAP). Moreover, the nucleoid body has to be constantly remodeled in response to environmental signals. How effective compaction by NAPs is compatible with these constraints is not well understood. H-NS is believed to play an essential role in the organization and compaction of bacterial chromatin [38, 52, 143] and acts by DNA-duplex bridging [39, 43]. Large regions of DNA can be bridged by adjacent H-NS dimers/multimers in a presumably cooperative manner [38, 39, 43, 58]. Due to its chromosome-wide structural impact it also acts as a global regulator of gene expression, essential for environmental adaptation and bacterial virulence [52, 143]. Limited knowledge is available regarding structural and kinetic aspects of these important H-NS-DNA interactions.

4.2 Results

Details of protein-mediated DNA-duplex bridging in general (but in particular by non-specific proteins) are hard to obtain with current bulk techniques. Also, using a sin-

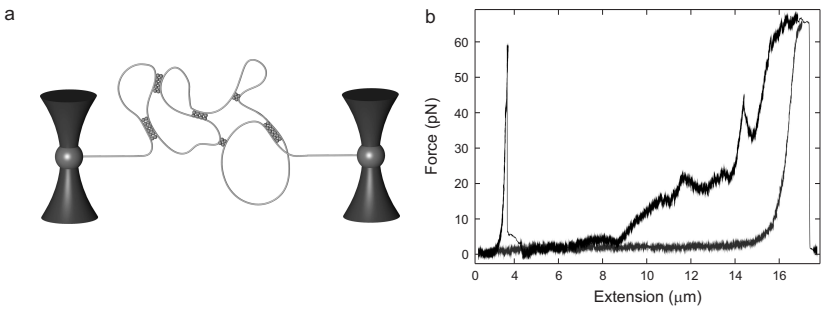

Figure 4.1: Single DNA molecule experiment: configuration and typical experimental data.a, One λ-DNA molecule is suspended between two polystyrene beads held with optical tweezers. **b**, The DNA is incubated with H-NS at low end-to-end distance (4 μm). This results in the formation of complex intra-molecular bridges in the DNA molecule (loop formation). If the beads are moved apart (at a rate of 22 nm s^{-1}) these loops are disrupted as evidenced by an increase in force followed by sudden large drops in force in the force-extension curve (black trace). The direction of the applied force (shearing or unzipping) is not known in these experiments. For comparison, a force-extension curve is shown for a bare λ-DNA molecule (gray)

gle DNA molecule to probe such DNA binding proteins [27, 3, 42] can be problematic, since the molecular details of DNA bridging are obscured by the large scale effects of multiple site DNA binding (compaction) (Fig. 4.1). We have designed and built an optical tweezers instrument with which we can simultaneously trap four micron-sized polystyrene beads (Methods) that are attached to the ends of two single DNA molecules (Fig. 4.2). Using two DNA molecules in an extended configuration allows us to address fundamental properties of DNA bridging proteins and their interaction with DNA. Finally, it opens up the possibility of high-throughput dynamic force spectroscopy on non-specific DNA binding proteins since in one experiment hundreds of unbinding events can be recorded, yielding an energy landscape for their interaction with DNA.

Figure 4.2: Dual DNA manipulation assay. λ-DNA molecules linked by H-NS suspended between polystyrene beads held with optical tweezers

With this instrument we have investigated the stability of the bridges in a DNA-H-NS-DNA assembly (H-NS-DNA_2) by exerting force through the duplexes. By building up a shearing force (Fig. 4.3, inset) we demonstrate that an H-NS-DNA_2 complex is formed by di/multimeric H-NS binding. When the beads are moved apart at a constant speed of $22\,\mathrm{nm\,s^{-1}}$, the force rises up to several tens of pN and then drops to zero after complete separation of the bridged region (Fig. 4.3). If the bead movement is stopped after reaching a pre-set force, the force gradually decreases, presumably due to the disruption of bridges at the extremities of the bridged regions (Fig. 4.3a). If we allow H-NS to coat a major part of both DNA duplexes *before* establishing a crossed configuration H-NS mediated DNA-DNA interactions are not observed (Fig. 4.3a). This observation indicates that protein-protein interactions are not responsible for bridge formation, but that instead each H-NS di/multimer interacts with two duplexes simultaneously. The application of an unzipping force (Fig. 4.3b, inset) gives rise to a rugged force landscape (Fig. 4.3b). The sign of the slope in such graphs is defined by the relative rates of bead movement and H-NS unbinding and as such reflects the local density of H-NS bridges. Depending on the bead's speed, a different force regime is associated with disruption: up to ∼1 pN at $6.5\,\mathrm{nm\,s^{-1}}$ (not shown), up to ∼7 pN at $22\,\mathrm{nm\,s^{-1}}$ and up to ∼25 pN at $88\,\mathrm{nm\,s^{-1}}$.

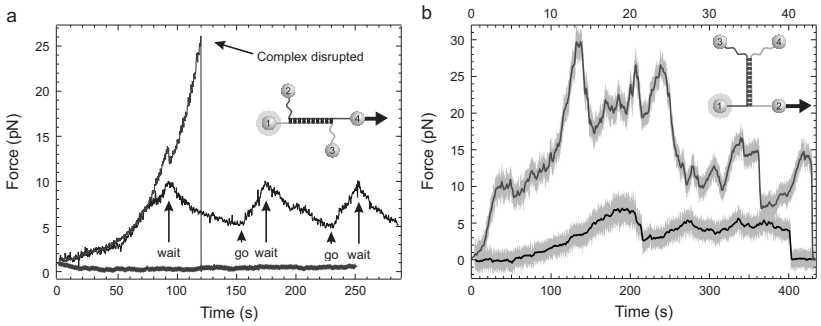

Figure 4.3: Dual DNA manipulation assay a, Shearing experiment. Beads are moved apart (at 22 nm s^{-1}) until the complex has been disrupted (top trace) or bead movement is stopped at 10 pN and the complex is allowed to disassemble (middle trace). DNA duplexes pre-coated with H-NS do not interact (bottom trace). Data displayed at 1 kHz. **b**, Unzipping experiment. Beads are moved apart until the DNA duplexes are separated (at 22 nm s^{-1} (bottom) and 88 nm s^{-1} (top)). Data displayed at 2 kHz (grey) and 4 Hz (dark). Insets: schematic representations of the experiments.

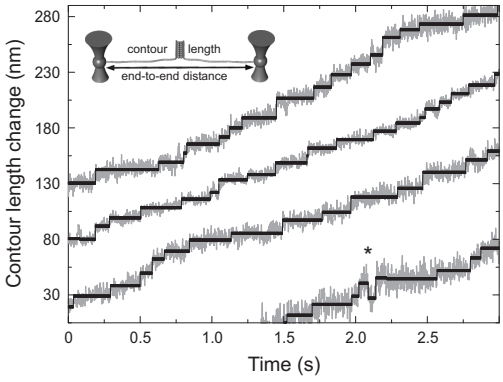

Figure 4.4: Dual DNA unzipping: steps. One-sided contour length change as a function of time in unzipping experiments. Data displayed at 1 kHz (grey) including staircase fits (black) [98].

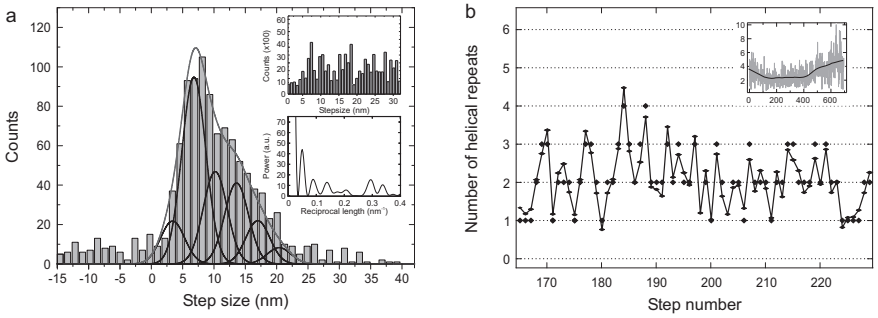

Figure 4.5: Characteristics of H-NS bridges. a, Histogram of all step sizes (N = 904). A multiple-Gaussian fit (grey) with the individual Gaussians (black). Inset, top: pdf of all the fitted steps for forces >10 pN (N = 458). Inset, bottom: Fourier transform of the pdf. **b**, Detailed view of the irregular spacing between adjacent H-NS bridges. Light squares correspond to a step sequence whose sequential order is plotted on the x-axis and the size of the step expressed in multiples of the DNA helical repeat on the y-axis. Dark squares, data rounded off to closest integer. Inset: Global view of spacing between H-NS bridges in a bridged region. Measured steps (grey) and smoothed (locally-weighted-regression) data (black).

In order to quantitatively analyze the unzipping of bridged areas, we converted our data to display contour length (see Materials and Methods). The steps observed in Figure 4.4 probably reflect the disruption of individual H-NS mediated bridges (note that occasionally rebinding occurs - indicated by an asterisk). We determined the size of these steps using a step-fitting algorithm [98]. When the sizes of the steps are plotted in a histogram (Fig. 4.5a) we observe a distribution which can be fit well to multiple Gaussians with identical spacing, yielding a repeating unit of 3.6 ± 0.4 nm. It has not escaped our notice that this spacing equals the length of a helical repeat ($\sim$3.5 nm for B-DNA). The Fourier transform of the combined pairwise distribution function (pdf) of our fits shows distinct peaks (0.09, 0.14 and 0.29 nm^{-1}, corresponding to three, two and one helical turn(s) respectively), further strengthening our observation that H-NS binding occurs with variable spacing in register with the DNA helical repeat (Fig. 4.5a, insets; Fig. 4.8; alternative analysis methods in Fig. 4.9 and 4.10). These analyses demonstrate that adjacent building blocks are positioned on opposite faces of two bridged DNA helices, as might be expected from DNA bridging models [43, 58]. Looking at the individual steps in a bridged region, we note that the density of H-NS binding is highly variable (Fig. 4.5b) which suggests that the H-NS units do not interact for cooperativity [58]. Rather, apparent cooperative behavior arises as an intrinsic property of DNA-bridging proteins due to duplex proximity [43].

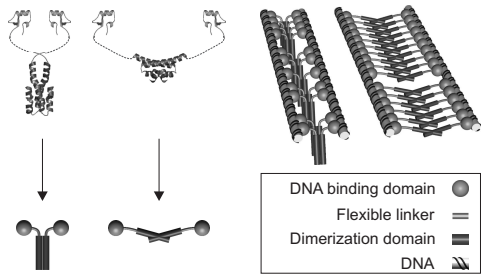

Figure 4.6: Structural models of H-NS and H-NS-DNA$_2$ complexes. Left, the hypothetical dimer structures of full-length H-NS, as derived from the individually resolved structures of the dimerization [58, 18] and DNA-binding domains [156]. These domains are connected through an unstructured flexible linker. Right, models for H-NS-DNA interaction. H-NS interacts with two DNA duplexes as a dimer in either a parallel [58] or anti-parallel [18] configuration.

What are the structural implications of our observations for the layout of H-NS-bridged regions? Only structures of the isolated C-terminal DNA-binding domain ($\varnothing$ ~3 nm) [156] and the N-terminal dimerization domain are available [143]. Interestingly, two alternative structures, which differ in the relative orientation of the dimerization interfaces (parallel [58] or anti-parallel [18]) have been proposed (Fig. 4.6). A fraction of ~10% of the steps can be assigned to a H-NS spacing of a single helical repeat (Fig. 4.5a). In combination with the absence of a regular (two step) unbinding pattern, we can effectively rule out the tetrameric (or larger multimeric) assemblies of H-NS observed in solution [32, 161] as the building blocks of H-NS bridged regions. Therefore, in our model each building block is a dimer that effectively extends over approximately one helical turn on the DNA (Fig. 4.6). Since sterical hindrance by swiveling of the ~6 nm 'tail' (the dimerization domain) [58] of the parallel H-NS dimer could yield the observed variations in the effective dimensions along the helix axis, it seems likely that the parallel H-NS structure prevails under our experimental conditions.

Little is known about the kinetics of the H-NS-DNA interaction. Usually, with dynamic force spectroscopy (DFS) [59] interactions between bodies are explored by determining the rupture force/loading rate dependence at pre-set loading rates. In our approach each individual experimental unzipping trace contains loading rate and unbinding force information for numerous individual rupture events in series, immediately yielding a dynamic force spectrum for the H-NS-DNA interaction (Fig. 4.7a). The resulting spectrum is characterized by two linear regions with different slopes reflecting the presence of two well-defined kinetic barriers in the energy landscape [59]. These two barriers are located at distances 1.2 ± 0.2 Å ($x_{\beta 1}$) (N = 34) and 5 ± 2 Å ($x_{\beta 2}$) (N = 479) from the ground state along the direction of the applied force (see Ma-

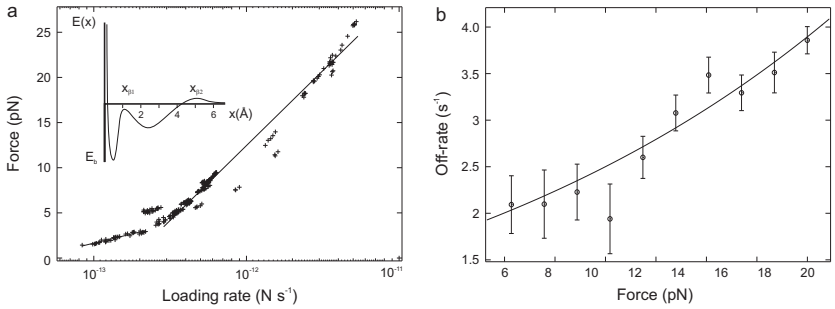

Figure 4.7: Kinetics of the H-NS-DNA interaction. **a**, Dynamic force spectrum of the H-NS-DNA interaction. The two distinct regions in the spectrum have been fitted to a straight line. Inset: Conceptual energy landscape for the H-NS-DNA interaction. **b**, The thermal off-rate of H-NS as a function of force with an Arrhenius fit (N = 904; error bars s.e.m.).

terials and Methods) probably reflects the docking of the DNA-binding domain to the DNA (presumably involving hydrogen bonds and Van der Waals interactions), whereas could correspond to a 'binding mode' that allows lateral diffusion [30]. When a diffusing H-NS dimer encounters a pre-existing bridge it becomes spatially restrained and will have ample time to cross the inner barrier. This would also make its binding to the second DNA duplex more probable and account for cooperativity. Therefore, an energy landscape with two well-defined barriers seems ideally suited to a protein that needs to bind to two DNA duplexes for functionality.

The thermal off-rate of H-NS shows an exponential increase as a function of the applied force (Fig. 4.7b). Assuming an Arrhenius relation ($k_{\mathrm{off}}(F) = k_{\mathrm{off}}(0) \cdot e^{\frac{aF}{k_B T}}$; where k_B is the Boltzman constant, T is the temperature) yields a barrier distance, $a = 2.0 \pm 0.3$ Å, which is likely the same as barrier $x_{\beta 1}$ determined using DFS. The small shift in distance is probably a reflection of the underlying assumption that the barrier doesn't shift due to the application of force [59]. The high off-rate at zero external force ($k_{\mathrm{off}} = 1.5 \pm 0.2 s^{-1}$) suggests that there is substantial breathing of bridged regions, potentiating effective competition for DNA binding by other proteins *in vivo*. Assuming diffusion-controlled association with a typical rate constant of $k_{\mathrm{on}} = 1.0 \cdot 10^5\ \mathrm{M}^{-1}\ \mathrm{s}^{-1}$ [54] for non-specific DNA-binding proteins yields an equilibrium constant of $K_D = k_{\mathrm{off}}/k_{\mathrm{on}} = 1.5 \cdot 10^{-5}\, M$, in good agreement with the K_D expected for sequence-unspecific binding [91]. Using $\Delta G° = RT \ln K_D$ we estimate the Gibbs' free energy difference of complex formation for H-NS binding to -27 kJ mol^{-1}, in line with bulk isothermal calorimetry estimates [131]. Our data thus yield a conceptual energy landscape as shown in Figure 4.7a (inset).

4.3 Discussion

How do our structural and kinetic findings relate to an *in vivo* situation? H-NS evidently has the ability to bridge DNA duplexes and is abundant, which provides support for the idea that this protein *in vivo* could act as a topological insulator on DNA loops [38, 74, 48]. H-NS binding nucleates in A/T rich areas [52, 143], which then probably recruit other areas without H-NS for binding in trans. This process is likely to be facilitated by plectonemic DNA supercoiling [38]. In a number of particular cases H-NS has been shown to play a functional regulatory role by acting as a roadblock, i.e. at the stage of promoter clearance *in vitro* [45, 153, 155] and during active elongation *in vivo* [51]. How then can we explain that in general transcription *in vivo* seems not strongly affected by supposedly ubiquitous H-NS roadblocks? RNAP can exert forces up to 25 pN [191]. Our data show that the maximum force for complex disruption is $\sim$7 pN at an unzipping rate of 70 bp s^{-1}, indicating that at this rate the barrier can easily be overcome. The combination of cooperative binding and a high off-rate allows H-NS to effectively stabilize DNA loops without compromising their susceptibility to dynamic reorganization (by transcription or by other NAPs [38, 110]). This is key to *E. coli* and other organisms in which restructuring the spatial organization of the genome is used for reprogramming of the global gene expression profile. Finally, these experiments demonstrate the potential of this dual DNA assay to study DNA bridging proteins and the ability to extract information neither accessible through bulk biochemistry nor with a single DNA approach. It also opens up a new range of *single-molecule* experiments including complex dynamic transactions between multiple DNA molecules.

4.4 Methods

An optical-tweezers instrument was designed and constructed with which four micron-sized beads attached to the ends of two DNA molecules can be simultaneously trapped (Quadruple or Q-trap). Optical traps are generated using a 1064 nm laser, which is first split on polarization. Subsequently one of the paths is led through an acousto-optic deflector to generate three time-shared traps at different locations. Experiments were performed in a flow cell with four channels. The use of laminar flow ensures that the channels do not mix [181]. By moving the sample perpendicular to the channels we can efficiently catch, manipulate and incubate two single DNA molecules. Streptavidin-coated polystyrene beads are captured in the optical traps and subsequently incubated in the channel with biotinylated DNA solution. After DNAmolecules have been captured between each set of beads they are tested for integrity and singularity in the buffer channel. The molecules are placed in the configuration required for the experiment and moved into the channel with H-NS solution. The position of the bead in the fixed trap is detected via back-focal-plane interferom-

etry using a quadrant photodiode. End-to-end distance is obtained by determination of the distance between the stationary and the moving bead from video microscopy. A detailed description of experimental conditions, data analysis and dynamic force spectroscopy is provided in the Appendix and Materials and methods section.

4.5 Acknowledgements

This research was supported by the Netherlands Organization for Scientific Research (NWO) through an NWO-Vernieuwingsimpuls grant (to GJLW), a FOM-projectruimte grant (to GJLW), an NWO-VENI grant (to RTD) and a grant from ALW-NWO (to GJLW). The authors thank Bram van den Broek, Nora Goosen, Joost van Mameren, Erwin Peterman, Rolf Wagner and Conrad Woldringh for their input and critical reading of the manuscript and Jacob Kerssemakers for providing the step-fitting algorithm and his assistance using it.

4.6 Materials and methods

4.6.1 Enzymes and buffers

H-NS was purified as described before [45]. DNA was captured and tested in a buffer containing 10 mM Tris-HCl (pH 7.5), 200 mM NaCl, 1 mM EDTA, 3.5 mM DTT. The binding reaction with H-NS (diluted from stock to a concentration of 2 μM) and measurements were done in a buffer containing 10 mM Tris-HCl (pH 7.5), 1 mM EDTA, 3.5 mM DTT, 60 mM∼KCl, 10 mM $MgCl_2$ at room temperature (20 °C). Before carrying out the unzipping or shearing experiments, the system is given ample time to reach equilibrium. Using a range of concentrations (down to 200 nM) yielded similar results due to the rapid saturation of the two DNA duplexes [42].

4.6.2 DNA constructs

Bacteriophage λ-DNA molecules (Roche) were labeled at each extremity with multiple biotin groups by filling the 12 bp cohesive ends with biotin-14-dATP, biotin-14-dCTP, dGTP and TTP (Invitrogen) using Klenow DNA Polymerase exo-minus (Fermentas).

4.6.3 Optical tweezers instrument (the Q-trap)/flow cell

Optical traps are generated using a 1064 nm laser, which is first split on polarization. Subsequently one of the paths is led through an acousto-optic deflector to generate three time-shared traps at different locations. Experiments were performed in a flow cell with four channels. The use of laminar flow ensures that the channels do not

mix [129]. In this manner, by moving the sample perpendicular to the channels we can efficiently catch, manipulate and incubate two single DNA molecules. 1.87 μm streptavidin-coated polystyrene beads (Spherotech) are captured in the optical traps and subsequently incubated in the channel with a DNA solution (∼2 pM). After DNA molecules have been captured between each set of beads they are tested for integrity and singularity in the buffer channel. The molecules are placed in the configuration required for the experiment and moved into the channel with H-NS solution. Position and motion are detected on the bead in the fixed trap via back focal plane interferometry using a quadrant photodiode. End-to-end distance is obtained by determination of the distance between the stationary and the moving bead from video microscopy.

4.6.4 Data analysis

Force data (4 kHz) and end-to-end distance (25 Hz) are measured during the assay. End-to-end distance is converted to contour length using a worm-like chain (WLC) estimation. The persistence length is obtained by fitting a WLC estimation to force-extension curves of single DNA molecules coated with H-NS. This value does not significantly differ from that of bare DNA molecules and can be estimated with an uncertainty of ∼10 %.

For the step size analysis, contour length information is averaged (4x). The size of individual steps (such as shown in Fig. 4.5) was determined using a recently published step-fitting algorithm [98]. This algorithm produces most reliable fits when a number of steps fractionally higher than indicated by the maximum of the step-indicator value (S) is used [52]. Typically the S value of fits to our data is around 1.5. The average size of steps detected does not change throughout the applied range of forces (4-22 pN), indicating that all H-NS bridge disruption events are detected. The observed increase in contour length arises from the unbridging of two oppositely located regions on the DNA. The contour length change is therefore divided by 2 (yielding one-sided contour length data).

We performed a weighted-fit with multiple Gaussians to the distribution of step sizes. The width, amplitude and unit step were fit parameters. The width was set to be identical for each of the Gaussians, while the position of each of the Gaussians was set to correspond to a multiple of the unit step. The quality of the fits was evaluated for different multiples of Gaussians from their reduced chi-squared values. The unit step obtained from fits with 4, 5, 6 and 7 Gaussians was identical within experimental error. The lowest reduced chi-squared value, yielding the statistically most relevant fit (as shown in Fig. 4.5a), was obtained for 6 Gaussians.

4.6.5 Dynamic force spectroscopy

The most probable force for the force-induced unbinding of two bodies shows a linear dependence on the natural logarithm of the loading rate for each kinetic barrier in the energy landscape of the interacting bodies [59]. Because the stiffness of the DNA (k_{DNA}) varies with force and contour length, we probe a wide range of loading rates in one unzipping assay. This distinguishes our approach from similar experiments done with scanning force microscopes, where the loading rate is changed by varying the speed. Since the H-NS dimer is bound to two DNA duplexes simultaneously, the probability of dissociation is doubled, which in turn halves the unbinding time. Since the increase in force between events is negligible and the loading rate is approximately linear, this can be accounted for by multiplying the thermal forces by 2. The loading rate (r_f) is calculated using $r_f = k_{DNA} \cdot \nu_{unzipping}$ where the stiffness of the DNA (k_{DNA}) can be calculated by assuming a worm-like-chain and calculating $\partial F/\partial z$, and where $\nu_{unzipping}$ is the unzipping rate. In a DFS spectrum a linear region reflects the presence of a well-defined kinetic barriers in the energy landscape. The location of the barriers can be calculated using the thermal force defined by the slope (equal to $k_\beta T/x_b$) [59].

4.7 Appendix

4.7.1 Analysis of step sizes in simulated data

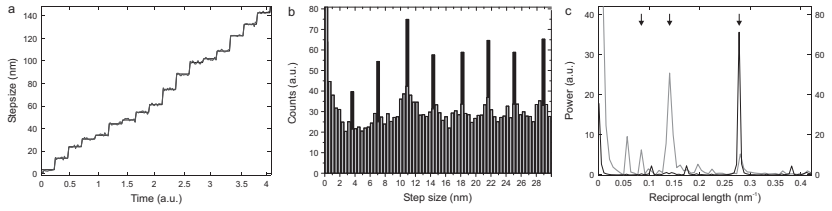

Figure 4.8: Analysis of step size in simulated data. **a**, Simulated step train with steps corresponding to 1, 2, 3 and 4 helical repeats (3.6 nm) distributed in random order (without (grey) and with (black) Gaussian noise of 1 nm). Steps of a given size occur with a frequency as extracted from the Gaussian fits of Figure 4.5a. **b**, Pdf's of the simulated data without (black) and with (grey) noise. The noise has a dramatic effect on the quality of the pdf, including the near absence of a peak at 3.6 nm. This demonstrates the limitations of pdf analysis for this type of stepping data. **c**, Fourier transform of the pdf's displays several peaks. A peak at 0.28 nm^{-1} dominates the data without noise, reproducing the helical repeat of 3.6 nm. When noise is added the dominant 0.28 nm^{-1} peak decreases markedly and additional peaks appear around multiples of the helical repeat (indicated by arrows).

4.7.2 Alternative analysis of H-NS step sizes I

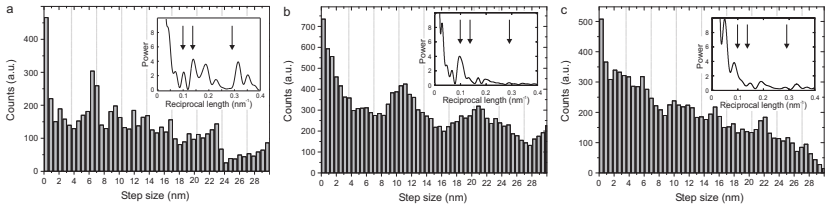

Figure 4.9: Analysis of H-NS step size using alternative methods - I: pairwise distribution functions. Histograms of pdf analysis based on the data from Figure 4.4. The distribution reveals a periodic signal, reflecting a regular organization in the H-NS-DNA_2 complex. Insets: The Fourier transforms of these pairwise distribution functions display peaks of varying intensities around multiples of the helical repeat as expected from the simulations in Figure 4.8 (indicated by arrows). As indicated in Figure 4.8,the use of pdf analysis is limited in these experiments since the correlation distance is smeared over all higher orders and not mostly concentrated in the first peak. Therefore it becomes harder to separate the peaks from the noise, which is close to a single helical repeat. Staircase fitting algorithms are better capable extracting irregular steps from data [98]).

4.7.3 Alternative analysis of H-NS step sizes II

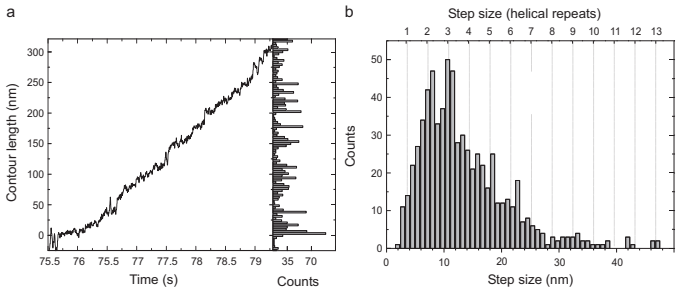

Figure 4.10: Analysis of H-NS step size using alternative methods - II: distribution histogram of the one-sided contour length change. a, In this approach a plateau in the time trace (left) appears as a peak in the histogram (right). The step size is defined as the distance between the centre of two adjacent peaks [19]. Measured data displayed at 400 Hz and median filtered, rank 6. **b**, When all steps are plotted in a histogram two dominant peaks are apparent (7.0 and 10.5 nm) that coincide with the distance between 2 and 3 helical turns. Drawbacks of this method are the difficulty identifying closely spaced peaks and the large variability in peak sizes. Nevertheless, the shape of the histogram is similar to what is found using the step-fitting algorithm.

Chapter 5

When lines are not in use, they must be stored into a configuration such that knots can not be introduced accidentally. This can be achieved by organizing them in bundles of loops.

H-NS promotes looped domain formation in the bacterial chromosome

Abstract – The bacterial chromosome is organized into loops, which constitute topologically isolated domains. It is unclear which proteins are responsible for the formation of the topological barriers between domains. The abundant DNA-binding histone-like nucleoid structuring protein (H-NS) is a key player in the organization and compaction of bacterial chromosomes [38, 52]. The protein acts by bridging DNA duplexes [40], thus allowing for the formation of DNA loops. Here, genome-wide studies of H-NS binding, based on earlier work of Oshima *et al.* [132] and Navarre *et al.* [128], suggest that this protein is directly involved in the formation or maintenance of topological domain barriers.

5.1 Introduction

Bacterial chromosomes are organized into topological domains that, on average, measure ∼10 kb, yielding on the order of 400 such domains per chromosome [48, 138]. Topological domains are regions where supercoiling is preserved due to, for instance, attachment to structural components of the cell or DNA duplex cross-linking. The ability of the DNA-binding protein H-NS to bridge DNA duplexes suggested it might serve as a domain barrier [38, 40]. Indeed, recently this protein was shown to be involved in topological domain formation *in vivo* [74]. Chromatin immunoprecipitation (ChIP) experiments demonstrate that H-NS binds to A/T rich regions within the genomes of *Salmonella typhimurium* [128, 108] and *Escherichia coli* [132, 69] where it generally silences transcription. Assuming that adjacent patches of DNA-bound H-NS interact to form a loop, the distance between these patches identified by ChIP corresponds to the size of the resulting loop.

5.2 Results

We have determined the location and size of H-NS-bound patches along the genomes of *S. typhimurium* and *E. coli* (see Fig. 5.1a and Fig. 5.3). The patch- spacing distribution follows an exponential decay (see Fig. 5.1b) indicating a stochastic placement of patches along the genome. The cumulative probability plot of loop length directly

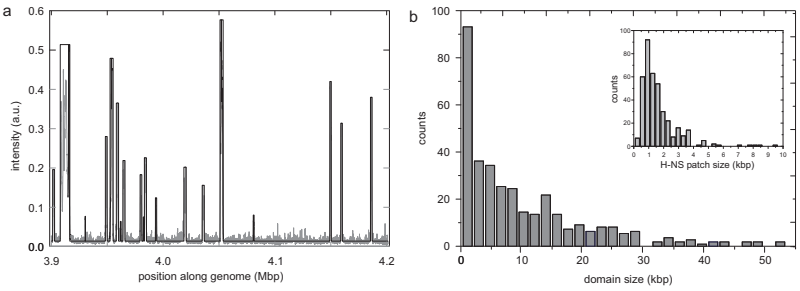

Figure 5.1: Applying a peak finding algorithm to ChIP-on-chip data for H-NS. **a**, ChIP-on-chip data for H-NS from *S. typhimurium* [128] (grey) and the result of a peak-detecting algorithm to these data (black). This algorithm detects peaks with intensity above a threshold, set to three times the background expression level, and a width >240bp. Shown is a 300 kb region representative for the whole genome (shown in the Appendix). Very similar results (not shown) were obtained for *E. coli*. **b**, Histogram of interspacing between H-NS patches along the genome. The interspacing between loops was obtained by calculating the distance between two peaks as detected by the algorithm. Inset: Histogram of H-NS patch size. The patch size corresponds directly to the width of the peaks detected.

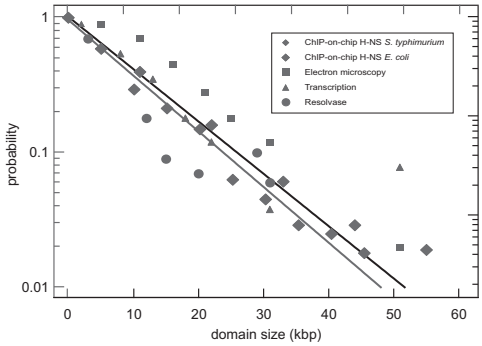

Figure 5.2: Comparing methods. Cumulative probability plot. Plotted along the x-axis is the probability that the size of a domain falls in a certain bin of domain sizes. Accordingly the probability that a domain has a size larger than 0 bp is by definition 1, while that probability for infinitely large loops is zero. Data from H-NS ChIP-on-chip for *S. typhimurium* and *E. coli* (yielding average loop sizes of 10.5 ± 1.0 and 12.3 ± 1.8 kbp respectively, from weighted exponential curve fits of the histogram of interspacing), electron microscopy images, transcription and resolvase assay (published data taken from [48, 138].

allows comparison with published data (see Fig. 5.2). The average distance measured between patches is ∼11 kb in both organisms, in excellent agreement with earlier estimates of topological domain size obtained using other approaches [48, 138] (see Fig. 5.2). In stationary phase, when the amount of H-NS is reduced by more than half, the domain size doubles [76]. This correlation between H-NS levels and domain size suggests that H-NS is a dominant factor in setting topological domain boundaries.

5.3 Discussion

There are ∼350 H-NS-bound patches along the genome, suggesting that other types of boundaries, for example, due to proteins such as gyrase [164], Fis or TktA [74], may account for the remaining ∼15 percent of the 400 topological domains formed during exponential growth [48, 138]. The size of a typical H-NS-bound patch is about 2 kb, resulting in 10-15 percent genome coverage in both *S. typhimurium* and *E. coli.* Combined with the average H-NS binding site size of 25 bp [40], this provides an upper limit for the amount of H-NS that is bound to the DNA - 10,000-15,000 dimers. This number agrees well with the estimate of ∼10,000 H-NS dimers per cell [38, 52], suggesting that most H-NS in the cell is DNA bound.

It is believed that chromosome folding preserves the linear order of genes on the DNA; newly replicated segments are condensed right after replication and then move to their final location [188]. If the ordering of the nucleoid is directly coupled to chromo-

some replication and segregation, a domain is formed when a newly replicated region prone to H-NS binding becomes available. This suggests a model in which the circular chromosome is arranged linearly with H-NS-stabilized loops stacked adjacently. Previously, it has been suggested that barriers are dynamic and formed stochastically [76]. Our current results refine this interpretation by including sequence determinants (A/T rich regions recognized by H-NS) that are apparently stochastically placed along the genome. The binding of H-NS at defined sites implies an underlying 'preferred order' in every cell. Nevertheless, the domains will be dynamic and not continuously fixed at one location in each cell within a population, as domain barriers will differ in stability (with smaller bridged regions being less stable than larger ones). Moreover, the looped domains are reorganized as a result of the effects of growth conditions on H-NS expression levels [38, 52], the interplay with other nucleoid-associated proteins [38] and transcription [40, 47]. Interestingly, hns$^-$ strains have a mild phenotype, suggesting that the looped domain organization is largely buffered by the action of other proteins. One such protein might be the H-NS paralogue StpA [209], but even hns-stpA double mutants do not exhibit a dramatic phenotype in rich medium [209], suggesting that additional proteins serve redundant functions in bacterial chromosome organization (e.g. Fis [9]). The genomes of *E. coli* and *Salmonella* are highly plastic and a large proportion of their content was obtained by horizontal gene transfer. Horizontally acquired genomic islands are generally A/T rich and thus specifically targeted by H-NS [128, 108, 132]. Any newly acquired sequence has the potential to decrease the fitness of its host bacterium by disrupting the organization of the genome. We propose that, in addition to silencing foreign DNA [128], H-NS prevents disruption of the overall nucleoid organization by newly acquired DNA, thereby expanding the role of H-NS as a defense against the potentially harmful effects of foreign DNA. Our hypothesis that H-NS is a key protein in looped domain formation should be used as a starting point for further experiments in which H-NS-bound patches are explicitly considered as potential domain barriers. It would be useful to systematically repeat the earlier transcription and resolution assays [138, 76] on defined regions along the genome. The use of microarrays to study transcription of genes within the proposed loops together with ChIP-on-chip could reveal the presence and dynamics of H-NS-induced domain barriers. The potentially least perturbative approach would be to probe the variance in the physical location of fluorescent tags placed within the proposed loops [188], as this should directly correlate with loop size.

5.4 Acknowledgements

This research was supported by the Netherlands Organization for Scientific Research (NWO) through a NWO VENI grant (to R.T.D.) and a NWO Vernieuwingsimpuls grant

(to G.J.L.W.). We thank Yipeng Wang, Steffen Porwollik and Michael McClelland for their help with the analysis of the *S. typhimurium* array data and Naotake Ogasawara for discussion and help with the analysis of the *E. coli* array data. We thank Nora Goosen, Jane' Kondev, Martijn Luijsterburg, Lisa Postow, Mariliis Tark, Paul Wiggins and Conrad Woldringh for discussion and critical reading of the manuscript.

5.5 Appendix

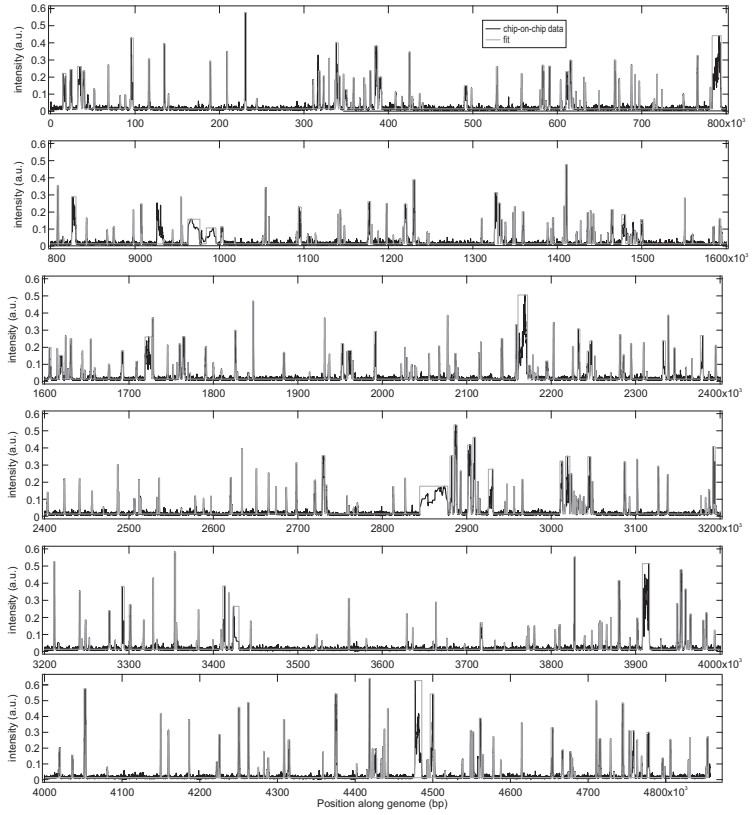

Figure 5.3: Applying a peak finding algorithm to ChIP-on-chip data of the entire genome for H-NS. ChIP-on-chip data for H-NS from *S. typhimurium* (black) and the result of a thresholded peak-detecting algorithm to these data (grey). An abbreviated version of this figure appears as Figure 5.1a in the text.

Chapter 6

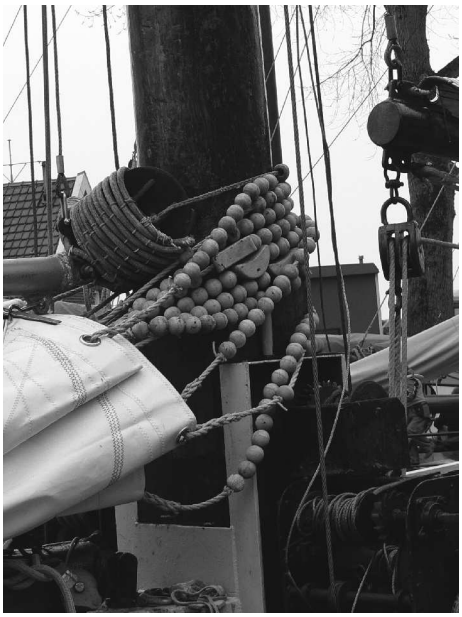

Some lines aboard a ship are used heavily and are therefore subject to increased wear and tear. To protect these lines, sometimes a protective cover of wooden beads is applied. In this particular case, the lines keep the mainsail close to the mast. When hoisting the sail, the wooden beads roll over the mast, protecting the line. Since the beads also slightly stiffen the line, hardly any knots occur.

Characterization of the archaeal protein Alba

Abstract – Alba is one of the most abundant proteins in Archaea and has been suggested to play an important role in DNA organization and regulation. Alba is a dimeric protein that binds DNA with no apparent sequence specificity. Earlier studies have shown that Alba is capable of dsDNA bridging which may be key to its organizational role. However, a comprehensive understanding regarding the action of Alba in DNA organization is currently lacking. Here, we employ a combination of scanning force microscopy, tethered particle motion, and optical tweezers experiments on single DNA molecules to define mechanistic, structural and kinetic aspects of the Alba-DNA interaction. We demonstrate that the protein has two modes of action, DNA bridging and DNA stiffening, depending on its concentration. Based on these observations we put forward a structural model that describes the multi-modal behavior of Alba in the context of the dynamic archaeal nucleoid.

6.1 Introduction

The length of the genomic DNA of organisms in all three domains of life typically exceeds the dimensions of the cell or organelle in which it is contained. To achieve the required considerable degree of compaction the DNA is associated with large numbers of architectural proteins [38, 119]. The action of such proteins is best characterized in eukaryotic organisms. Eukaryotes predominantly employ DNA wrapping (into nucleosomes) as a mechanism of compaction [100, 109]. Bacteria on the other hand have evolved proteins that either induce bends into DNA or bridge DNA duplexes [39, 110].

In general, Archaea combine traits of both eukaryotes and bacteria. This seems no different for the mechanisms they employ to organize their genome. Many Archaea do possess histones, that are homologous to their eukaryotic counterparts, and form nucleosomes, but rather than being an octamer, the archaeal histones form a tetrameric protein core [147]. Moreover, in many archaeal species at least one type of DNA bending protein has been identified [196]. In addition, most archaeal genomes code for the Alba protein from the Sac10b family, an abundant nucleoid-associated protein that was first identified in *Sulfolobus acidocaldarius* [72]. In some archaeal species two homologues of Alba are found, Alba 1 and Alba 2. Alba 2 is expressed at only 5% of the level of Alba 1 [90] in these species. The majority of Alba *in vivo* exists in the form of Alba 1 homo dimers while a small fraction exists as Alba 1-Alba 2 hetero dimers. The Alba 1 structure has two extended beta-hairpin arms extending from a highly basic body [192]. The arms are separated by ∼40 Å, which has led to the idea that the protein-dimer is bound in *cis* and that the two arms are inserted into two adjacent minor grooves [192]. Using electron microscopy it was shown that this protein is also capable of bridging DNA into filaments, in which the two DNA duplexes are possibly wound around each other [90, 111]. However, the characteristics of the Alba-DNA interaction and the DNA bridging mechanism remain unclear. In order to obtain a deeper molecular mechanistic and kinetic understanding of DNA looping by Alba and DNA-Alba-DNA complex (Alba-DNA_2) formation, we have employed a series of complementary approaches with four different single-molecule techniques.

6.2 Results

To characterize the structural effect of the binding of Alba to dsDNA, we used optical tweezers to analyze the force extension behavior of single λ-DNA molecules incubated with Alba 1 dimer in a flow chamber (see Materials and methods for details). The mechanical response (Fig. 6.1) of a bare λ-DNA molecule (light grey) changes significantly in response to the addition of Alba (dark grey). The experimental data can be fitted between 0-50 pN with a modified Worm-Like Chain (WLC) model [10] (see Fig. 6.1). This fitting allows for quantification of protein induced changes in

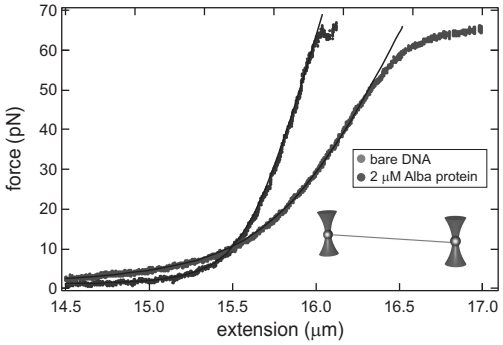

Concentration	P (nm)			N
0	38	±	1	41
2	65	±	6	11
600	147	±	6	4
2000	136	±	9	22

Concentration	L (μm)			N
0	16.48	±	0.03	41
2	16.23	±	0.07	11
600	16.14	±	0.01	4
2000	16.03	±	0.01	22

Concentration	S (pN)			N
0	2300	±	100	41
2	4800	±	200	11
600	5400	±	800	4
2000	5700	±	900	22

Figure 6.1: Force extension behavior of Alba - DNA$_1$ complexes. Force-extension curves of individual λ-DNA molecules acquired without (light grey) or with 2 μM Alba (dark grey). Both traces can be fitted with a modified WLC (black solid lines). The traces exhibit a clear difference in contour length and stiffness. **inset bottom right**, Schematic illustration of the experimental assay. **Table**,Values obtained from FE-curves for contour length, persistence length and stretch modulii. The stretch modulii are not used any further.

the contour length (CL) and the effective persistence length (P, a measure for the flexibility) of DNA. These parameters were estimated for Alba concentrations in the range of 0-2000 nM (Fig. 6.1, Inset). The parameters obtained for bare DNA are in good agreement with previous estimates [172]. Addition of Alba leads to stiffening of the DNA molecule in a concentration dependent manner. The change in both CL and P appears to level off at concentrations exceeding 600 nM (see Fig. 6.1, Inset and Fig. 6.3, Inset). At these conditions, where the DNA is apparently close to saturation with Alba, the stiffness obtained is almost four times higher than that of bare DNA whereas the contour length is shortened by ∼3%.

How does the protein exactly bind to the DNA? The structure of the Alba-DNA complex has not been resolved, but the DNA-binding domain of Alba is structurally homologous to the DNA-binding domain of DNAseI [192], comprising a β-hairpin. The co-crystal structure of this domain (residues 1-86) shows that binding of DNAseI deforms the helical structure of dsDNA mildly [195] by inserting a β-hairpin in the minor groove of the DNA. However, there are also clear differences between the structures of Alba and DNAse I; the β-hairpin of Alba is considerably longer, indicating that the orientation of the DNA in the Alba-DNA complex could be very different. Proteins with a similar β-hairpin configuration are the bacterial nucleoid associated proteins IHF and HU. These proteins also distort the helical structure of the DNA by locally 'kinking' the DNA [110, 184] leading to an effective shortening of the DNA contour length. At saturating conditions, where filament formation of Alba on DNA was previously [192] hypothesized, we measure a shortening of the DNA contour length of ∼3%. This ob-

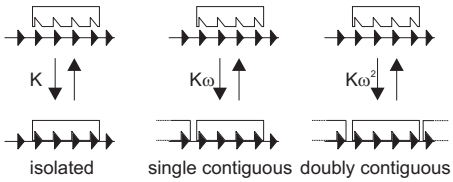

Figure 6.2: Summary of cooperativity theory. Three different types of binding events can occur [121], isolated, single contiguous and doubly contiguous. Protein induced cooperativity enhances the association constant K in the latter two events with a factor ω and ω^2 respectively.

servation and the structural similarities correspond well with a model for Alba binding to DNA that is analogous to DNA binding of IHF or HU, where the DNA helix is deformed. Disperse binding of Alba along the DNA would then indeed lead to the observed shortening of contour length.

In order to assess the kinetics of the Alba–DNA interaction we used the McGhee and von Hippel [121] theory that describes protein binding to a one-dimensional lattice (in this case DNA). In this theory, protein binding to DNA is characterized with an equilibrium binding rate constant K and a 'footprint' n, the effective binding site size in base pairs. Typically for DNA binding proteins, K ranges from 10^4-10^8 $M^{-1}$and n ranges from 2-20 bp. The theory explains that due to this finite sized footprint, 'vacant' positions on the DNA smaller than n make it very hard to achieve 'perfect' protein coverage on a DNA duplex. Instead, one obtains only a fractional coverage ν, which is concentration, C, dependent, according to:

$$\frac{\nu}{C} = K(1-n\nu)\cdot\left(\frac{1-n\nu}{1-(n-1)\nu}\right)^{n-1} \tag{6.1}$$

When cooperativity between proteins influences the binding constant, a cooperativity factor, ω, can be introduced that modulates the effective equilibrium association rate constant K (see Fig. 6.2) according to:

$$\frac{\nu}{C} = K(1-n\nu)\cdot\left(\frac{(2\omega-1)(1-n\nu)+\nu-R}{2(\omega-1)(1-n\nu)}\right)^{n-1}\cdot\left(\frac{1-(n+1)\nu+R}{2(1-n\nu)}\right)^{2} \tag{6.2}$$

where $R=\sqrt{[1-(n-1)\nu]^2+4\omega\nu(1-n\nu)}$. For $\omega>1$, indicating a cooperative effect, this results in an enhancement of the binding constant whereas an $\omega<1$ indicates anti-cooperativity. In the case $\omega=1$, Equation 6.2 reduces (using l'Hôpital's rule) to Equation 6.2 for non-interacting proteins. By measuring the fractional protein coverage as a function of concentration, the association constant K, as well as the cooperativity factor ω can be determined. We now know from the optical tweezers experiments that the protein coverage is directly linked to the shortening of the

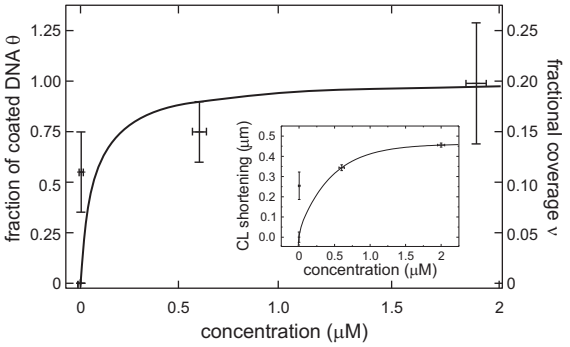

Figure 6.3: Fractional shortening vs concentration. The fractional shortening ν is plotted against concentration. The data points correspond to the contour length measured for each concentration. Error bars indicate s.e.m.. The data is fitted using Equation 6.2 (solid line). inset, Change in contour length versus concentration. Data points are determined from fits shown in Figure 6.1, and the line is a fit to an exponential function to determine L_{min}. Error bars indicate s.e.m..

contour length of DNA in a concentration dependent manner. In order to calculate the *fractional* shortening of DNA in our experiments, a value for the contour length of DNA at 'perfect' lattice filling, L_{min} is necessary. We therefore plotted the contour length obtained from the DNA-stretching experiments as a function of concentration (see Fig. 6.3, Inset). We estimate L_{min} by assuming that the value for L at an infinite Alba concentration, as obtained from the exponential fit (see Fig. 6.3, Inset) approaches L_{min}. Now the concentration dependent binding density, ranging from 0 for bare DNA to 1 for perfect lattice saturation, can be calculated using:

$$\theta = \frac{L_{\text{bareDNA}} - L_{\text{Alba}}}{L_{\text{bareDNA}} - L_{\text{min}}} = n \cdot \nu \tag{6.3}$$

where θ is the fraction of the DNA that is coated with Alba. Figure 6.3 shows the fractional coverage as a function of concentration measured by taking force-extension-curves. The size of the Alba protein suggests that one Alba dimer has a maximal footprint of ∼15 bp. However, it was found that DNA binding is saturated at three times higher stochiometry than expected [192]. Based on these observations a model was suggested where Alba dimers are tightly packed around the DNA in a helical structure, each dimer effectively occupying ∼5 bp. Thus assuming $n = 5$ and fitting this curve with the McGhee-von Hippel binding isotherm described in Equation 6.2 yields a cooperativity factor $\omega = 18 \pm 1 \text{ x } 10^3$ and an equilibrium binding constant $K = 2.9 \pm 0.3 \text{ x } 10^6 \text{ M}^{-1}$. This result, $\omega \gg 1$, confirms the previously observed cooperativity of Alba binding on DNA [11, 192].

stochiometrie (Alba/bp)	fractional overlap
no Alba	2 ± 1 nm
1 : 60	16 ± 5 nm
1 : 30	26 ± 2 nm
1 : 15	52 ± 6 nm

Table 6.1: fractional overlap in SFM images for different concentrations of Alba protein

Based on electron microscopy (EM) experiments [90, 111] it has been suggested that a second mode of binding of Alba is the ability to condense DNA by holding two separate tracts of a DNA molecule together. This mode could play an important role in the organization of DNA in Archaea since DNA bridging is considered a key organization mechanism in for example the bacterial nucleoid. Here, we performed Scanning Force Microscopy (SFM) experiments on Alba-DNA_2 complexes at different protein-DNA stochiometries (see Materials and methods for details). Open circular DNA (obtained by nicking a 5.4 kb plasmid, see Materials & Methods) instead of a linear DNA fragment was used in these experiments to increase the probability of bridging. In the absence of Alba most DNA molecules appeared circular and uncondensed (see Fig. 6.4a). A very small fraction of molecules exhibit regions where the DNA crosses ($2 \pm 1\%$, fraction of contour length in overlapping regions). This fractional overlap region increases with Alba concentration as more self-overlapping regions are detected and DNA condensation becomes more evident (see Fig. 6.4b-d). We therefore use the fractional interaction as a measure for the bridging activity of Alba protein. At a ratio of 15 bp/Alba the plasmids attain shapes with stiffened branches (See Fig. 6.4d). The concentration dependent increase of bridged regions, from ~2 to ~50% of the contour length (see Table), indicates that Alba as a dimer can progressively bridge long DNA tracts. This progressive bridging behavior is probably facilitated by the increased local DNA concentration that occurs when one bridge is formed [43, 42].

The images obtained with the SFM experiments display the condensation of the plasmid DNA by the formation of bridges by Alba protein. As a result of this condensation process, the Alba-DNA complexes at intermediate stochiometries form loops along the contour of the DNA (see Fig. 6.4c and Fig. 6.5, Inset). The sizes of these loops are determined by the balance between the adhesive free energy density of Alba binding to DNA and the conformational free energy penalty that results from the energy cost of DNA loop formation. The distribution of loop-sizes directly measured from SFM images is shown in Figure 3 ($N = 42$). The probability for a loop with certain contour length L in equilibrium is related [200] to the looping free energy, G_{loop}, by

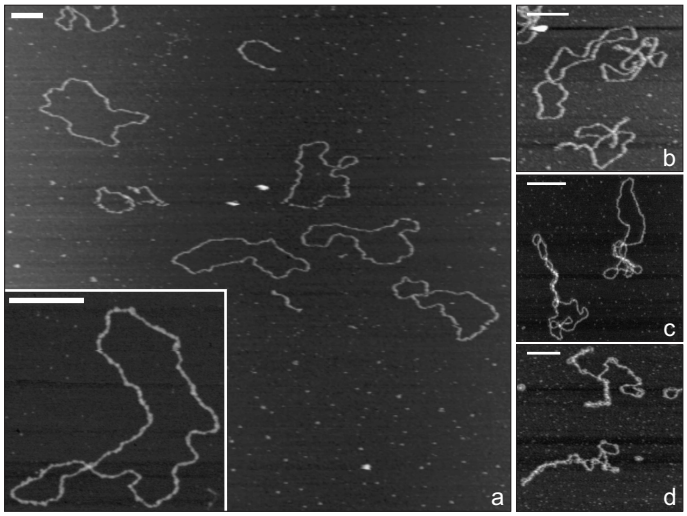

Figure 6.4: Scanning Force Microscopy of Alba-DNA complexes. SFM images (N = 54) of ϕX174RFII nicked circular DNA molecules. Scale bars indicate 150 nm. **a**, Bare DNA molecules. Inset, Zoom of bare circular DNA molecule. **b**, SFM image of the same plasmid DNA incubated with Alba at a ratio of 1 Alba dimer per 60 bp. **c**, Idem, but with Alba at a ratio of 1 Alba dimer per 30 bp. **d**, Idem, but with Alba at a ratio of 1 Alba dimer per 15 bp.

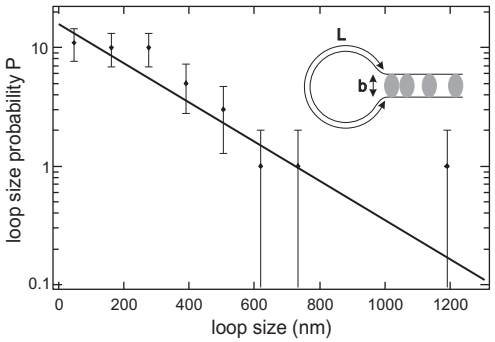

Figure 6.5: Size of loops in Alba-DNA complexes imaged by SFM. Loop size probability obtained from SFM-image analysis. Error bars indicate s.e.m., solid line is a fit to the data. inset, Schematic illustration of a loop formed by Alba. *L* is the size of the loop, *b* depicts the bridge spacing.

the Boltzmann Distribution:

$$P(L) = e^{-\frac{G_{\text{loop}}(L)}{k_{\text{B}}T}} \tag{6.4}$$

with k_{B} the Boltzmann constant and T the temperature. The free energy of an Alba mediated DNA loop is dominated by the bridge spacing (*b* in Fig. 6.5, Inset), whereas for large loop sizes the Alba–mediated adhesion energy per unit length of DNA, ρ [200] becomes more dominant. Since there are hardly any small loops, G_{loop} is probably only adhesion energy dominated and no information about the loop spacing can be obtained. In this case the free energy of a loop is given by $G_{\text{loop}}(L,\rho) = \frac{1}{2} \cdot \rho \cdot L$ and the prediction for *P(L)* in Equation 6.4 becomes an exponential decay. Fitting the distribution, obtained from analyzing the SFM images, with this function (see Fig. 6.5) results in an adhesion energy $\rho = 0.008 \pm 0.03\,\text{kT}\,\text{nm}^{-1}$. When comparing the adhesion energy ρ obtained from the loop-size distribution with values obtained for another DNA bridging protein, H-NS, $\rho = 0.13 \pm 0.03\,\text{kT}\,\text{nm}^{-1}$ (unpublished results) [200], we find that the Alba-DNA interaction is much weaker than the H-NS-DNA interaction. The much lower adhesion energy, compared to H-NS, suggests that -if at all- *in vivo* Alba does not give rise to relatively stable loops or bridging.

As the SFM images only provide a static image of protein-DNA complexes, we performed optical tweezers [40, 129] experiments with two dsDNA duplexes, to study the structure and dynamics of the Alba-DNA_2 complex. With this technique, (protein-induced) interactions between two DNA molecules can be probed in detail since two DNA molecules can be manipulated independently and interaction forces can be measured with sub-pN resolution (see Fig. 6.6 Inset). After catching two single DNA molecules with four optical tweezers, we incubated the two DNA molecules in a solution containing Alba protein. By measuring the force-extension behavior of the

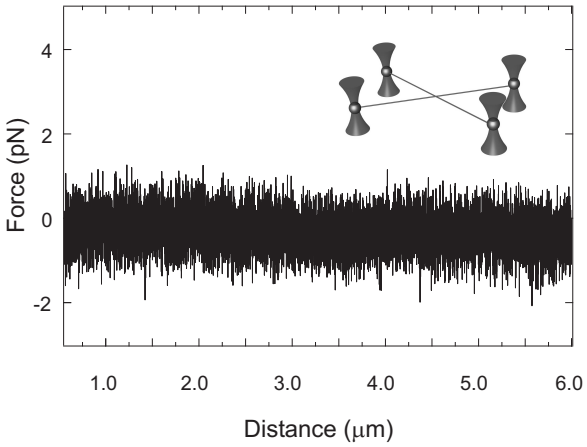

Figure 6.6: Dual DNA assay on Alba. Typical data trace showing no bridging activity of Alba protein in the dual DNA assay. Similar data obtained in 17 experiments over a concentration range of 2-2000 nM. inset, Schematic illustration of the dual DNA assay. The ends of two λ-DNA molecules are attached to four beads held with optical tweezers.

individual DNA molecules the binding of Alba to the DNA was confirmed. To facilitate inter-duplex bridging we placed the two DNA molecules in a crossed configuration (see Fig. 6.6) in a buffer containing Alba protein and the system was given time to equilibrate. We systematically tested a large range of protein concentrations (2-2000 nM) but no bridging of the DNA duplexes was observed.

What is the mechanistic basis of our observation that Alba bridges DNA in the SFM experiments while only Alba coating of single DNA duplexes is observed in the dual DNA assay? There is an important distinction between the two experiments: the ratio of DNA molecules and Alba proteins is very different in both experiments. In an SFM experiment DNA is incubated with Alba at a pre-set ratio. In tweezers experiments, however, the Alba-DNA ratio is considerably larger as the total number of DNA molecules is only two [42]. This leads us to hypothesize that the mode of Alba-DNA complex formation is highly concentration dependent and that this is reflected in the two different assays due to fundamentally different incubation conditions. At low Alba-DNA ratios, when two tracts of dsDNA are in close proximity to each other, bridging can occur. However, at higher Alba-DNA ratios, filament formation of Alba on a single DNA molecule prevails over bridge formation.

In order to test this hypothesis we performed tethered particle motion (TPM) experiments [139, 140, 141, 182, 207] (see Materials and methods for details). TPM allows for measuring the kinetics of the Alba-DNA interaction without exerting forces that could possibly perturb the formation of Alba-DNA_2 complexes while more closely approaching the Alba-DNA ratio used in the SFM experiments. The Brownian motion of the

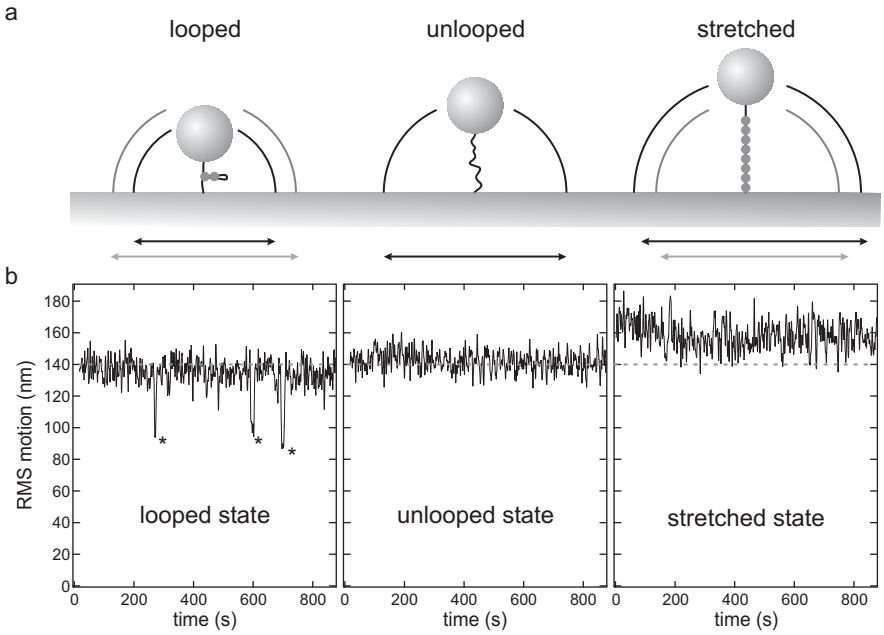

Figure 6.7: Tethered Particle Motion. **a**, Schematic representation of three possible effects of Alba binding to DNA and the effect on the RMS value. When a tethered DNA molecule is looped, the DNA is effectively shortened compared to the unlooped state (see middle panel) and as a result, a (sudden) decrease of the RMS value can be observed (indicated by the arrows on the bottom of the panel). At high concentrations of Alba, the DNA can be stiffened (right panel) resulting in an increased RMS value compared to an unlooped tether. **b**, For a normal, looped and stretched tether the resulting data trace is shown. In the left panel, showing looping events, black stars indicate the occurrence of a loop formation event. Grey dashed line indicates normal RMS value.

tethered beads (N = 20) was recorded over time at Alba concentrations from 0 to almost saturating conditions (2000 nM). Protein induced stiffening or bridging should result in a larger or smaller amplitude of RMS motion respectively (see Fig. 6.7a). In the range 25 - 2000 nM, besides the tethers that showed no effect at all (10%), basically three effects where measured. First, ∼25% of the DNA tethers showed sudden drops of 32 ± 4% in the RMS value, observed at intermediate concentrations (∼500 nM). This indicates the formation of DNA loops transiently stabilized by Alba (see Fig. 6.7, left panels). The looped states had an average duration of ∼22 seconds indicating an off rate k_{off}=∼0.04 s^{-1}. Second, at almost saturating conditions, ∼20% of the tethers showed an increase in RMS values of 20 ± 10%, indicating that the DNA stiffens (see Fig. 6.7, right panels). Based on Monte Carlo simulations (data not shown) we found that the observed 20% increase in RMS motions corresponds with a ∼3-fold increase in persistence length, in good agreement with the optical tweezers experiment. Third: a significant number, 45% of the tethers did not move anymore, indicating that the bead is in contact with the surface, inhibiting any Brownian motion of the DNA. This occurred at intermediate and high concentrations of Alba protein (>200 nM). Upon flushing the sample with buffer solution, all tethers return to normal length and display normal Brownian motion. It is likely that Alba causes the tether to stick to the surface via non-specific interactions despite coating the surface with BSA. Since looping occurs only at non-saturating conditions (concentrations « 2000 nM), we conclude that these results match our prediction that bridging occurs at intermediate concentrations and cooperative coating of single DNA strands occurs at high concentrations. The cooperative coating inhibits any further bridging to occur. The increased stiffness of saturated Alba-DNA filaments might interfere with bridge formation.

6.3 Discussion

How do the results from the four different experimental approaches combine to a structural model? From the single DNA tweezers experiments we find that Alba binding to DNA shortens the contour length, probably by locally bending the DNA helix. Second, we find that Alba cooperatively forms filaments on DNA. SFM experiments confirm the bridging behavior of the Alba dimer, be it with low binding strength, but this behavior is not detected in the dual DNA assay. Finally, the TPM experiments confirm the stiffening of the DNA helix as well as the weak bridging of DNA by Alba. The effects of the structural model we propose for the functioning of Alba based on these data are highly concentration dependent; at low concentrations Alba exhibits bridging behavior with a low binding strength at locations where DNA occasionally self-crosses (see Fig. 6.8a). When one bridge is formed, the probability to form an-

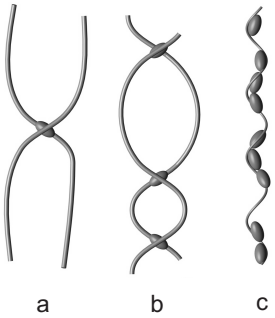

Figure 6.8: Model for Alba-DNA interaction. **a**, At low concentrations an Alba 1 dimer can join sites where DNA self-crosses. **b**, These sites can expand into larger regions due to DNA induced cooperativity. **c**, At increasing concentrations of Alba protein, the DNA is stiffened, breaking the bridges formed at lower concentrations. Each individual Alba protein slightly bends the DNA resulting in a slightly shortened DNA helix wrapped around a filament of proteins resulting in a 'super helix'.

other bridge close by is relatively high due to the increased local DNA concentration resulting in an Alba-DNA_2 structure as shown in Figure 5b. The resulting structure (see Fig. 6.8c) resembles the images taken by Lurz *et al.* [111] and Jelinska *et al.* [90] very well. *In vivo*, this bridging behavior could provide the cell means to compact its DNA. However, the low binding strength indicates that this compaction of Alba 1 will be very dynamic in nature.

At increasing concentrations, the cooperative nature of Alba-DNA binding causes the DNA to be coated with Alba, shifting the balance from DNA bridging to the formation of a protein filament around the DNA, effectively shortening the end-to-end distance (see Fig. 6.7c). The protein-induced increase in stiffness of the DNA might drive the release of bridges, since the energy penalty for forming a small loop will increase along with the persistence length.

6.4 Outlook

The structural model for the interaction of Alba with DNA as presented above provides a unique view of the binding modes of the Alba 1 homo-dimer. The model we have presented here is very much in line with previous experimental results on Alba protein as well as the structural model that was proposed by Lurz *et al.* [111] but offers more insight and better explains the bridging function of Alba. The observation that Alba mediated bridging is much weaker than for instance that of H-NS, indicates that this bridging function probably does not play an important architectural role. However, the described concentration dependent functioning of Alba might suggest that Alba's

role in the cell changes with the growth phase of the cell: it has been shown that the expression of Alba is highly growth phase dependent [50]. If, for instance due to a change in environment, the cell experiences different growth conditions in which the expression level of another DNA architectural protein is increased, the functioning of Alba might shift from bridging towards filament formation on the DNA or vice versa. Such a mechanism, a growth phase dependent ratio of proteins with antagonistic functions, was previously suggested for prokaryotes [38, 110] and might also apply to Archaea.

6.5 Acknowledgements

This research was supported by the Netherlands Organization for Scientific Research (NWO) through a NWO-vernieuwingsimpuls grant (to G.J.L.W.) and a NWO-VENI grant (to R.T.D.). We thank Niels Laurens for his help with the TPM experiments and the MC-simulations and Paul Wiggins for useful discussions and for critically reading the manuscript.

6.6 Materials and methods

6.6.1 Protein

Purification of the Alba 1 protein was carried out as described earlier [192]. The protein was stored at a concentration of 0.91 mM. For experiments the protein was diluted into buffer containing 10 mM Tris-HCl (pH 7.5), 1 mM EDTA, 3.5 mM DTT, 60 mM KCl, 10 mM $MgCl_2$ at room temperature (20 °C).

6.6.2 Experimental setup

Optical tweezers

DNA To allow specific binding to streptavidin-coated beads (1.87 μm diameter, Spherotech Inc.), bacteriophage λ-DNA molecules (Roche) were labeled at each extremity with multiple biotin groups by filling the 12 bp cohesive ends with biotin-14-dATP, biotin-14-dCTP, dGTP and TTP (Invitrogen) using Klenow DNA Polymerase exo-minus (Fermentas). DNA was captured and tested in a buffer containing 10 mM Tris-HCl (pH 7.5), 200 mM NaCl, 1 mM EDTA, 3.5 mM DTT [181].

Instrument The optical-tweezers instrument used for both the single- and dual DNA molecule experiments was previously described in detail [129]. Micron-sized beads, attached to the ends of DNA molecules, can be manipulated by optical traps. Optical

traps are generated using a 1064 nm laser, which is split on polarization. In the case of single DNA molecule experiments the resulting two beams are used to generate two optical traps, one of which is then fixed and the other can be moved using a set of telescope lenses. In the case of dual DNA experiments one of the paths is led through an acousto-optic deflector to generate three moveable time-shared traps at different locations. Experiments were performed in a laminar flow cell with four channels. By moving the sample perpendicular to the channels we can efficiently catch, manipulate and incubate two single DNA molecules [129]. Streptavidin-coated polystyrene beads are captured in the optical traps and subsequently incubated in the channel with biotinylated DNA solution. After DNA molecules have been captured between each set of beads they are tested for integrity and singularity in the buffer channel. The molecules are placed in the configuration required for the experiment and moved into the channel with Alba solution. Before carrying out the experiments, the system is given ample time to reach equilibrium. The position of the bead in the fixed trap is detected via back-focal-plane interferometry using a quadrant photodiode. End-to-end distance is obtained by determination of the distance between the stationary and the moving bead from video microscopy [129].

Data acquisition and analysis For two traps, we recorded bead displacements within the traps in *x*- and *y*-directions using two quadrant photodiodes and a data acquisition board (AD16 module on an analog data acquisition board (National Instruments) [64, 186]. We calibrated voltages to forces using power spectrum analysis [64]. For concurrent force and extension recordings of the captured DNA molecules, we measured the distances between pairs of beads on-line using pattern matching on a digitized microscope image (IMAQ PCI-1409, National Instruments).

Scanning Force microscopy

DNA, Sample Preparation Commercially obtained ϕX174RFII nicked circular DNA (Westburg B.V.) was diluted from stock into buffer containing 40 mM Hepes (pH 7.9), 10 mM $MgCl_2$ and 60 mM KCl and incubated at different Alba-DNA stochiometries for 35 min at 30 °C. This reaction was then diluted 20x in deposition buffer containing 3 mM Hepes (pH 7.9) and 5 mM $MgCl_2$. Subsequently a droplet of 40 µl was deposited on a mica disk. After allowing 1.5 min for the adsorption of the DNA-protein complexes, the surface was gently rinsed with HPLC water. The sample was then dried by gentle exposure to a flow of filtered argon gas [43].

Instrument Images of Alba–DNA complexes were acquired on a Nanotec microscope (Nanotec) operating in tapping mode in air, with NanoDevices Metrology Probes. The cantilevers that were used had nominal spring constants of 40 N m^{-1},

calibrated by using a thermal-oscillations method, and had a resonance frequency of ∼275 kHz. The tip radii of the cantilevers were ∼10 nm.

Data acquisition and analysis Data was acquired using WsXM software (Nanotec). To measure the contour length of open loops, DNA molecules were manually traced using WsXM [82].

Tethered Particle Motion

DNA and sample preparation For the tethered particle motion experiments, single DNA molecules were labelled with digoxigenin on one end and biotin on the other end. The DIG end was then attached to an anti-DIG coated glass surface and the biotin end to a 440 nm diameter streptavidin-coated polystyrene bead (G. Kisker). DNA constructs were assembled in a flow cell consisting of a microscope slide and a cover slip, using double stick tape as spacer. After assembly the chamber was incubated for 20 minutes with a solution containing 20 $\mu g\,mL^{-1}$ anti-DIG (Roche Applied Science) and BSA in order to passivate the glass surfaces. Next, 0.4 ml of labeled DNA (12.5 nM) was flowed in. After incubation for 1 hour, the chamber was again washed with ∼0.5 ml of buffer without protein before the experiment [182].

Instrument The sample containing the tethers was imaged under an inverted microscope (Nikon TE-2000). The brightfield image of Brownian motion of the beads was analyzed by tracking the *x*- and *y*- (in plane) displacement using custom made on-line video analysis (LabVIEW, National Instruments).

Data acquisition and analysis The bead displacements were obtained at $30\,fps^{-1}$. Typically, 30 beads are simultaneously tracked for ∼30 min per experiment. Afterwards, the data was analyzed as previously described [182]. The root mean square (RMS) of the displacement is a direct measure for the DNA tether length. The data was filtered using a 1 s filter. This allows for detecting bridging events in the order of seconds, any shorter events were omitted from analysis. When protein induced bridging occurs, this effectively shortens the DNA tether length reducing the RMS-motion of the bead.

Chapter 7

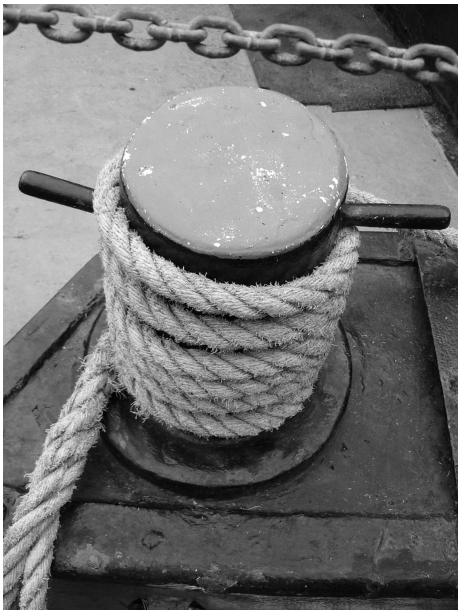

Moorings must be able to withstand very large forces. A set of equally sized loops around a mooring bollard allow for easy adjustment of the length of the mooring since the line can 'roll' over the mooring bollard.

Visualizing the formation and collapse of DNA toroids

Abstract – In living organisms, DNA is often confined into very small volumes. In most viruses, positively charged multivalent ions assist the condensation of DNA into tightly packed toroidal structures. Interestingly, such cations can also induce the spontaneous formation of DNA toroids *in vitro*. Despite many experimental and theoretical studies, the condensation dynamics and stability of DNA toroids are still not understood. Furthermore, in optical- and magnetic tweezers studies, condensates with toroidal shape are often assumed, yet no evidence for such structures under these conditions exists. Using a combination of optical tweezers and fluorescence imaging, we visualize in real-time the spermine-induced DNA condensation in single DNA molecules. By actively controlling the DNA extension, we are able to follow (de)condensation with high temporal and spatial resolution. Finally, we demonstrate that both processes occur in a quantized manner, caused by addition or removal of individual DNA loops from a toroidal condensate that is much smaller than previously assumed.

7.1 Introduction

In eukaryotic and prokaryotic organisms as well as in viruses, strongly positively charged polyamines, like spermine (4+) and spermidine (3+), play an important role in the compaction of DNA among a broad range of cellular processes [83, 174]. *In vitro*, polyamines can cause DNA to undergo a sharp condensation phase transition [201, 34, 67, 198]. In this process, DNA molecules aggregate into highly ordered structures, generally with toroidal or rod-like shapes, consisting of many (circumferentially wound) DNA strands [21, 85, 116, 117, 148]. Toroidal DNA condensates are of particular interest because of their striking similarity with the morphology of compacted DNA found in viruses and sperm cells. Moreover, despite previous (single-molecule) experiments addressing the forces and energies involved in the process of DNA (de)condensation [10, 126], little is known about the dynamics of toroid formation and the stability of such a condensate. In addition, an extensive, quantitative understanding of DNA toroid formation dynamics will be pertinent to the development and optimization of applications based on DNA-condensation, such as gene therapy [112, 187, 87]. Exploiting recent advances in single-molecule technology [113] we aim to address these issues.

7.2 Results

Here we visualize the reversible spermine-induced condensation of single DNA molecules into toroidal structures with high spatial- and temporal resolution using a combination of optical-tweezers and epi-fluorescence detection [129, 183]. This is achieved by attaching the endpoints of single λ-DNA molecules, sparsely labeled with the fluorescent dye YOYO-1, between two streptavidin-coated beads in a multi-channel flow chamber [129] (see Materials and methods).

In the presence of spermine (0.1 – 1 mM), the condensation force [10] keeps the sparsely stained DNA stretched and therefore visible at all end-to-end lengths. Any DNA condensates are expected to appear brighter, because of the increased local DNA density and thus dye concentration. Indeed, upon moving the endpoints of the DNA closer together, a single bright fluorescent DNA condensate emerges (see Fig. 7.1), a process that is fully reversible. The most immediate result of this experiment is that it provides direct evidence that DNA in solution under tension condenses into one single collapsed structure. Furthermore, the results demonstrate that in this case the surfaces of the polystyrene beads do not act as nucleation point for DNA condensation, nor do they seem to affect the process of DNA condensation in any other way. Comparison with the contour length reduction of the uncondensed part of the DNA molecule (grey dotted line) shows that most of the 'missing' DNA length is indeed included in the condensate (Fig. 7.1c, black trace).

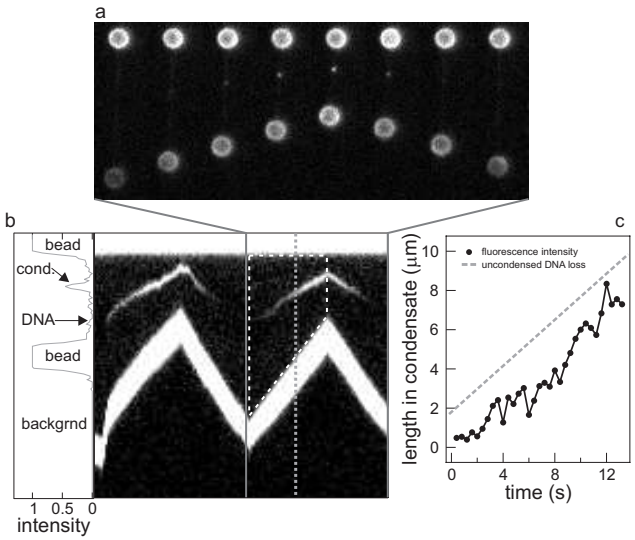

Figure 7.1: Real-time DNA condensation observed with fluorescence. a, Snapshots from a movie showing condensation in a single λ-DNA molecule fixed between two beads. As the extension is reduced by moving the lower bead, a bright condensate appears along the DNA contour, which increases in intensity. Upon DNA stretching at approximately the same rate, the intensity of the spot fades again, until bare DNA is left. Note that at all times, the uncondensed DNA remains in focus due to the force applied by the condensate. The constant condensation force [16, 176] suppresses lateral fluctuations of the DNA that occur in buffer without condensing agent. **b**, Kymograph of the complete movie, (duration 20 seconds), showing repeated condensation and decondensation of the same DNA molecule. The fraction of the movie in the top panel is highlighted by the solid line. The slope of the condensate is half that of the moving bead, implying that DNA condenses from both sides of the condensate at equal rates Similar results were obtained from other traces where the condensate was not situated in the middle of the DNA contour ($N = 7$). The dashed line shows the section that is used for the analysis in the inset. **c**, Quantitative analysis of the fluorescence intensity per pixel calibrated to the amount of DNA per pixel during condensation. Dashed gray line: DNA length in the condensate calculated from loss of uncondensed DNA length. Black data points: total fluorescence intensity of the DNA condensate in units of length, calculated from the kymograph (see Materials and methods). Quenching of dyes in the condensate due to close packing in the condensate might cause the observed fluorescence to be slightly less than expected.

To analyze how the condensate incorporates DNA we quantified the *fractional velocity* of the condensate with respect to the translocating bead. Its displacement over time was determined with sub-pixel resolution by fitting the spot in each image with a 2-D Gaussian. The fractional velocity of the condensate in the trace was found to be 0.50 ± 0.02, indicating that there is no preference from which of the two ends the DNA is added, i.e. the condensate is reeling in DNA from both sides. The same holds for de-condensation: DNA condensates unravel from both ends at equal rates. Based on this result one can envision diffusion-driven 'rolling' of condensates along DNA. However, at present we are cannot discriminate between such a diffusion mechanism and thermally driven fluctuations of a condensate fixed at one location.

The kinetics of DNA condensation formation in relaxed DNA molecules can be probed by changing buffer conditions for a single DNA molecule held in optical tweezers. Rapidly moving a relaxed DNA molecule into a buffer containing 100 μM spermine (< 1 s) using our laminar flow chamber results in the immediate formation of a DNA condensate. Likewise, upon removal of the condensed molecule from the spermine solution the condensate disappears just as quickly, and the worm-like chain (WLC) behavior of the DNA is restored. Using light-scattering techniques, condensation rates faster than 1 min^{-1}, the maximal attainable resolution, have been reported. Our results indicate that association and dissociation kinetics of condensing agent, in low ionic strength buffer, can be two orders of magnitude faster [75, 198].

Using fluorescence, we directly visualized the formation of DNA-condensates, but the initial formation and perhaps the structure of such a condensate can be studied by analyzing force-extension curves with high spatial resolution. To this end we let the DNA condense by reducing the end-to-end distance in a controlled fashion using two high-stiffness traps ($\sim$300 pN/μm). The force-extension curve of λ-DNA in the presence of 1 mM spermine (see Fig. 7.2) reveals a marked hysteresis. Relaxation of an uncondensed DNA molecule below a certain extension triggers an abrupt force increase (< 0.1 s) up to a rugged force plateau at $\sim$4 pN, similar to forces reported for other condensing agents [10, 126]. We attribute this event to the sudden initiation of a spermine-induced DNA condensate, as also observed in the fluorescence data. At the force plateau, the condensation force is balanced by the external DNA tension exerted by the optical traps. Markedly, upon stretching of the condensed molecule, the force plateau remains present at extensions considerably larger than the end-to-end length at nucleation. A distinct force drop then signifies the complete disruption of the condensate. The force-extension hysteresis, which is reproducibly observed in all stretch-release cycles (see Fig. 7.3), can be explained as follows: a gradual decrease in end-to-end distance results in increasing slack in the DNA molecule, modulating the energy landscape until at a critical force F_c the energy barrier to an unfavorable transition state has been lowered enough to initiate condensation. The formation of the DNA condensate under tension is thus nucleation-limited. This conclusion is

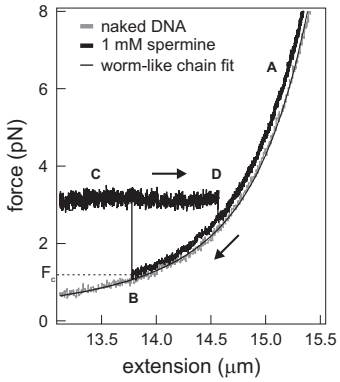

Figure 7.2: Toroid Kinetics. High-resolution force-extension curves of λ-DNA with (black) and without (grey) 1 mM spermine in the solution (N = 19). The extension of fully stretched DNA is slowly decreased until the tension reaches a critical force F_c at approximately 85% of the contour length. Then, suddenly the WLC behavior (A) disappears and the force rises abruptly (within 50-100 ms) to a value of ∼3.1 pN (B). This marked force jump indicates the collapse of part of the DNA into a condensate. With any further reduction in the extension, the force on the DNA stays roughly constant at forces of generally 2-5 pN. (C). When stretched again, this force balance remains stable up to significantly higher extensions (90% of the contour length), until a distinct force reduction down to the WLC curve signifies the disruption of the last piece of condensed DNA (D).

further supported by the results of the same experiment performed under constant force conditions (see Fig. 7.4). In this case, a larger fraction of the DNA abruptly (< 0.5 s) condenses when the imposed force drops below the critical force F_c. Our results are consistent with condensation behavior found in earlier constant-force experiments [16, 166], and is in good agreement with the finding that the onset of DNA condensation is the formation of a DNA loop due to random fluctuations of the polymer [16].

We also used force-extension analysis to study the condensation process after nucleation. We found that the observed 'roughness' of the force plateau [126] in fact consists of series of sawtooth-like steps. To elucidate this feature, the force-extension data was converted into *effective contour length* (see Materials and methods). Contour length traces of the relaxation of DNA in the presence of 1 mM spermine (see Fig. 7.5a) clearly show that the DNA molecule condenses in a stepwise manner: individual DNA segments of a defined length are added to the growing condensate one at a time. The stepwise behavior can be fitted with a step-fitting algorithm [98], yielding a broad distribution of step sizes (see Fig. 7.5b) with a dominant peak at ∼40 nm and a substantial number of back steps of the same length.

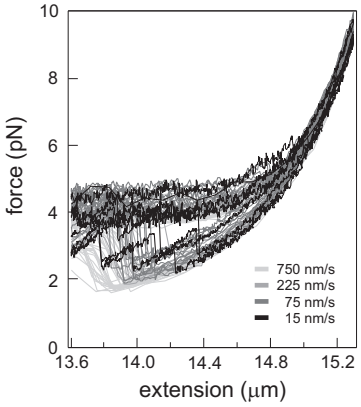

Figure 7.3: DNA relaxation speed dependence of nucleation hysteresis. a, The graph shows force-extension data from repeated stretch-release cycles with different speeds on the same λ-DNA molecule. In this dynamic force spectroscopy approach, the critical condensation force F_c depends on the relaxation speed of the DNA.

If the peak in the distribution of step sizes represents loops added onto the condensate, the step size would correspond to loops with a diameter of only 12 nm. How does this small step size fit with the observed larger toroids (50-100 nm in diameter) reported for bulk experiments [20, 87]? Compared to bulk studies where the DNA is free in solution during condensation, the minimum energy state for condensed DNA is dramatically altered for DNA kept under tension. While bending of relaxed DNA disfavors the formation of very small DNA loops, under tension the reduction of the end-to-end distance due to looping requires work that has to be performed against the opposing external force. These two energy contributions (bending and extension reduction) determine the energetically most favorable loop size. The total energy of a circular DNA loop with diameter d and persistence length l_p under an applied force F is:

$$E_{\text{loop}} = \frac{2\pi k_B T l_p}{d} + d\pi F \tag{7.1}$$

Energy minimization leads to the most probable diameter of a loop [16]:

$$d = 2\sqrt{\frac{k_B T l_p}{2F}} \tag{7.2}$$

For an external force of 2–5 pN as applied here and $l_p \approx 50$ nm, Equation 7.2 results in $d = 14$–9 nm, or a circumference of 30–45 nm, almost an order of magnitude smaller than the diameter of DNA toroids in the absence of tension [85, 87]. The optimal loop length for DNA under an applied tension matches very well with a condensation

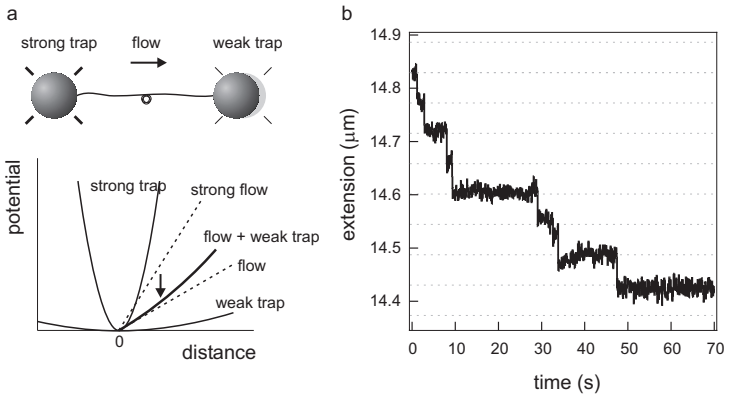

Figure 7.4: condensation against a nearly constant force. a, When a DNA condensing experiment as described in the main text is performed under constant force conditions (one bead in an optical trap, one bead in flow), a substantial fraction (»50%) of the DNA is abruptly (< 500 ms) condensed. This is consistent with the nucleation-limited condensation as found in earlier constant-force experiments [16, 166]. In order to slow down DNA condensation against a constant force, a slightly parabolically rising potential was created by applying a second optical trap with substantially reduced stiffness ($\sim$0.3 pN/μm). The maximum applicable force with such a weak trap is too low to oppose the pulling force of the DNA condensate. Therefore, the required force was predominantly created by added hydrodynamic flow on the free bead. The superimposed weak trap causes a slight increase in tension with distance from the trap center. **b**, When the drag force on uncondensed DNA is reduced below a threshold value, stepwise condensation is observed. As the decrease in DNA extension pulls the bead out of the trap center, the force increases just enough to put up a small energy barrier preventing the wrapping of the next loop. This way, consecutive condensation steps, with a mean step size of $\sim$50 nm, were observed until the bead was completely pulled out of the optical trap. Further condensation proceeded at the usual rapid pace.

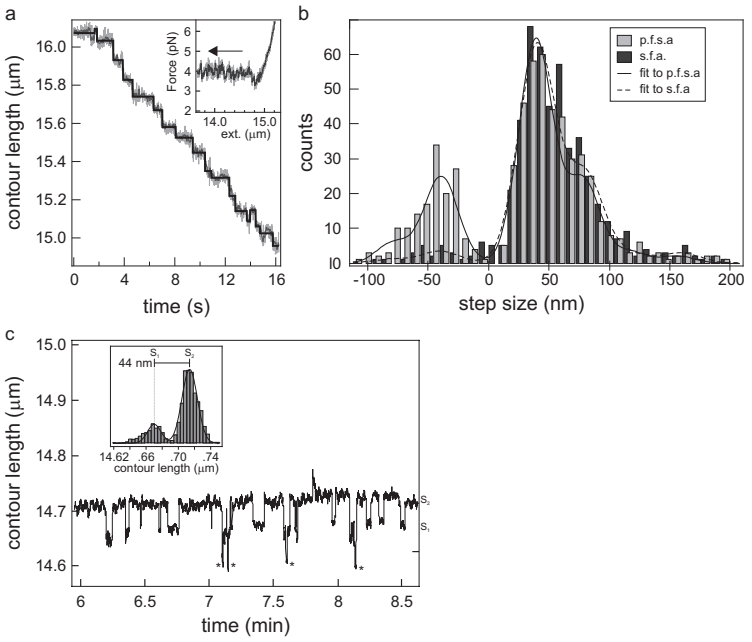

Figure 7.5: Stepwise DNA condensation. **a**, Contour length plot of condensing DNA, constructed from the measured force and extension data. Data is shown at 128 Hz (grey), and averaged to 16 Hz, rank 2 median filtered (dark grey). The data show that DNA condensation proceeds in discrete steps. The solid black line is the output of the step fitting algorithm (s.f.a). Occasionally, transient back steps can be problematic (see top left and bottom right). The fits are therefore checked manually using a plateau fitting step analysis (p.f.s.a). The inset shows the corresponding force-extension curve. **b**, Histograms of step sizes, acquired from several condensation traces on different DNA molecules. The distributions obtained from p.f.s.a (light bars, $N = 592$ steps) and s.f.a. (dark bars, $N = 501$ steps) virtually overlap, but the p.f.s.a yields an accurate amount of back-steps. The data is weighed fit with a function consisting of multiple Gaussians having equal widths σ, spaced at integer multiples of the elementary step size x_0. Obtained parameters are: $x_0 = 40 \pm 1$ nm, $\sigma = 22$ nm with normalized $\chi^2 = 1.1$ (s.f.a.) and $x_0 = 39 \pm 1$ nm, $\sigma = 20$ nm with normalized $\chi^2 = 1.3$ (p.f.s.a.). **c**, Reversible wrapping of a single DNA loop. The effective contour length of the DNA switches between two distinct values. The distance between the two peaks in the dwell time histogram (inset) is 44 nm, indicative of a single toroid loop. Occasionally, a second loop is transiently added to the toroid (marked with stars).

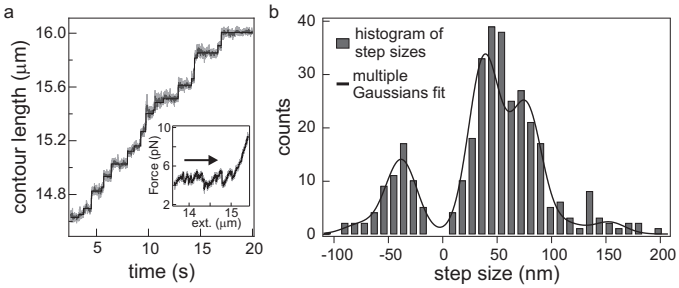

Figure 7.6: Stepwise disruption of DNA toroids. **a**, Contour length plot of forced stepwise de-condensing of DNA. Like the condensation process, DNA de-condensation proceeds in discrete steps. The solid line shows the output of the step fitting algorithm. The inset displays the force-extension curve corresponding to the data. **b**, Histograms of disruption step sizes, acquired from multiple de-condensation traces on several DNA molecules. Steps were analyzed by plateau fitting. The distribution is quantitatively similar to the toroid formation histograms in Figure 7.5b. Fitting with the same function as used for stepwise condensation results in $x_0 = 39 \pm 1$ nm, $\sigma = 20$ nm (normalized $\chi^2 = 1.2$), essentially the same parameters as found for condensing DNA.

scheme in which condensation proceeds by wrapping equally sized small DNA loops of ∼40 nm onto a toroidal condensate. When plotting the time evolution of steps, we observe that this is indeed the case; the size of the loops added to the condensate remains constant over time (see Fig. 7.7).

We can use this result to explain the broad distribution of step sizes to arise from the winding of single- and multiple loops of the same diameter. Based on this interpretation the distribution should be well described by multiple equidistant Gaussians with equal widths. Indeed we find a DNA loop length of 40 ± 1 nm (s.e.m.) (see Fig. 7.5a), as predicted above. An identical stepwise increase of the contour length (39 ± 1 nm) is observed when the condensed DNA is disrupted (see Fig. 7.6).

In many of the DNA relaxation and stretching (toroid formation and disruption) traces, transient back steps are observed (see for example Fig. 7.5a). The contour length change in these steps is found to be comparable to that of one toroid loop, approximately 40 nm (see Fig. 7.5b and Fig. 7.6b). This apparent reversible wrapping of DNA loops onto the toroid can most clearly be demonstrated when the DNA end-to-end distance is held fixed when a condensate is present, i.e., somewhere in the force plateau (see Fig. 7.5c). The contour length is observed to switch between two distinct values, in this case 44 nm apart, signifying the reversible addition and removal of a single toroid loop. As the winding is done against an external force of ∼5 pN, the gained binding energy of such a loop is enormous: $\sim 60\, k_B T$ ($\sim 0.4\, k_B T$/bp). However, the inclusion of a DNA loop into the toroid causes a shortening of the uncondensed DNA, which increases the mechanical strain in the molecule. Due to this effect the

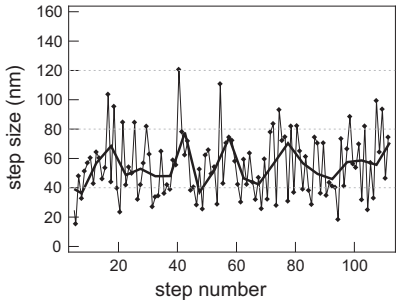

Figure 7.7: Time evolution of observed steps in a condensing DNA molecule. Data points show consecutive positive step sizes obtained from two different traces, acquired with s.f.a. Black line indicates the mean step size, averaged over 5 steps. This graph indicates that there is no significant trend in the size of individual loops wrapped onto the DNA toroid.

difference between the two energy states (S_1 and S_2) becomes small enough to be overcome by thermal fluctuations to overcome. From the relative occupancies of the two states in the trace (see Fig. 7.5c, inset) we calculate the energy difference between S_1 and S_2 to be only $\sim$1.5 k_BT. Together with the occasional second loop that is transiently added to the toroid (marked with stars) this also indicates that the energy barrier between the two states is only several k_BT maximum.

In order to investigate the energy landscape of toroid formation, we performed dynamic force spectroscopy [59] on the formation of the initial toroid. As DNA tension influences transitions from one state to another, the critical force F_c (the DNA tension at which condensation commences (see Fig. 7.2)), should depend on the rate at which this force is reduced. In our approach, we decreased the energy barrier to the transition state for nucleation by lowering the force at various unloading rates (by relaxing the DNA with pre-set speeds). We measured F_c as a function of DNA relaxation rate in several stretch-release cycles on the same λ-DNA molecule (see Fig. 7.3). The resulting spectrum reveals that the nucleation hysteresis indeed depends on the unloading rate (see Fig. 7.8). It can be characterized by a linear fit, indicating that there is a single kinetic barrier in the energy landscape of the transition state. From the slope of the fit we determine the distance to the transition state, the energetically disfavored state in the condensation pathway, to be 27 ± 3 nm, about two thirds of the observed toroid loop length. We hypothesize that, when thermal fluctuations are able to create a local molecular slack larger than $\sim$27 nm, a first DNA loop can be formed. In the presence of spermine, the attraction between close DNA segments somewhat stabilizes this loop, facilitating expansion of the "overlapping" DNA regions. The condensate then quickly recruits more of its neighboring DNA until a force balance between condensate and traps is achieved (see also Fig. 7.9). Apparently, this process

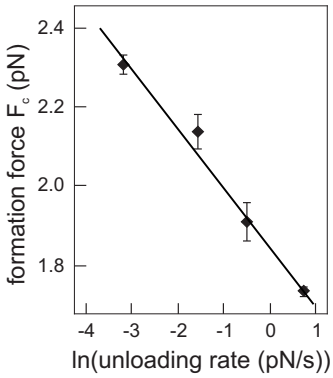

Figure 7.8: Dynamic force spectroscopy on condensing DNA. The critical condensation force F_c depends on the relaxation speed of the DNA (see Fig. 7.3. Hence, the kinetic barrier in the energy landscape impeding DNA condensation is lowered by reducing the force. By fitting the slope of F_c versus the natural logarithm of the unloading rate with a line (linear correlation coefficient r = -0.93, normalized $\chi^2 = 0.9$), the distance to this barrier is found to be ∼27 nm.

starts as soon as a single loop is present. However, one would only expect a stable condensate when there is sufficient overlap, i.e. when more than one loop is present.

To further investigate the nature of DNA condensates we focus on an intriguing feature of the force-extension curve: the point where, when stretching the polymer, the force plateau changes back into WLC-elasticity (Fig 7.2a, step D). The sudden transition, marked by an irreversible drop in tension, suggests that this last step in the disruption process represents the destruction of the smallest stable condensed structure. Figure 7.10a displays a distribution of the contour length gained in such last steps. The measured distribution fits the same function of multiple Gaussians as before; again we find an elementary step size of 38 nm. Interestingly, no steps smaller than 50 nm are observed; the first peak is located at 76 nm. This implies that a stable toroid structure comprises a minimum of two DNA loops, in line with our expectation. This behavior can be understood when a hexagonally packed toroidal condensate [85, 87] structure is assumed. Because of removal of shared nearest-neighbor interactions, the average binding energy per remaining DNA loop decreases non-linearly with the number of turns still present in the toroid [20, 85, 87]. The number of inter-strand interactions per DNA loop declines steeply when only approximately four DNA loops are left (see Fig. 7.10b). Eventually, the energy barrier for removing the next DNA loop in the disruption process becomes sufficiently small for thermal fluctuations to release all of the residual loops rapidly after each other (see Fig. 7.10a, inset). The experimental results are in agreement with this idea: the most frequent step size we find is equal to 150 nm, or about four loops. Within this model a toroid consisting of only one

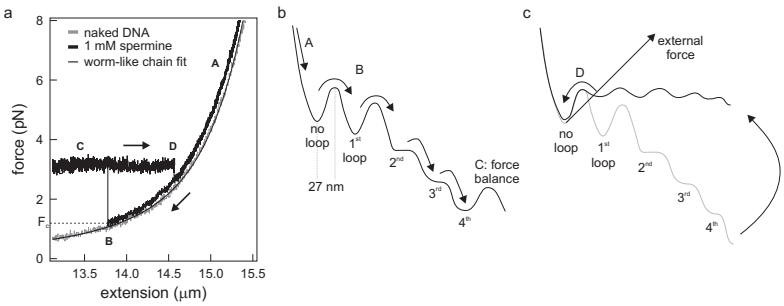

Figure 7.9: Toroid formation energy landscape. a, Force-extension curves of λ-DNA with (black) and without (gray) 1 mM spermine in the solution (the same as Figure 7.2). Slowly decreasing the extension of fully stretched DNA until the tension reaches a critical force the WLC-behavior (A) suddenly disappears and the force abruptly rise to a value of ∼3.5 pN (B). This indicates the collapse of part of the DNA. Further condensation occurs at constant force (C). When stretched again, this balance remains stable up to much higher extensions until a distinct force jump down to the WLC-curve signifies the disruption of the last piece of condensed DNA (D). **b**, Energy landscape of toroid formation. Letters correspond to the letters in panel a. As soon as the critical force is reached, the attraction caused by the presence of spermine somewhat stabilizes the first looped state and slightly lowers the barrier to the second looped state (B). As soon as a stable condensate is formed, subsequent loops can be added to the condensate until a balance between the condensation force and the external (trapping) force is reached (C). **c**, Under an external force, as indicated in the Figure and in our experiments induced by the optical tweezers, the energy landscape is tilted and as a result the energy barriers between the different states are lowered. This causes the toroid to unravel until no loops are present in the condensate.

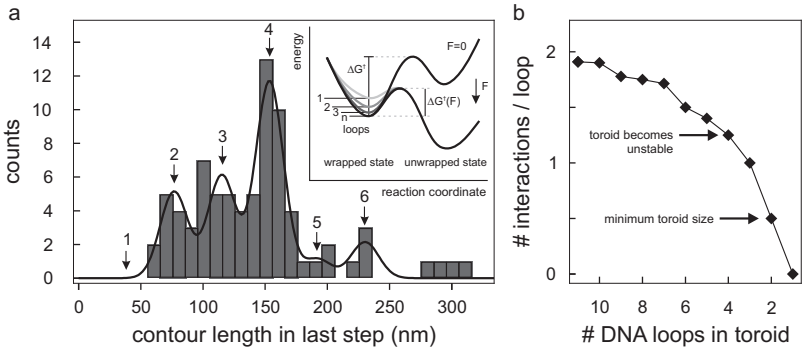

Figure 7.10: Minimum stable toroid size. **a**, Distribution of observed last-step sizes in the toroid disruption process (N = 74). No steps of 40 nm are detected (indicated with the arrow at "1"). The most common last step is ∼150 nm, comprising four DNA loops. The data is fit with multiple Gaussians, resulting in a step size $x_0 = 38 \pm 1$ nm with width $\sigma = 17$ nm. **Inset**, Schematic diagram of the energy landscape during the unraveling of a loop. Extending the DNA increases the force on the toroidal condensate, resulting in a lowered energy barrier to the unwrapped state. **b**, Number of interactions per remaining DNA loop in a toroid-shaped condensate, assuming a hexagonally packed structure. The curve shows a steep decline starting roughly at four loops.

loop does not have sufficient overlap and is unstable. Indeed, while we regularly find smallest toroids consisting of two and three loops, we never observe single loops as last disruption steps.

7.3 Discussion

Our (de-)condensation data (see Fig. 7.5 and Fig. 7.6) show the continues (de-)formation of small (∼40 nm) DNA loops throughout the condensation process. Why does the size of these loops stay constant? To release bending strain, DNA loops could in principle slide along each other, increasing their size and decreasing their number, while maintaining maximal contact area. Apparently this does not happen. From our data, it thus appears that the size of the nucleation loop, rather than thermodynamics, determines the final diameter of the fully formed DNA toroid [36]. Nonetheless, if the loops would slide along each other and thermodynamical parameters eventually dictate the toroid size, only a weak dependence of the loop length on the number of loops is expected as described by Schnurr *et al.* [152]. Due to the small loop length of ∼40 nm our data traces of condensation of several micrometers of DNA must contain over a hundred DNA turns. In a proposed toroid model [86], contiguous DNA loops of equal size presses around the toroid axis. The radius of each such loop is equal to the average of the inside and outside radii of the toroid.

But why do DNA condensates unfold in a stepwise manner? Gradually reeling in or peeling off DNA appears to be energetically more favorable than condensing or disrupting it in a quantized manner. However, it was recently demonstrated that a spool-like structure is kinetically protected from mechanical disruption because an unfavorable rotation of the toroid under tension is required for unwrapping [102]. Both our formation and disruption data are in agreement with such a model.

The disruption of DNA condensates with optical tweezers has been reported earlier [10, 126] and circumferences of individual turns of DNA toroids in low monovalent salt buffer were found to peak around 300 nm. What is the explanation for the large mismatch with the much smaller step sizes that we find, suggesting much smaller DNA toroids? From the previous experiments it was thought that there are two regimes in DNA condensation. The first, so-called 'stick-release' events, observed in high concentrations of condensing agent, were viewed upon as the discrete unfolding of the condensate. The second regime, the constant force plateau observed at lower concentrations, was associated with a continuous transition between condensed and relaxed DNA. We reveal here that there is no qualitative difference between 'plateau' and stick-slip. Both regimes are characteristic of the stepwise unraveling of condensed DNA, yet at high concentrations of condensing agent, the enhanced attraction between DNA tracts in the toroid causes disruption to occur in irregular large steps comprising multiple toroid loops. This conclusion is further supported by analysis of some of our force-extension curves in which we observed modest stick-slip behavior. By evaluating those events, we could qualitatively reproduce the shape of the step size distribution obtained previously [126] with in this case a most frequent step size of 150-200 nm (see Fig. 7.11).

7.4 Outlook

In conclusion, we have demonstrated the formation of toroidal structures due to DNA condensation (by visualizing DNA condensation in real-time). With the observation that toroids reel in DNA from both ends we have first demonstrated a mechanism for toroid formation. Second, this observation provides a starting point for diffusion-driven mobility, explaining the formation of closely spaced toroids as observed in sperm cells [84]. We therefore expect our results to be a basis for more sophisticated *in vivo* models of DNA condensates. Future experiments could for instance involve diffusion of DNA toroids 'rolling' along the DNA contour. Furthermore, DNA toroids are a major candidate as a delivery vehicle in gene therapy [87, 112, 187]. Extensive and quantitative assays of formation and deformation kinetics will be relevant for developments in this direction.

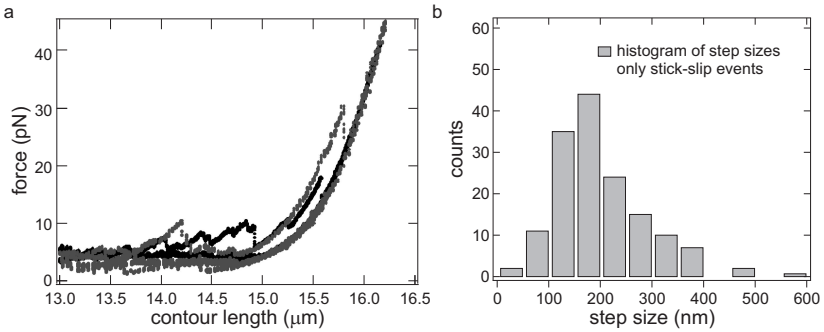

Figure 7.11: Stepwise disruption of DNA toroids. a, High-resolution force-extension curves of λ-DNA in the presence of 0.25-1 mM spermine that exhibit modest stick-slip behavior. **b**, Distribution of stick-release events, analyzed by plateau fitting. Notice the difference in most frequent step size with the main graph. The stepwise unraveling of condensed DNA, in the case of high concentrations, is apparently dominated by the enhanced attraction between DNA tracts in the toroid and causes disruption to occur in irregular large steps comprising multiple toroid loops.

7.5 Acknowledgements

We thank F.C. MacKintosh, H. Schiessel, K. Besteman and S.G. Lemay for useful discussions.

7.6 Materials and methods

7.6.1 DNA and spermine

Lambda phage dsDNA (Roche Applied Science) was biotinylated on both ends, as described previously [181]. Spermine (Fluka Biochemika - Sigma-Aldrich) was dissolved into distilled de-ionized water (milliQ) to a stock concentration of 100 mM and stored at 4 °C. Spermine stock solutions were used for up to two weeks. In all experiments spermine was diluted to a final concentration of 100 μM to 1 mM in TE buffer containing 10 mM Tris and 1 mM EDTA, pH 7.5.

7.6.2 Experimental setup

The experimental setup used was described previously [129]. For the experiments reported here two optical traps were employed. One stationary trap was used for force detection, while the other trap could be steered through the sample with nanometer precision using acousto-optical deflectors (AODs). The motion of the bead during DNA stretching and relaxation was continuous with speeds varying from 15 to

750 nm s^{-1}. Inter-bead distances were calculated in real-time by video image analysis at 8 Hz. Raw force data was sampled at 8 kHz and pre-averaged to 128 Hz before analysis. The combined dual optical trap and fluorescence excitation and detection system has been described previously [113]. High-sensitivity fluorescence imaging is obtained using a 473 nm laser excitation source and a Cascade 512B CCD camera interfaced with the WinView software package (both from Roper Scientific). In order to leave the elastic properties of DNA unaffected and prevent interference of the (positively charged) fluorescent YOYO-1 with the condensation process [199, 208], the number of dye molecules per DNA was kept low enough to prevent detectable dye-induced lengthening of the DNA [13]. DNA condensation and de-condensation was imaged without fluorescent dye in the solution, in a buffer containing ∼1 mM spermine, with an exposure time of 0.4 seconds. The size of observed DNA condensates in the fluorescence images is limited by diffraction of the excitation light (473 nm) and is spread out over several pixels. Its position along the DNA can however be extracted with sub-pixel precision by fitting the spot with a 2-D Gaussian [175].

7.6.3 Fluorescence analysis

From the fluorescence images, a kymograph was constructed. This was done by a) selecting a narrow box encompassing the DNA contour in all frames, b) integrating the pixel values across the DNA to obtain a single line of pixels per frame, c) subtracting background values, and d) pasting these pixel lines into consecutive columns of a single image. Thus, in the kymograph pixel columns represent the total fluorescence intensity of the DNA, while rows indicate time. From the kymograph, the total DNA length incorporated in the condensate was calculated by comparing the fluorescence intensity of the bright condensate with that of the uncondensed DNA on both sides of it, averaged over a width of 7 pixels. This way, in-homogeneities of the excitation light are corrected for.

7.6.4 Step analysis

For each data point with force F and extension x the apparent DNA length L is calculated by rewriting the well-known interpolation formula for worm-like chain elasticity [28] into:

$$L(x,F) = \frac{1}{x}\left(1 - \sqrt{\frac{k_B T}{F l_p}}\right)\left(1 + \frac{F}{K}\right). \tag{7.3}$$

Here is k_B the Boltzmann constant, T the temperature and K the stretch modulus of double stranded DNA [130, 159]. For uncondensed DNA this simply results in a

constant value L_0 (~16.4 μm for λ-DNA) for all extensions. In a partially condensed λ-DNA molecule, the uncondensed part of the DNA still obeys the worm-like chain, but a DNA length x is lost into a small ($d \ll L$) and inextensible condensate. The measured elasticity then corresponds to that of a DNA molecule with length $L = L_0 - x$. Changes in L over time thus correspond to DNA being incorporated into or released from the DNA condensate. To extract DNA loop sizes from the contour length traces, we used a semi-automated fitting procedure [98]. This algorithm has been proved successful in fitting steps in noisy data [40, 162]. The number of steps in each trace was optimized by thoroughly inspecting the obtained fits. The step fitting algorithm sometimes had problems finding transient back steps, occasionally leading to a misfit (an example can be seen in Fig. 7.5a). To test whether this has an effect on the step size distribution, we also tracked step sizes of the same traces by a different method. This was done by computing the differences between averages of the data in each (hand-picked) plateau. In both procedures, analysis was performed on data re-sampled to 128 Hz. The distribution obtained from this plateau fitting step analysis is virtually identical to the one acquired by using the step fitting algorithm (Fig. 7.5b). The only significant difference is the amount of detected back steps. Fitting results in a value of 39 ± 1 nm for the DNA loop length, equivalent to that obtained with the step fitting algorithm (40 ± 1 nm).

Bibliography

[1] B. M. Ali, R. Amit, I. Braslavsky, A. B. Oppenheim, O. Gileadi, and J. Stavans. Compaction of single DNA molecules induced by binding of integration host factor (IHF). *Proc Natl Acad Sci U S A*, 98(19):10658–63, 2001.

[2] M. W. Allersma, F. Gittes, M. J. deCastro, R. J. Stewart, and C. F. Schmidt. Two-dimensional tracking of ncd motility by back focal plane interferometry. *Biophysical Journal*, 74(2 Pt 1):1074–85, 1998.

[3] R. Amit, A. B. Oppenheim, and J. Stavans. Increased bending rigidity of single DNA molecules by H-NS, a temperature and osmolarity sensor. *Biophys J*, 84(4):2467–73, 2003.

[4] Y. Arai, R. Yasuda, K. Akashi, Y. Harada, H. Miyata, Jr. Kinosita, K., and H. Itoh. Tying a molecular knot with optical tweezers. *Nature*, 399(6735):446–8, 1999.

[5] A. Ashkin. Acceleration and Trapping of Particles by Radiation Pressure. *Physical Review Letters*, 24(4):156–&, 1970.

[6] A. Ashkin and J. M. Dziedzic. Optical Trapping and Manipulation of Viruses and Bacteria. *Science*, 235(4795):1517–1520, 1987.

[7] A. Ashkin, J. M. Dziedzic, and T. Yamane. Optical Trapping and Manipulation of Single Cells Using Infrared-Laser Beams. *Nature*, 330(6150):769–771, 1987.

[8] C. Badaut, R. Williams, V. Arluison, E. Bouffartigues, B. Robert, H. Buc, and S. Rimsky. The degree of oligomerization of the H-NS nucleoid structuring protein is related to specific binding to DNA. *Journal of Biological Chemistry*, 277(44):41657–41666, 2002.

[9] C. A. Ball, R. Osuna, K. C. Ferguson, and R. C. Johnson. Dramatic changes in Fis levels upon nutrient upshift in Escherichia coli. *J Bacteriol*, 174(24):8043–56, 1992.

[10] C. G. Baumann, V. A. Bloomfield, S. B. Smith, C. Bustamante, M. D. Wang, and S. M. Block. Stretching of single collapsed DNA molecules. *Biophysical Journal*, 78(4):1965–1978, 2000.

[11] S. D. Bell, C. H. Botting, B. N. Wardleworth, S. P. Jackson, and M. F. White. The interaction of Alba, a conserved archaeal chromatin protein, with Sir2 and its regulation by acetylation. *Science*, 296(5565):148–51, 2002.

[12] C. Beloin, J. Jeusset, B. Revet, G. Mirambeau, F. Le Hegarat, and E. Le Cam. Contribution of DNA conformation and topology in right-handed DNA wrapping by the Bacillus subtilis LrpC protein. *J Biol Chem*, 278(7):5333–42, 2003.

[13] M. L. Bennink, O. D. Scharer, R. Kanaar, K. Sakata-Sogawa, J. M. Schins, J. S. Kanger, B. G. de Grooth, and J. Greve. Single-molecule manipulation of double-stranded DNA using optical tweezers: interaction studies of DNA with RecA and YOYO-1. *Cytometry*, 36(3):200–8, 1999.

[14] O. G. Berg, R. B. Winter, and P. H. von Hippel. Diffusion-driven mechanisms of protein translocation on nucleic acids. 1. Models and theory. *Biochemistry*, 20(24):6929–48, 1981.

[15] K. Berg-Sorensen and H. Flyvbjerg. Power spectrum analysis for optical tweezers. *Review of Scientific Instruments*, 75(3):594–612, 2004.

[16] K. Besteman, S. Hage, N. H. Dekker, and S. G. Lemay. Role of tension and twist in single-molecule DNA condensation. *Phys Rev Lett*, 98(5):058103, 2007.

[17] G. Binnig, C. F. Quate, and C. Gerber. Atomic force microscope. *Physical Review Letters*, 56(9):930–933, 1986.

[18] V. Bloch, Y. Yang, E. Margeat, A. Chavanieu, M. T. Auge, B. Robert, S. Arold, S. Rimsky, and M. Kochoyan. The H-NS dimerization domain defines a new fold contributing to DNA recognition. *Nat Struct Biol*, 10(3):212–8, 2003.

[19] S. M. Block and K. Svoboda. Analysis of high resolution recordings of motor movement. *Biophys J*, 68(4 Suppl):2305S–2395S; discussion 2395S–2415S, 1995.

[20] V. A. Bloomfield, S. He, A. Z. Li, and P. B. Arscott. Light scattering studies on DNA condensation. *Biochem Soc Trans*, 19(2):496, 1991.

[21] C. Bottcher, C. Endisch, J. H. Fuhrhop, C. Catterall, and M. Eaton. High-yield preparation of oligomeric C-type DNA toroids and their characterization by cryoelectron microscopy. *Journal of the American Chemical Society*, 120(1):12–17, 1998.

[22] L. R. Brewer, M. Corzett, and R. Balhorn. Protamine-induced condensation and decondensation of the same DNA molecule. *Science*, 286(5437):120–3, 1999.

[23] A. B. Brinkman, T. J. Ettema, W. M. de Vos, and J. van der Oost. The Lrp family of transcriptional regulators. *Mol Microbiol*, 48(2):287–94, 2003.

[24] R. A. Britton, D. C. Lin, and A. D. Grossman. Characterization of a prokaryotic SMC protein involved in chromosome partitioning. *Genes Dev*, 12(9):1254–9, 1998.

[25] Robert Brown. A brief account of microscopical observations made in the months of June, July and August, 1827, on the particles contained in the pollen of plants; and on the general existence of active molecules in organic and inorganic bodies. *Phil. Mag.*, 4:161–173, 1828.

[26] Robert Brown. Observations on the organs and mode of fecundation in Orchideae and Asclepiadeae. *Trans. Linn. Soc. London*, 16:685–745, 1932.

[27] C. Bustamante, J. C. Macosko, and G. J. L. Wuite. Grabbing the cat by the tail: Manipulating molecules one by one. *Nature Reviews Molecular Cell Biology*, 1(2):130–136, 2000.

[28] C. Bustamante, J. F. Marko, E. D. Siggia, and S. Smith. Entropic elasticity of lambda-phage DNA. *Science*, 265(5178):1599–600, 1994.

[29] J. M. Calvo and R. G. Matthews. The leucine-responsive regulatory protein, a global regulator of metabolism in Escherichia coli. *Microbiol Rev*, 58(3):466–90, 1994.

[30] C. J. Camacho and S. Vajda. Protein docking along smooth association pathways. *Proc Natl Acad Sci U S A*, 98(19):10636–41, 2001.

[31] P. Ceci, S. Cellai, E. Falvo, C. Rivetti, G. L. Rossi, and E. Chiancone. DNA condensation and self-aggregation of Escherichia coli Dps are coupled phenomena related to the properties of the N-terminus. *Nucleic Acids Res*, 32(19):5935–44, 2004.

[32] S. Ceschini, G. Lupidi, M. Coletta, C. L. Pon, E. Fioretti, and M. Angeletti. Multimeric self-assembly equilibria involving the histone-like protein H-NS. A thermodynamic study. *J Biol Chem*, 275(2):729–34, 2000.

[33] G. Charvin, A. Vologodskii, D. Bensimon, and V. Croquette. Braiding DNA: experiments, simulations, and models. *Biophys J*, 88(6):4124–36, 2005.

[34] D. K. Chattoraj, L. C. Gosule, and A. Schellman. DNA condensation with polyamines. II. Electron microscopic studies. *J Mol Biol*, 121(3):327–37, 1978.

[35] S. Chu, L. Hollberg, J. E. Bjorkholm, A. Cable, and A. Ashkin. 3-Dimensional Viscous Confinement and Cooling of Atoms by Resonance Radiation Pressure. *Physical Review Letters*, 55(1):48–51, 1985.

[36] C. C. Conwell, I. D. Vilfan, and N. V. Hud. Controlling the size of nanoscale toroidal DNA condensates with static curvature and ionic strength. *Proc Natl Acad Sci U S A*, 100(16):9296–301, 2003.

[37] Y. Cui, Q. Wang, G. D. Stormo, and J. M. Calvo. A consensus sequence for binding of Lrp to DNA. *J Bacteriol*, 177(17):4872–80, 1995.

[38] R. T. Dame. The role of nucleoid-associated proteins in the organization and compaction of bacterial chromatin. *Mol Microbiol*, 56(4):858–70, 2005.

[39] R. T. Dame, M. S. Luijsterburg, E. Krin, P. N. Bertin, R. Wagner, and G. J. Wuite. DNA bridging: a property shared among H-NS-like proteins. *J Bacteriol*, 187(5):1845–8, 2005.

[40] R. T. Dame, M. C. Noom, and G. J. Wuite. Bacterial chromatin organization by H-NS protein unravelled using dual DNA manipulation. *Nature*, 444(7117):387–90, 2006.

[41] R. T. Dame, J. van Mameren, M. S. Luijsterburg, M. E. Mysiak, A. Janicijevic, G. Pazdzior, P. C. van der Vliet, C. Wyman, and G. J. Wuite. Analysis of scanning force microscopy images of protein-induced DNA bending using simulations. *Nucleic Acids Res*, 33(7):e68, 2005.

[42] R. T. Dame and G. J. Wuite. On the role of H-NS in the organization of bacterial chromatin: from bulk to single molecules and back. *Biophys J*, 85(6):4146–8, 2003.

[43] R. T. Dame, C. Wyman, and N. Goosen. H-NS mediated compaction of DNA visualised by atomic force microscopy. *Nucleic Acids Res*, 28(18):3504–10, 2000.

[44] R. T. Dame, C. Wyman, and N. Goosen. Structural basis for preferential binding of H-NS to curved DNA. *Biochimie*, 83(2):231–4, 2001.

[45] R. T. Dame, C. Wyman, R. Wurm, R. Wagner, and N. Goosen. Structural basis for H-NS-mediated trapping of RNA polymerase in the open initiation complex at the rrnB P1. *J Biol Chem*, 277(3):2146–50, 2002.

[46] T. den Blaauwen, A. Lindqvist, J. Lowe, and N. Nanninga. Distribution of the Escherichia coli structural maintenance of chromosomes (SMC)-like protein MukB in the cell. *Mol Microbiol*, 42(5):1179–88, 2001.

[47] S. Deng, R. A. Stein, and N. P. Higgins. Transcription-induced barriers to supercoil diffusion in the Salmonella typhimurium chromosome. *Proc Natl Acad Sci U S A*, 101(10):3398–403, 2004.

[48] S. Deng, R. A. Stein, and N. P. Higgins. Organization of supercoil domains and their reorganization by transcription. *Mol Microbiol*, 57(6):1511–21, 2005.

[49] G. M. Dhavan, D. M. Crothers, M. R. Chance, and M. Brenowitz. Concerted binding and bending of DNA by Escherichia coli integration host factor. *J Mol Biol*, 315(5):1027–37, 2002.

[50] M. E. Dinger, G. J. Baillie, and D. R. Musgrave. Growth phase-dependent expression and degradation of histones in the thermophilic archaeon Thermococcus zilligii. *Molecular Microbiology*, 36(4):876–885, 2000.

[51] S. Dole, V. Nagarajavel, and K. Schnetz. The histone-like nucleoid structuring protein H-NS represses the Escherichia coli bgl operon downstream of the promoter. *Mol Microbiol*, 52(2):589–600, 2004.

[52] C. J. Dorman. H-NS: a universal regulator for a dynamic genome. *Nat Rev Microbiol*, 2(5):391–400, 2004.

[53] K. Drlica and J. Rouviere-Yaniv. Histonelike proteins of bacteria. *Microbiol Rev*, 51(3):301–19, 1987.

[54] R. Eckel, S. D. Wilking, A. Becker, N. Sewald, R. Ros, and D. Anselmetti. Single-molecule experiments in synthetic biology: an approach to the affinity ranking of DNA-binding peptides. *Angew Chem Int Ed Engl*, 44(25):3921–4, 2005.

[55] M. Eltsov and B. Zuber. Transmission electron microscopy of the bacterial nucleoid. *J Struct Biol*, 156(2):246–54, 2006.

[56] M. Engelhorn, F. Boccard, C. Murtin, P. Prentki, and J. Geiselmann. In vivo interaction of the Escherichia coli integration host factor with its specific binding sites. *Nucleic Acids Res*, 23(17):2959–65, 1995.

[57] V. Epshtein, F. Toulme, A. R. Rahmouni, S. Borukhov, and E. Nudler. Transcription through the roadblocks: the role of RNA polymerase cooperation. *Embo J*, 22(18):4719–27, 2003.

[58] D. Esposito, A. Petrovic, R. Harris, S. Ono, J. F. Eccleston, A. Mbabaali, I. Haq, C. F. Higgins, J. C. Hinton, P. C. Driscoll, and J. E. Ladbury. H-NS oligomerization domain structure reveals the mechanism for high order self-association of the intact protein. *J Mol Biol*, 324(4):841–50, 2002.

[59] E. Evans. Probing the relation between force–lifetime–and chemistry in single molecular bonds. *Annu Rev Biophys Biomol Struct*, 30:105–28, 2001.

[60] M. Falconi, M. T. Gualtieri, A. Lateana, M. A. Losso, and C. L. Pon. Proteins from the Prokaryotic Nucleoid - Primary and Quaternary Structure of the 15-Kd Escherichia-Coli DNA-Binding Protein H-Ns. *Molecular Microbiology*, 2(3):323–329, 1988.

[61] W Flemming. *Zellsubstanz, Kern und Zelltheilung*. FCW Vogel, Leipzig, 1882.

[62] D. Frenkiel-Krispin, I. Ben-Avraham, J. Englander, E. Shimoni, S. G. Wolf, and A. Minsky. Nucleoid restructuring in stationary-state bacteria. *Mol Microbiol*, 51(2):395–405, 2004.

[63] W. Fritzsche, L. Takac, and E. Henderson. Application of atomic force microscopy to visualization of DNA, chromatin, and chromosomes. *Crit Rev Eukaryot Gene Expr*, 7(3):231–40, 1997.

[64] F. Gittes and C. F. Schmidt. Interference model for back-focal-plane displacement detection in optical tweezers. *Optics Letters*, 23(1):7–9, 1998.

[65] F. Gittes and C. F. Schmidt. Signals and noise in micromechanical measurements. *Methods in Cell Biology, Vol 55*, 55:129–156, 1998.

[66] J. A. Goodrich, M. L. Schwartz, and W. R. McClure. Searching for and predicting the activity of sites for DNA binding proteins: compilation and analysis of the binding sites for Escherichia coli integration host factor (IHF). *Nucleic Acids Res*, 18(17):4993–5000, 1990.

[67] L. C. Gosule and J. A. Schellman. Compact form of DNA induced by spermidine. *Nature*, 259(5541):333–5, 1976.

[68] D. M. Gowers and S. E. Halford. Protein motion from non-specific to specific DNA by three-dimensional routes aided by supercoiling. *Embo J*, 22(6):1410–8, 2003.

[69] D. C. Grainger, D. Hurd, M. D. Goldberg, and S. J. Busby. Association of nucleoid proteins with coding and non-coding segments of the Escherichia coli genome. *Nucleic Acids Res*, 34(16):4642–52, 2006.

[70] R. A. Grant, D. J. Filman, S. E. Finkel, R. Kolter, and J. M. Hogle. The crystal structure of Dps, a ferritin homolog that binds and protects DNA. *Nat Struct Biol*, 5(4):294–303, 1998.

[71] P. L. Graumann. SMC proteins in bacteria: Condensation motors for chromosome segregation? *Biochimie*, 83(1):53–59, 2001.

[72] M. Grote, J. Dijk, and R. Reinhardt. Ribosomal and DNA-Binding Proteins of the Thermoacidophilic Archaebacterium Sulfolobus-Acidocaldarius. *Biochimica Et Biophysica Acta*, 873(3):405–413, 1986.

[73] S. E. Halford, A. J. Welsh, and M. D. Szczelkun. Enzyme-mediated DNA looping. *Annu Rev Biophys Biomol Struct*, 33:1–24, 2004.

[74] C. D. Hardy and N. R. Cozzarelli. A genetic selection for supercoiling mutants of Escherichia coli reveals proteins implicated in chromosome structure. *Mol Microbiol*, 57(6):1636–52, 2005.

[75] S. He, P. G. Arscott, and V. A. Bloomfield. Condensation of DNA by multivalent cations: experimental studies of condensation kinetics. *Biopolymers*, 53(4):329–41, 2000.

[76] N. P. Higgins, X. Yang, Q. Fu, and J. R. Roth. Surveying a supercoil domain by using the gamma delta resolution system in Salmonella typhimurium. *J Bacteriol*, 178(10):2825–35, 1996.

[77] N.P. Higgins, S. Deng, Z. Pang, R. Stein, K. Champion, and D. Manna. Domain behavior and supercoil dynamics in bacterial chromosomes. In N. P. Higgins, editor, *The bacterial chromosome*, pages 133–153, Chapter 6. ACM Press, Washington D.C., 2005.

[78] D. A. Hiller, J. M. Fogg, A. M. Martin, J. M. Beechem, N. O. Reich, and J. J. Perona. Simultaneous DNA binding and bending by EcoRV endonuclease observed by real-time fluorescence. *Biochemistry*, 42(49):14375–85, 2003.

[79] M. Hirano and T. Hirano. Positive and negative regulation of SMC-DNA interactions by ATP and accessory proteins. *Embo Journal*, 23(13):2664–2673, 2004.

[80] M. Hirano and T. Hirano. Opening closed arms: Long-distance activation of SMC ATPase by hinge-DNA interactions. *Molecular Cell*, 21(2):175–186, 2006.

[81] K. P. Hopfner, A. Karcher, D. S. Shin, L. Craig, L. M. Arthur, J. P. Carney, and J. A. Tainer. Structural biology of Rad50 ATPase: ATP-driven conformational control in DNA double-strand break repair and the ABC-ATPase superfamily. *Cell*, 101(7):789–800, 2000.

[82] I. Horcas, R. Fernandez, J. M. Gomez-Rodriguez, J. Colchero, J. Gomez-Herrero, and A. M. Baro. WSXM: A software for scanning probe microscopy and a tool for nanotechnology. *Review of Scientific Instruments*, 78(1):–, 2007.

[83] D. M. Hougaard. Polyamine cytochemistry: localization and possible functions of polyamines. *Int Rev Cytol*, 138:51–88, 1992.

[84] N. V. Hud, M. J. Allen, K. H. Downing, J. Lee, and R. Balhorn. Identification of the elemental packing unit of DNA in mammalian sperm cells by atomic force microscopy. *Biochem Biophys Res Commun*, 193(3):1347–54, 1993.

[85] N. V. Hud and K. H. Downing. Cryoelectron microscopy of lambda phage DNA condensates in vitreous ice: the fine structure of DNA toroids. *Proc Natl Acad Sci U S A*, 98(26):14925–30, 2001.

[86] N. V. Hud, K. H. Downing, and R. Balhorn. A constant radius of curvature model for the organization of DNA in toroidal condensates. *Proc Natl Acad Sci U S A*, 92(8):3581–5, 1995.

[87] N. V. Hud and I. D. Vilfan. Toroidal DNA condensates: unraveling the fine structure and the role of nucleation in determining size. *Annu Rev Biophys Biomol Struct*, 34:295–318, 2005.

[88] J. H. G. Huisstede, K. O. van der Werf, M. L. Bennink, and V. Subramaniam. Force detection in optical tweezers using backscattered light. *Optics Express*, 13(4):1113–1123, 2005.

[89] S. Jafri, S. Evoy, K. Cho, H. G. Craighead, and S. C. Winans. An Lrp-type transcriptional regulator from Agrobacterium tumefaciens condenses more than 100 nucleotides of DNA into globular nucleoprotein complexes. *J Mol Biol*, 288(5):811–24, 1999.

[90] C. Jelinska, M. J. Conroy, C. J. Craven, A. M. Hounslow, P. A. Bullough, J. P. Waltho, G. L. Taylor, and M. F. White. Obligate heterodimerization of the archaeal Alba2 protein with Alba1 provides a mechanism for control of DNA packaging. *Structure*, 13(7):963–71, 2005.

[91] L. Jen-Jacobson. Protein-DNA recognition complexes: conservation of structure and binding energy in the transition state. *Biopolymers*, 44(2):153–80, 1997.

[92] R. C. Johnson, M. F. Bruist, and M. I. Simon. Host protein requirements for in vitro site-specific DNA inversion. *Cell*, 46(4):531–9, 1986.

[93] R. C. Johnson, L. M. Johnson, J. W. Schmidt, and J. F. Gardner. *Major nucleoid proteins in the structure and function of the Escherichia coli chromosome*. The bacterial chromosome. ASM Press, Washington, D. C., 2005.

[94] B. J. A. M. Jordi, A. E. Fielder, C. M. Burns, J. C. D. Hinton, N. Dover, D. W. Ussery, and C. F. Higgins. DNA binding is not sufficient for H-NS-mediated repression of proU expression. *Journal of Biological Chemistry*, 272(18):12083–12090, 1997.

[95] Y. Kano and F. Imamoto. Requirement of integration host factor (IHF) for growth of Escherichia coli deficient in HU protein. *Gene*, 89(1):133–7, 1990.

[96] S. Kar, R. Edgar, and S. Adhya. Nucleoid remodeling by an altered HU protein: reorganization of the transcription program. *Proc Natl Acad Sci U S A*, 102(45):16397–402, 2005.

[97] S. Kasas, N. H. Thomson, B. L. Smith, H. G. Hansma, X. Zhu, M. Guthold, C. Bustamante, E. T. Kool, M. Kashlev, and P. K. Hansma. Escherichia coli RNA polymerase activity observed using atomic force microscopy. *Biochemistry*, 36(3):461–8, 1997.

[98] J. W. Kerssemakers, E. L. Munteanu, L. Laan, T. L. Noetzel, M. E. Janson, and M. Dogterom. Assembly dynamics of microtubules at molecular resolution. *Nature*, 442(7103):709–12, 2006.

[99] S. J. Koch, A. Shundrovsky, B. C. Jantzen, and M. D. Wang. Probing protein-DNA interactions by unzipping a single DNA double helix. *Biophys J*, 83(2):1098–105, 2002.

[100] R. D. Kornberg. Structure of chromatin. *Annu Rev Biochem*, 46:931–54, 1977.

[101] S. C. Kowalczykowski, D. A. Dixon, A. K. Eggleston, S. D. Lauder, and W. M. Rehrauer. Biochemistry of homologous recombination in Escherichia coli. *Microbiol Rev*, 58(3):401–65, 1994.

[102] I. M. Kulic and H. Schiessel. DNA spools under tension. *Phys Rev Lett*, 92(22):228101, 2004.

[103] A. Lammens, A. Schele, and K. P. Hopfner. Structural biochemistry of ATP-driven dimerization and DNA-stimulated activation of SMC ATPases. *Curr Biol*, 14(19):1778–82, 2004.

[104] P. M. Leonard, S. H. Smits, S. E. Sedelnikova, A. B. Brinkman, W. M. de Vos, J. van der Oost, D. W. Rice, and J. B. Rafferty. Crystal structure of the Lrp-like transcriptional regulator from the archaeon Pyrococcus furiosus. *Embo J*, 20(5):990–7, 2001.

[105] J. C. Lindow, R. A. Britton, and A. D. Grossman. Structural maintenance of chromosomes protein of Bacillus subtilis affects supercoiling in vivo. *J Bacteriol*, 184(19):5317–22, 2002.

[106] S. M. Lindsay, L. A. Nagahara, T. Thundat, U. Knipping, R. L. Rill, B. Drake, C. B. Prater, A. L. Weisenhorn, S. A. Gould, and P. K. Hansma. STM and AFM images of nucleosome DNA under water. *J Biomol Struct Dyn*, 7(2):279–87, 1989.

[107] M. Lorenz, A. Hillisch, S. D. Goodman, and S. Diekmann. Global structure similarities of intact and nicked DNA complexed with IHF measured in solution by fluorescence resonance energy transfer. *Nucleic Acids Res*, 27(23):4619–25, 1999.

[108] S. Lucchini, G. Rowley, M. D. Goldberg, D. Hurd, M. Harrison, and J. C. Hinton. H-NS mediates the silencing of laterally acquired genes in bacteria. *PLoS Pathog*, 2(8):e81, 2006.

[109] K. Luger, A. W. Mader, R. K. Richmond, D. F. Sargent, and T. J. Richmond. Crystal structure of the nucleosome core particle at 2.8 A resolution. *Nature*, 389(6648):251–60, 1997.

[110] M. S. Luijsterburg, M. C. Noom, G. J. Wuite, and R. T. Dame. The architectural role of nucleoid-associated proteins in the organization of bacterial chromatin: A molecular perspective. *J Struct Biol*, 2006.

[111] R. Lurz, M. Grote, J. Dijk, R. Reinhardt, and B. Dobrinski. Electron microscopic study of DNA complexes with proteins from the Archaebacterium Sulfolobus acidocaldarius. *Embo J*, 5(13):3715–3721, 1986.

[112] R. I. Mahato, Y. Takakura, and M. Hashida. Nonviral vectors for in vivo gene delivery: physicochemical and pharmacokinetic considerations. *Crit Rev Ther Drug Carrier Syst*, 14(2):133–72, 1997.

[113] J. Mameren, M. Modesti, R. Kanaar, C. Wyman, G. J. Wuite, and E. J. Peterman. Dissecting elastic heterogeneity along DNA molecules coated partly with Rad51 using concurrent fluorescence microscopy and optical tweezers. *Biophys J*, 91(8):L78–80, 2006.

[114] G. S. Manning. Limiting laws and counterion condensation in polyelectrolyte solutions. V. Further development of the chemical model. *Biophys Chem*, 9(1):65–70, 1978.

[115] J. F. Marko and E. D. Siggia. Stretching DNA. *Macromolecules*, 28(26):8759–8770, 1995.

[116] K. A. Marx and G. C. Ruben. Evidence for hydrated spermidine-calf thymus DNA toruses organized by circumferential DNA wrapping. *Nucleic Acids Res*, 11(6):1839–54, 1983.

[117] K. A. Marx and G. C. Ruben. Studies of DNA organization in hydrated spermidine-condensed DNA toruses and spermidine-DNA fibres. *J Biomol Struct Dyn*, 1(5):1109–32, 1984.

[118] J. Mascarenhas, A. V. Volkov, C. Rinn, J. Schiener, R. Guckenberger, and P. L. Graumann. Dynamic assembly, localization and proteolysis of the Bacillus subtilis SMC complex. *BMC Cell Biol*, 6:28, 2005.

[119] S. J. McBryant, V. H. Adams, and J. C. Hansen. Chromatin architectural proteins. *Chromosome Res*, 14(1):39–51, 2006.

[120] J. D. McGhee and G. Felsenfeld. Nucleosome structure. *Annu Rev Biochem*, 49:1115–56, 1980.

[121] J. D. McGhee and P. H. von Hippel. Theoretical aspects of DNA-protein interactions: co-operative and non-co-operative binding of large ligands to a one-dimensional homogeneous lattice. *J Mol Biol*, 86(2):469–89, 1974.

[122] T. E. Melby, C. N. Ciampaglio, G. Briscoe, and H. P. Erickson. The symmetrical structure of structural maintenance of chromosomes (SMC) and MukB proteins: long, antiparallel coiled coils, folded at a flexible hinge. *J Cell Biol*, 142(6):1595–604, 1998.

[123] R. Merkel, P. Nassoy, A. Leung, K. Ritchie, and E. Evans. Energy landscapes of receptor-ligand bonds explored with dynamic force spectroscopy. *Nature*, 397(6714):50–3, 1999.

[124] M. Meselson and F. W. Stahl. The Replication of DNA in Escherichia-Coli. *Proceedings of the National Academy of Sciences of the United States of America*, 44(7):671–682, 1958.

[125] A. Minsky, E. Shimoni, and D. Frenkiel-Krispin. Stress, order and survival. *Nat Rev Mol Cell Biol*, 3(1):50–60, 2002.

[126] Y. Murayama, Y. Sakamaki, and M. Sano. Elastic response of single DNA molecules exhibits a reentrant collapsing transition. *Phys Rev Lett*, 90(1):018102, 2003.

[127] K. Nasmyth and C. H. Haering. The structure and function of SMC and Kleisin complexes. *Annual Review of Biochemistry*, 74:595–648, 2005.

[128] W. W. Navarre, S. Porwollik, Y. Wang, M. McClelland, H. Rosen, S. J. Libby, and F. C. Fang. Selective silencing of foreign DNA with low GC content by the H-NS protein in Salmonella. *Science*, 313(5784):236–8, 2006.

[129] M. C. Noom, B. van den Broek, J. van Mameren, and G. J. Wuite. Visualizing single DNA-bound proteins using DNA as a scanning probe. *Nat Methods*, 4(12):1031–6, 2007.

[130] T. Odijk. Stiff Chains and Filaments under Tension. *Macromolecules*, 28(20):7016–7018, 1995.

[131] S. Ono, M. D. Goldberg, T. Olsson, D. Esposito, J. C. Hinton, and J. E. Ladbury. H-NS is a part of a thermally controlled mechanism for bacterial gene regulation. *Biochem J*, 2005.

[132] T. Oshima, S. Ishikawa, K. Kurokawa, H. Aiba, and N. Ogasawara. Escherichia coli histone-like protein H-NS preferentially binds to horizontally acquired DNA in association with RNA polymerase. *DNA Res*, 13(4):141–53, 2006.

[133] C. Q. Pan, S. E. Finkel, S. E. Cramton, J. A. Feng, D. S. Sigman, and R. C. Johnson. Variable structures of Fis-DNA complexes determined by flanking DNA-protein contacts. *J Mol Biol*, 264(4):675–95, 1996.

[134] T. T. Paull, M. J. Haykinson, and R. C. Johnson. The nonspecific DNA-binding and -bending proteins HMG1 and HMG2 promote the assembly of complex nucleoprotein structures. *Genes Dev*, 7(8):1521–34, 1993.

[135] T. T. Paull and R. C. Johnson. DNA looping by Saccharomyces cerevisiae high mobility group proteins NHP6A/B. Consequences for nucleoprotein complex assembly and chromatin condensation. *J Biol Chem*, 270(15):8744–54, 1995.

[136] M. M. Pena and G. S. Bullerjahn. The DpsA protein of Synechococcus sp. Strain PCC7942 is a DNA-binding hemoprotein. Linkage of the Dps and bacterioferritin protein families. *J Biol Chem*, 270(38):22478–82, 1995.

[137] D. E. Pettijohn and O. Pfenninger. Supercoils in Prokaryotic DNA Restrained Invivo. *Proceedings of the National Academy of Sciences of the United States of America-Biological Sciences*, 77(3):1331–1335, 1980.

[138] L. Postow, C. D. Hardy, J. Arsuaga, and N. R. Cozzarelli. Topological domain structure of the Escherichia coli chromosome. *Genes Dev*, 18(14):1766–79, 2004.

[139] N. Pouget, C. Dennis, C. Turlan, M. Grigoriev, M. Chandler, and L. Salome. Single-particle tracking for DNA tether length monitoring. *Nucleic Acids Res*, 32(9):e73, 2004.

[140] H. Qian. A mathematical analysis for the Brownian dynamics of a DNA tether. *J Math Biol*, 41(4):331–40, 2000.

[141] H. Qian and E. L. Elson. Quantitative study of polymer conformation and dynamics by single-particle tracking. *Biophys J*, 76(3):1598–605, 1999.

[142] P. A. Rice, S. Yang, K. Mizuuchi, and H. A. Nash. Crystal structure of an IHF-DNA complex: a protein-induced DNA U-turn. *Cell*, 87(7):1295–306, 1996.

[143] S. Rimsky. Structure of the histone-like protein H-NS and its role in regulation and genome superstructure. *Curr Opin Microbiol*, 7(2):109–14, 2004.

[144] C. Rivetti, M. Guthold, and C. Bustamante. Wrapping of DNA around the E.coli RNA polymerase open promoter complex. *Embo J*, 18(16):4464–75, 1999.

[145] J. Rouviere-Yaniv, M. Yaniv, and J. E. Germond. E. coli DNA binding protein HU forms nucleosomelike structure with circular double-stranded DNA. *Cell*, 17(2):265–74, 1979.

[146] D. Sagi, N. Friedman, C. Vorgias, A. B. Oppenheim, and J. Stavans. Modulation of DNA conformations through the formation of alternative high-order HU-DNA complexes. *J Mol Biol*, 341(2):419–28, 2004.

[147] K. Sandman and J. N. Reeve. Structure and functional relationships of archaeal and eukaryal histones and nucleosomes. *Arch Microbiol*, 173(3):165–9, 2000.

[148] J. A. Schellman and N. Parthasarathy. X-ray diffraction studies on cation-collapsed DNA. *J Mol Biol*, 175(3):313–29, 1984.

[149] M.F. Schleiden. Beiträge zur Phytogenesis. *Archiv für Anatomie, Physiologie und wissenschaftliche Medicin. Hg. Johannes Müller*, Berlin: Veit 1838:137–176, 1838.

[150] R. Schneider, R. Lurz, G. Luder, C. Tolksdorf, A. Travers, and G. Muskhelishvili. An architectural role of the Escherichia coli chromatin protein FIS in organising DNA. *Nucleic Acids Res*, 29(24):5107–14, 2001.

[151] R. Schneider, A. Travers, T. Kutateladze, and G. Muskhelishvili. A DNA architectural protein couples cellular physiology and DNA topology in Escherichia coli. *Mol Microbiol*, 34(5):953–64, 1999.

[152] B. Schnurr, F. Gittes, and F. C. MacKintosh. Metastable intermediates in the condensation of semiflexible polymers. *Phys Rev E Stat Nonlin Soft Matter Phys*, 65(6 Pt 1):061904, 2002.

[153] O. Schroder and R. Wagner. The bacterial DNA-binding protein H-NS represses ribosomal RNA transcription by trapping RNA polymerase in the initiation complex. *J Mol Biol*, 298(5):737–48, 2000.

[154] N. Shimamoto. One-dimensional diffusion of proteins along DNA - Its biological and chemical significance revealed by single-molecule measurements. *Journal of Biological Chemistry*, 274(22):15293–15296, 1999.

[155] M. Shin, M. Song, J. H. Rhee, Y. Hong, Y. Kim, Y Seok, K Ha, S. Jung, and H. E. Choy. DNA looping-mediated repression by histone-like protein H-NS: specific requirement of E.sigma70 as a cofactor for looping. *Genes Dev*, 19(19):2388–98, 2005.

[156] H. Shindo, T. Iwaki, R. Ieda, H. Kurumizaka, C. Ueguchi, T. Mizuno, S. Morikawa, H. Nakamura, and H. Kuboniwa. Solution structure of the DNA binding domain of a nucleoid-associated protein, H-NS, from Escherichia coli. *FEBS Lett*, 360(2):125–31, 1995.

[157] H. Shindo, A. Ohnuki, H. Ginba, E. Katoh, C. Ueguchi, T. Mizuno, and T. Yamazaki. Identification of the DNA binding surface of H-NS protein from Escherichia coli by heteronuclear NMR spectroscopy. *FEBS Lett*, 455(1-2):63–9, 1999.

[158] D. Skoko, J. Yan, R. C. Johnson, and J. F. Marko. Low-force DNA condensation and discontinuous high-force decondensation reveal a loop-stabilizing function of the protein Fis. *Phys Rev Lett*, 95(20):208101, 2005.

[159] S. B. Smith, Y. Cui, and C. Bustamante. Overstretching B-DNA: the elastic response of individual double-stranded and single-stranded DNA molecules. *Science*, 271(5250):795–9, 1996.

[160] S. Smolik. Image of Drosophila Salivary Gland, optimized by Aurelie Snyder. *Private communication*, 2007.

[161] C. P. Smyth, T. Lundback, D. Renzoni, G. Siligardi, R. Beavil, M. Layton, J. M. Sidebotham, J. C. Hinton, P. C. Driscoll, C. F. Higgins, and J. E. Ladbury. Oligomerization of the chromatin-structuring protein H-NS. *Mol Microbiol*, 36(4):962–72, 2000.

[162] Y. Sowa, A. D. Rowe, M. C. Leake, T. Yakushi, M. Homma, A. Ishijima, and R. M. Berry. Direct observation of steps in rotation of the bacterial flagellar motor. *Nature*, 437(7060):916–9, 2005.

[163] R. Spurio, M. Durrenberger, M. Falconi, A. Lateana, C. L. Pon, and C. O. Gualerzi. Lethal Overproduction of the Escherichia-Coli Nucleoid Protein H-Ns - Ultramicroscopic and Molecular Autopsy. *Molecular & General Genetics*, 231(2):201–211, 1992.

[164] P. Staczek and N. P. Higgins. Gyrase and Topo IV modulate chromosome domain size in vivo. *Mol Microbiol*, 29(6):1435–48, 1998.

[165] A. V. Strunnikov. SMC complexes in bacterial chromosome condensation and segregation (vol 55, pg 135, 2006). *Plasmid*, 56(3):235–235, 2006.

[166] T. J. Su, E. Theofanidou, J. Arlt, D. T. Dryden, and J. Crain. Single molecule fluorescence imaging and its application to the study of DNA condensation. *J Fluoresc*, 14(1):65–9, 2004.

[167] K. Svoboda and S. M. Block. Biological Applications of Optical Forces. *Annual Review of Biophysics and Biomolecular Structure*, 23:247–285, 1994.

[168] K. K. Swinger, K. M. Lemberg, Y. Zhang, and P. A. Rice. Flexible DNA bending in HU-DNA cocrystal structures. *Embo J*, 22(14):3749–60, 2003.

[169] K. K. Swinger and P. A. Rice. IHF and HU: flexible architects of bent DNA. *Curr Opin Struct Biol*, 14(1):28–35, 2004.

[170] A.A. Talukder, A. Iwata, A. Nishimura, S. Ueda, and A. Ishihama. Growth phase-dependent variation in protein composition of the Escherichia coli nucleoid. *J. Bacteriol.*, 181:6361–6370, 1999.

[171] H. Tanaka, K. Yasuzawa, K. Kohno, N. Goshima, Y. Kano, T. Saiki, and F. Imamoto. Role of HU proteins in forming and constraining supercoils of chromosomal DNA in Escherichia coli. *Mol Gen Genet*, 248(5):518–26, 1995.

[172] W. H. Taylor and P. J. Hagerman. Application of the Method of Phage-T4 DNA Ligase-Catalyzed Ring-Closure to the Study of DNA-Structure.2. Nacl-Dependence of DNA Flexibility and Helical Repeat. *Journal of Molecular Biology*, 212(2):363–376, 1990.

[173] P. Thaw, S. E. Sedelnikova, T. Muranova, S. Wiese, S. Ayora, J. C. Alonso, A. B. Brinkman, J. Akerboom, J. van der Oost, and J. B. Rafferty. Structural insight into gene transcriptional regulation and effector binding by the Lrp/AsnC family. *Nucleic Acids Res*, 34(5):1439–49, 2006.

[174] T. Thomas and T. J. Thomas. Polyamines in cell growth and cell death: molecular mechanisms and therapeutic applications. *Cell Mol Life Sci*, 58(2):244–58, 2001.

[175] R. E. Thompson, D. R. Larson, and W. W. Webb. Precise nanometer localization analysis for individual fluorescent probes. *Biophys J*, 82(5):2775–83, 2002.

[176] B. A. Todd and D. C. Rau. Interplay of ion binding and attraction in DNA condensed by multivalent cations. *Nucleic Acids Res*, 2007.

[177] W. Trabesinger, G. J. Schutz, H. J. Gruber, H. Schindler, and T. Schmidt. Detection of individual oligonucleotide pairing by single-molecule microscopy. *Analytical Chemistry*, 71(1):279–283, 1999.

[178] A. Travers and G. Muskhelishvili. Bacterial chromatin. *Current Opinion in Genetics & Development*, 15(5):507–514, 2005.

[179] M. Ueda and K. Yoshikawa. Phase Transition and Phase Segregation in a Single Double-Stranded DNA Molecule. *Physical Review Letters*, 77(10):2133–2136, 1996.

[180] M. van den Bosch, P. H. Lohman, and A. Pastink. DNA double-strand break repair by homologous recombination. *Biol Chem*, 383(6):873–92, 2002.

[181] B. van den Broek, M. C. Noom, and G. J. L. Wuite. DNA-tension dependence of restriction enzyme activity reveals mechanochemical properties of the reaction pathway. *Nucleic Acids Research*, 33(8):2676–2684, 2005.

[182] B. van den Broek, F. Vanzi, D. Normanno, F. S. Pavone, and G. J. Wuite. Real-time observation of DNA looping dynamics of Type IIE restriction enzymes NaeI and NarI. *Nucleic Acids Res*, 34(1):167–74, 2006.

[183] J. van Mameren, M. Modesti, R. Kanaar, C. Wyman, G. J. L. Wuite, and E. J. G. Peterman. Dissecting elastic heterogeneity along DNA molecules coated partly with Rad51 using concurrent fluorescence microscopy and optical tweezers. *Biophysical Journal*, 91(8):L78–L80, 2006.

[184] J. van Noort, S. Verbrugge, N. Goosen, C. Dekker, and R. T. Dame. Dual architectural roles of HU: formation of flexible hinges and rigid filaments. *Proc Natl Acad Sci U S A*, 101(18):6969–74, 2004.

[185] S. J. van Noort, K. O. van der Werf, A. P. Eker, C. Wyman, B. G. de Grooth, N. F. van Hulst, and J. Greve. Direct visualization of dynamic protein-DNA interactions with a dedicated atomic force microscope. *Biophys J*, 74(6):2840–9, 1998.

[186] K. C. Vermeulen, J. van Mameren, G. J. M. Stienen, E. J. G. Peterman, G. J. L. Wuite, and C. F. Schmidt. Calibrating bead displacements in optical tweezers using acousto-optic deflectors. *Review of Scientific Instruments*, 77(1):013704, 2006.

[187] V. Vijayanathan, T. Thomas, and T. J. Thomas. DNA nanoparticles and development of DNA delivery vehicles for gene therapy. *Biochemistry*, 41(48):14085–94, 2002.

[188] P. H. Viollier, M. Thanbichler, P. T. McGrath, L. West, M. Meewan, H. H. McAdams, and L. Shapiro. Rapid and sequential movement of individual chromosomal loci to specific subcellular locations during bacterial DNA replication. *Proc Natl Acad Sci U S A*, 101(25):9257–62, 2004.

[189] A. V. Volkov, J. Mascarenhas, C. Andrei-Selmer, H.D. Ulrich, and P.L. Graumann. A prokaryotic condensin/cohesin-like complex can actively compact chromosomes from a single position on the nucleoid and binds to DNA as a ring-like structure. *Mol. Cell. Biol.*, 23:5638–5650, 2003.

[190] P. H. von Hippel and O. G. Berg. Facilitated target location in biological systems. *J Biol Chem*, 264(2):675–8, 1989.

[191] M. D. Wang, M. J. Schnitzer, H. Yin, R. Landick, J. Gelles, and S. M. Block. Force and velocity measured for single molecules of RNA polymerase. *Science*, 282(5390):902–7, 1998.

[192] B. N. Wardleworth, R. J. Russell, S. D. Bell, G. L. Taylor, and M. F. White. Structure of Alba: an archaeal chromatin protein modulated by acetylation. *Embo J*, 21(17):4654–62, 2002.

[193] J. D. Watson and F. H. C. Crick. Molecular Structure of Nucleic Acids - a Structure for Deoxyribose Nucleic Acid. *Nature*, 171(4356):737–738, 1953.

[194] S. C. West. Molecular views of recombination proteins and their control. *Nat Rev Mol Cell Biol*, 4(6):435–45, 2003.

[195] S. A. Weston, A. Lahm, and D. Suck. X-Ray Structure of the Dnase I-D(Ggtatacc)(2) Complex at 2.3-Angstrom Resolution. *Journal of Molecular Biology*, 226(4):1237–1256, 1992.

[196] M. F. White and S. D. Bell. Holding it together: chromatin in the Archaea. *Trends Genet*, 18(12):621–6, 2002.

[197] J. Widom. Toward a unified model of chromatin folding. *Annu Rev Biophys Biophys Chem*, 18:365–95, 1989.

[198] J. Widom and R. L. Baldwin. Cation-induced toroidal condensation of DNA studies with Co3+(NH3)6. *J Mol Biol*, 144(4):431–53, 1980.

[199] J. Widom and R. L. Baldwin. Inhibition of cation-induced DNA condensation by intercalating dyes. *Biopolymers*, 22(6):1621–32, 1983.

[200] Paul A. Wiggins, R.T. Dame, M.C. Noom, and G.J.L. Wuite. Demystifying the bridging motif: the mechanism of H-NS induced bacterial nucleoid organization. *Manuscript in preparation*, 2008.

[201] R. W. Wilson and V. A. Bloomfield. Counterion-induced condesation of deoxyribonucleic acid. a light-scattering study. *Biochemistry*, 18(11):2192–6, 1979.

[202] C. R. Woese. Interpreting the universal phylogenetic tree. *Proc Natl Acad Sci U S A*, 97(15):8392–6, 2000.

[203] H. Y. Wu, S. H. Shyy, J. C. Wang, and L. F. Liu. Transcription generates positively and negatively supercoiled domains in the template. *Cell*, 53(3):433–40, 1988.

[204] G. J. Wuite, R. J. Davenport, A. Rappaport, and C. Bustamante. An integrated laser trap/flow control video microscope for the study of single biomolecules. *Biophys J*, 79(2):1155–67, 2000.

[205] M. Yamazoe, T. Onogi, Y. Sunako, H. Niki, K. Yamanaka, T. Ichimura, and S. Hiraga. Complex formation of MukB, MukE and MukF proteins involved in chromosome partitioning in Escherichia coli. *Embo Journal*, 18(21):5873–5884, 1999.

[206] S. W. Yang and H. A. Nash. Comparison of protein binding to DNA in vivo and in vitro: defining an effective intracellular target. *Embo J*, 14(24):6292–300, 1995.

[207] H. Yin, R. Landick, and J. Gelles. Tethered particle motion method for studying transcript elongation by a single RNA polymerase molecule. *Biophys J*, 67(6):2468–78, 1994.

[208] N. Yoshinaga, T. Akitaya, and K. Yoshikawa. Intercalating fluorescence dye YOYO-1 prevents the folding transition in giant duplex DNA. *Biochem Biophys Res Commun*, 286(2):264–7, 2001.

[209] A. Zhang, S. Rimsky, M. E. Reaban, H. Buc, and M. Belfort. Escherichia coli protein analogs StpA and H-NS: regulatory loops, similar and disparate effects on nucleic acid dynamics. *Embo J*, 15(6):1340–9, 1996.

Samenvatting

DNA Organisatie Mechanismen Ontrafeld met Nieuwe Enkele-Molecuul Methodes

Over het algemeen wordt aangenomen dat al het dierlijk leven op aarde afstamt van dezelfde voorouders: een-cellige organismen. Door evolutie is er uiteindelijk diversiteit ontstaan en rezen er grote verschillen tussen groepen organismen. Uiteindelijk heeft dit geleid tot de grote diversiteit in de natuur zoals we die nu kennen. Echter, aan aantal aspecten zijn opmerkelijk genoeg voor alle soorten hetzelfde gebleven. Een van die aspecten is de genetische informatie van een organisme. Hoewel de genetische informatie van soort tot soort en zelfs van persoon tot persoon verschilt zijn er toch opmerkelijke overeenkomsten. Genetische informatie is in alle organismen opgeslagen in lange moleculen, DNA genaamd (zie Fig. 1.2). Wat nog opmerkelijker is: al het DNA bestaat maar uit vier verschillende bouwstenen die de genetische code vormen door ze in een bepaalde volgorde aan elkaar te schakelen. Een opeenvolging van drie van die bouwstenen vormt de code voor een bepaald aminozuur en een hele reeks aminozuren vormt de basis voor eiwitten(zie Fig. 1.3), de 'werkpaarden' in de cel . De code op het DNA voor een eiwit, een sequentie van telkens drie bouwstenen, wordt een gen genoemd. Door bepaalde genen aan of uit te zetten kan een cel dus reguleren wat er precies in de cel gebeurt. Het DNA speelt dus een essentiële rol.

Tegenwoordig kan je geen krant meer openslaan of ergens wordt wel een onderwerp aangesneden dat met DNA te maken heeft. De blauwdruk van onze cellen met daarin de persoonsgebonden eigenschappen opgeslagen die voor iedereen uniek zijn. Het kleinste beetje DNA achtergelaten op een *plaats delict* is genoeg om een dader

achter de tralies te krijgen. Maar hoeveel DNA heb je eigenlijk in je lichaam zitten? Elke cel van het menselijk lichaam bevat ∼1.8 meter DNA. Dat is op zich al veel, maar het menselijk lichaam bestaat uit ∼10-50 biljoen (miljoen x miljoen) cellen. Stel dat je alle stukjes DNA dan aan elkaar zou kunnen knopen, dan levert dat een lengte van ongeveer 36.000 miljoen kilometer DNA op! Hoe past dat allemaal in je lichaam? Welnu, DNA is ontzettend dun, het is slechts een miljoenste van een millimeter dik, maar nog is het een ingewikkelde taak om het DNA op te vouwen zodat het in een cel past. Het moet namelijk nog steeds kunnen worden gekopieerd, afgelezen om eiwitten te maken en eventueel gerepareerd. Wij zijn natuurlijk niet de enige die met dit probleem 'worstelen'. Alle andere (zoog)dieren maar ook bacteriën, gistcellen en virussen hebben dit probleem. Interessant genoeg doen ze dit niet allemaal op dezelfde manier. Er zijn eigenlijk drie methodes te onderscheiden, waarop DNA wordt georganiseerd en opgevouwen in organismen. Het blijkt dat dit bij mensen heel anders gebeurd dan bij bijvoorbeeld bacteriën. Daarnaast zijn er soorten die een beetje van de ene methode gebruiken en een beetje van de andere methode. Er is inmiddels veel bekend over de DNA organisatie in het menselijk lichaam maar nog steeds weinig over hoe dit in bacteriën gebeurt. Dit is echter precies waar ik met mijn promotie onderzoek naar heb gekeken. De manier waarop we dat gedaan hebben is vrij bijzonder; terwijl een DNA molecuul ontzettend dun is kunnen we toch één DNA molecuul 'vangen'met behulp van lasers en een mikroscoop. Door één DNA molecuul te manipuleren onder de microscoop zijn we meer te weten gekomen over hoe de organisatie van bacterieel DNA in elkaar zit. Alvorens de resultaten van mijn onderzoek te beschrijven zal ik eerst een korte introductie geven over de DNA organisatie en de technieken die ik heb gebruikt.

DNA organisatie

De genoemde diversiteit van soorten heeft veel mensen geïnspireerd een classificatie aan te brengen op basis van overeenkomsten en verschillen tussen soorten. Vroeger gebeurde dat op uiterlijke kenmerken maar dit leidt onherroepelijk tot problemen, denk bijvoorbeeld maar aan het vogelbekdier, hoe moet dit dier geclassificeerd worden? Met ontdekking van DNA is er een nieuwe classificatie ontstaan die is gebaseerd de genetische informatie van een organisme. Er zijn dan drie domeinen te onderscheiden, *eukaryoten*, *prokaryoten* en *archaea* (zie Figuur 1.5). Waar eukaryoten vaak complexe organismen zijn die bestaan uit vele triljoenen cellen, bijvoorbeeld mensen, bestaan prokaryoten en archaea vaak slechts uit één cel, denk dan bijvoorbeeld aan bacteriën. Deze cel is dan ook nog eens veel kleiner dan de gemiddelde eukaryote cel (zie Figuur 1.6). Als we kijken wat er nu precies in die verschillende cellen zit, zien we ook dat sommige componenten ook verschillen, met name diegene die te maken hebben met de organisatie van het genetisch materiaal.

DNA organisatie in eukaryoten

In eukaryoten is het DNA, dat soms wel 18.000x langer kan zijn dan de lengte van de cel, georganiseerd in één of meer chromosomen. Deze chromosomen zijn enorm gecompacteerde stukken DNA en ze zijn allemaal gelokaliseerd in de *celkern*. Hoe kan het DNA zo enorm gecompacteerd worden en toch tegelijkertijd heel toegankelijk zijn voor processen die moeten plaatsvinden op het DNA, zoals bijvoorbeeld het kopiëren of aflezen van het DNA? In eukaryoten gebeurt dit in een aantal compactie-stappen, weergegeven in Figuur 1.7. Allereerst is het DNA ∼1.7 keer om een eiwitcomplex, een histon, gewikkeld. De structuur die dan ontstaat lijkt een beetje op een kralenketting. Het DNA is dan een factor zes compacter. Deze 'kralenketting' wordt vervolgens verder opgevouwen, wat resulteert in weer een factor zes compactie, en in een geluste structuur gebracht. Deze geluste structuur wordt verder opgerold en in elkaar gevouwen totdat de uiteindelijke structuur ontstaat (zie Fig. 1.7).

DNA organisatie in prokaryoten en archaea

In tegenstelling tot menselijke lichaamscellen hebben bacteriën geen celkern. De genetische informatie 'drijft' schijnbaar vrijelijk rond in de cel, als ware het noedels in een bord met soep. Het is dan ook wat losser en dynamischer georganiseerd dan bij eukaryoten. Het DNA wordt eigenlijk simpelweg georganiseerd door 50-400 in elkaar gedraaide lussen te maken (zie Figuur 1.4) die bij elkaar worden gehouden door een groep kleine eiwitten. Dit geheel wordt de nucleoid genoemd. De groep eiwitten die hierbij betrokken is heeft naast het organiseren en compacteren van het DNA vaak ook nog andere functies in de cel en dat maakt het heel lastig om uit te zoeken hoe de organisatie nu precies in zijn werk gaat. We kunnen deze eiwitten classificeren door te kijken naar wat ze nu structureel met het DNA doen. De één buigt het DNA bijvoorbeeld terwijl de ander stukken DNA kan bruggen door twee plekken op het DNA 'beet te pakken'. In eerste instantie hebben deze eiwitten de naam "histon-achtige eiwitten"gekregen omdat gedacht werd dat ze ongeveer dezelfde rol vervulde als histonen bij eukaryoten, maar inmiddels is duidelijk dat ze daar erg van verschillen. Een betere naam is dan ook "nucleoid geassocieerde eiwitten".

In Figuur 1.5 is te zien dat archaea eigenlijk een beetje tussen de prokaryoten en eukaryoten inzitten en dat blijkt ook uit de manier waarop zij hun DNA organiseren. Veel archaea bevatten bijvoorbeeld histonen, maar ook DNA organiserende eiwitten die voorkomen in bacterien. Behalve het compacteren van het DNA is er bij archaea vaak nog een andere eis aan de organisatie van het DNA: bescherming. Veel archaea zijn extremophilen; zij leven op plaatsen waar andere organismen niet kunnen over-

leven. Bijvoorbeeld op plaatsen met extreem hoge (80°) of lage (-45°) temperaturen of op plaatsen waar een hele hoge zuurgraad heerst. Al deze omstandigheden zijn heel gevaarlijk voor het DNA en vraagt dus om extra bescherming. Dit maakt archaea tot hele fascinerende organismen.

Het manipuleren van enkele moleculen

Om te begrijpen hoe een cel in elkaar zit moeten we niet alleen weten wat er in zit, maar ook hoe structuren ontstaan en weer verbroken worden. De vragen die hierbij gesteld worden hebben vaak een biologisch, maar ook een heel fysisch karakter: als het DNA sterk compacteerd is, hoeveel kracht kost het dan om het weer los te trekken? Is een eiwit dan wel sterk genoeg? En hoe sterk is een DNA molecuul eigenlijk? Veel van dit soort bio-fysische vragen zijn moeilijk te beantwoorden met traditionele technieken. In het geval van reacties van eiwitten met DNA wordt er dan vaak gekeken naar het gemiddelde resultaat van biljoenen reacties. Op deze manier is het moeilijk details van reacties te ontrafelen. 'Enkele molecuul' biofysica kan soms wel antwoord geven op die vragen. Door een DNA molecuul te vangen (zie Fig. 1.10) en er een eiwit op te laten werken kan precies worden gevolgd wat er gebeurt. Een groot nadeel is dat je dit wel erg vaak moet doen voordat je een solide resultaat hebt.

Het 'optisch pincet' is zo'n techniek waarbij enkele moleculen gemanipuleerd kunnen worden. Met een optisch pincet is het mogelijk glazen microbolletjes (met een diameter van 1 miljoenste van een meter) vast te pakken. Het principe is gebaseerd op het feit dat licht een kracht kan uitoefenen als het van richting wordt veranderd (zie Fig. 1.11). Weliswaar een hele kleine kracht maar genoeg om hele kleine objecten mee te bewegen. De glazen bolletjes zijn gemaakt van glas en iedereen die wel eens door een grote glazen knikker of bol heeft gekeken weet dat je dan een vervormd beeld ziet. Dit komt doordat het glas licht 'breekt'; het veranderd de richting van het licht. Een knikker zal niet zo snel bewegen, maar door een hele sterke laserbundel te focusseren kun je op deze manier wel microknikkers bewegen en zelfs vastpakken. Belangrijk gegeven is dat we de microbolletjes niet alleen kunnen vasthouden, maar ook kunnen meten hoeveel kracht we er op uitoefenen. Die krachten zijn ook ontzettend klein, in de orde van een *picoNewton*. Het is moeilijk je voor te stellen hoeveel dat precies is maar een mug die op tafel zit oefent door de zwaartekracht een kracht uit van $\sim$1 miljoenste Newton. Een picoNewton is nog een miljoen keer kleiner! In dit regime spelen zich ook de processen af die in een cel plaats vinden en dus is het optisch pincet een uitermate geschikt stuk gereedschap om deze processen te onderzoeken. Door de microballetjes een beetje plakkerig te maken kun je er van alles aanplakken, bijvoorbeeld een DNA molecuul. Door twee van deze pincetten te gebruiken kun je de uiteinden van een DNA molecuul 'vastpakken' en dus manipuleren! Om het DNA en de eiwitten goed te kunnen bestuderen, halen we ze uit de cel, we

doen dus *in vitro* experimenten. Het zou anders veel te ingewikkeld worden vanwege alle processen die tegelijkertijd plaats vinden in de cel. Om te zorgen dat we toch de juiste omstandigheden hebben en snel achter elkaar experimenten kunnen doen, hebben we een flow-kamer ontwikkeld (zie Fig. 1.12). Door verschillende vloeistoffen vanuit hun eigen reservoir naast elkaar te laten stromen kunnen we snel een experiment 'in elkaar zetten' (zie Fig. 1.13). Als we bijvoorbeeld drie kanalen hebben, i, ii en iii, één met een vloeistof met microballetjes, één met een vloeistof met DNA en één met eiwit, dan beginnen we met het vangen van twee balletjes in kanaal i. Daarna bewegen we de twee pincetten een klein stukje zodat ze in het DNA kanaal, kanaal ii, zitten. Als we dan een stuk DNA hebben gevangen verplaatsen we dat *construct* naar het kanaal met de eiwitten, kanaal iii, waar we vervolgens bestuderen wat het effect is van de eiwitten op het DNA.

Het manipuleren van twee DNA moleculen

Het vangen van één DNA molecuul werd voor het eerst gedaan in de vroege jaren '90 en dit leverde een schat aan mogelijke experimenten op die voorheen niet mogelijk waren. Voor het bestuderen van DNA organisatie en met name de rol van DNA-bruggende eiwitten bleek het noodzakelijk niet één maar twee DNA moleculen te manipuleren om daar bruggen tussen te laten ontstaan en meten. Op het eerste gezicht lijkt dit niet moeilijk maar er komt toch veel bij kijken. Voor één DNA molecuul zijn twee optisch pincetten nodig, één voor elk uiteinde. Nu is het door gebruik te maken van de optische eigenschappen van licht niet moeilijk om uit één laserbundel twee bundels te maken, maar voor twee DNA moleculen zijn vier optisch pincetten en dus vier laserbundels nodig. De manier waarop we dit opgelost hebben, beschreven in Hoofdstuk 2, is door 1 laserbundel te "verdelen" over drie optisch pincetten. Dit doen we door één laserbundel door een akoestisch afstelbaar kristal heen te sturen. Dat wil zeggen dat door een geluidsgolf door het kristal heen te sturen de laserbundel een klein beetje verplaatst kan worden. Het gebruik van zo'n kristal heeft als voordeel dat dit heel snel kan. Door de geluidsgolf heel snel (∼20.000 keer per seconde) 3x te veranderen kunnen we met één laserbundel drie optisch pincetten maken. Fysisch gezien gebeurt dat ook nog eens op een leuke manier: uiteindelijk maken we met elektriciteit eerst een geluidsgolf, waarmee we licht manipuleren, terwijl we met dat licht iets "tastbaars" (de microballetjes) vasthouden! Samen met de door ons ontwikkelde flow-kamer kunnen we nu twee DNA moleculen vangen (zie Fig. 2.1). Om dit systeem te karakteriseren hebben we eerst gekeken wat er gebeurt als je de twee moleculen langs elkaar wrijft. Opmerkelijk genoeg konden de beide moleculen schier wrijvingsloos langs elkaar bewegen. Zelfs als we het ene molecuul een aantal keer om het andere molecuul wikkelden was er nog steeds amper sprake van wrijving. Dit komt waarschijnlijk omdat een DNA molecuul een klein beetje negatief geladen is.

De negatieve ladingen van de twee moleculen stoten elkaar af met als resultaat dat wij amper wrijving konden meten. Vervolgens hebben we gekeken of we met zo'n lusje van DNA om een tweede DNA molecuul eiwitten, die op dat laatste DNA molecuul zitten, kunnen detecteren. Verassend genoeg bleek dit het geval te zijn. Door het lusje strakker of juist minder strak te trekken konden we zelfs eiwitten van het DNA aftrekken of juist laten zitten. Deze nieuwe *dubbele DNA methode* biedt nieuwe mogelijkheden om DNA-eiwit interacties te meten die voorheen niet gemeten konden worden.

Het openritsen van een kluwen DNA

Bacteriën zijn veel eenvoudiger dan onze lichaamscellen maar dat maakt het verrassend genoeg juist lastiger om uit te vissen hoe DNA in een kernloze bacteriecel is georganiseerd. Tot de laserpincet in beeld kwam, was het bijvoorbeeld niet goed mogelijk om de ruimtelijke organisatie van bacterieel DNA in beeld te brengen en te bestuderen. In menselijke en dierlijke cellen zijn DNA-strengen, opgerold tot chromosomen, uitermate georganiseerd. Het bacteriële chromosoom is veel dynamischer georganiseerd door een kleine groep eiwitten die het DNA a-specifiek bindt. Ze hebben daardoor meerdere algemene functies. Het DNA ligt schijnbaar ongeorganiseerd, als een kluwen noedels in de cel, zo lijkt het tenminste. We hebben, beschreven in Hoofdstuk 3, een nieuwe classificatie voorgesteld voor de meest voorkomende nucleoid geassocieerde eiwitten op basis van het structurele effect dat ze hebben op DNA, bijvoorbeeld het bruggen of buigen van DNA (zie bijvoorbeeld Fig. 3.1 en Fig. 3.2).

Een van de belangrijkste eiwitten in de organisatie van het bacterieel chromosoom is H-NS. Dit kleine eiwit heeft twee DNA-bindende domeinen en is (dus) in staat twee stukken DNA aan elkaar te 'bruggen'. Hoewel bekend was dat dit eiwit kon bruggen was onbekend hoe sterk die bruggen dan precies zijn. Dit is een belangrijke vraag want stel dat het ontzettend sterk brugt, dan wordt het DNA eigenlijk geblokkeerd voor andere processen! In Hoofdstuk 4 wordt beschreven hoe we eerst hebben geprobeerd dit te bestuderen met één DNA molecuul maar als snel bleek dat we op deze manier heel makkelijk een grote DNA knoop kregen (zie Fig. 4.1). Door onze dubbele DNA methode te gebruiken konden we heel geordend bruggen laten ontstaan (zie Fig. 4.2). Vervolgens konden we deze bruggen openbreken door de twee stukken DNA uit elkaar te bewegen en de bruggen als het ware open te 'ritsen'. Hierdoor was het mogelijk om voor H-NS een *bindingsgrootte* op het DNA de definiëren; één H-NS eiwit neemt effectief ongeveer tien baseparen (de eerder genoemde 'bouwstenen' van DNA) in beslag. Bovendien bleek dat de H-NS-bruggen krachten tot $\sim$ 10 picoNewton konden weerstaan, maar dat dit geen bezwaar hoefde te zijn voor andere eiwitten die over het DNA bewegen; inmiddels was aangetoond dat deze eiwitten $\sim$25 picoNew-

ton aan kracht kunnen uitoefenen. Onze metingen toonden dus aan dat de H-NS bruggen een dynamisch georganiseerde nucleoid niet in de weg staan. Daarnaast hebben we met dit experiment voor het eerst de 'dubbele DNA methode' succesvol toegepast.

De organisatie van het bacterieel genoom

Het bacterieel genoom wordt georganiseerd door ∼50-400 in elkaar gedraaide lussen (zie Figuur 1.4) die bij elkaar worden gehouden door een groep kleine eiwitten. De lussen zijn niet gefixeerd maar kunnen naar believen worden opengebroken en weer opgenieuw gevormd. Een belangrijke vraag was welk eiwit nu precies verantwoordelijk is voor het stabiliseren van deze lussen. Een mogelijke kandidaat daarvoor was H-NS, dat door zijn bruggende functie mogelijk zo'n lus in stand zou kunnen houden. Om te kijken hoe het DNA georganiseerd zou worden als H-NS lussen in stand zou houden hebben we gebruik gemaakt van de experimentele resultaten van William Navarre en zijn medewerkers en Taku Oshima en zijn medewerkers (zie Hoofdstuk 5). Zij hadden namelijk in een eerdere studie bekeken waar H-NS bij voorkeur bindt op het DNA. We hebben toen bekeken wat voor lussen er mogelijk zouden kunnen ontstaan als H-NS op deze plekken zou binden. De verdeling van lussen die daaruit volgde kwam precies overeen met de resultaten eerder behaalt door andere groepen (zie Fig. 5.2). Bovendien konden we, door de voorkeurs plekken voor H-NS op het DNA te vergelijken met de bindingsgrootte die we eerder hadden gevonden (Hoofdstuk 4) een schatting maken van het aantal H-NS eiwitten dat aanwezig was in de cel en ook dit komt uitstekend overeen met hoeveelheiden die eerder gevonden waren. Tesamen heeft dit ertoe geleidt dat H-NS als belangrijkste kandidaat overblijft als lus-stabilisator en dat we nu beter begrijpen hoe het bacterieel chromosoom wordt (ge-re)organiseerd.

De rol van Alba in de DNA organisatie in archaea

In alle drie de domeinen, eukaryoten, prokaryoten en archaea, is de lengte van het genoom vele malen langer dan de grootte van de cel waarin het moet passen. Om een compact genoom de verkrijgen zijn er een groot aantal eiwitten betrokken bij de organisatie van het genoom. Waar in eukaryoten deze eiwitten met name DNA wikkelen, spelen buigen en bruggen waarschijnlijk een belangrijkere rol in prokaryoten. Over het algemeen combineren archaea de voordelen van zowel eukaryoten en prokaytoten. De manier waarop zij hun genoom organiseren lijkt hierbij geen uitzondering te zijn. Veel archaea gebruiken histonen, eiwitten waarbij het DNA om het eiwit heen gewikkeld zit, maar ook DNA-buigende en bruggende eiwitten komen voor in archaea. Een belangrijk eiwit in de organisatie van archaeal DNA lijkt het eiwit Alba te zijn. Het komt in bijna alle archaea voor, maar ook in sommige eukaryoten.

Met behulp van electronen mikroscopie was aangetoond dat dit eiwit waarschijnlijk in staat is om DNA te bruggen, analoog aan hoe bijvoorbeeld H-NS dit doet. Om uit te zoeken hoe Alba dit nu precies doet hebben we drie technieken gebruikt om te onderzoeken hoe Alba nu precies aan DNA bindt (zie Hoofdstuk 6). Met behulp van twee optisch pincetten hebben we één DNA molecuul gevangen en vervolgens Alba hier aan laten binding. Daaruit bleek dat Alba snel het hele DNA 'bezet' waardoor het DNA plots 3x zo stijf wordt. Daarbij konden we uit deze resultaten afleiden dat Alba waarschijnlijk 'samenwerkt' bij het binden aan DNA; als er een Alba eiwit al aan het DNA is gebonden wordt het makkelijker voor andere Alba eiwitten om aan het DNA te binden. Om een beter beeld te krijgen van hoe Alba zou kunnen bruggen, hebben we plaatjes gemaakt van hele korte DNA moleculen die met Alba waren geincubeerd. Dit hebben we gedaan door ze eerst op een oppervlak te deponeren en vervolgens op te laten drogen. Door met een heel klein naaldje (met een diameter 30 miljoenste van een millimeter) vervolgens over het oppervlak te 'scannen', analoog aan hoe een blinde met zijn stok 'voelt' of er obstakels zijn, kan DNA en de eiwitten die erop zitten 'zichtbaar' worden gemaakt (zie Fig. 1.17 en 6.4). Met behulp van deze techniek, Atomic Force Microscopy (AFM) genaamd, zagen we dat Alba inderdaad in staat is om DNA te bruggen. Het nadeel van deze techniek is echter dat het nogal statisch is; zodra het DNA op het oppervlak lag konden wij er alleen nog een plaatje van maken. Om mogelijke dynamica te meten hebben we dus vervolgens de dubbele DNA methode toegepast om te kijken of we op dezelfde manier bruggen tot stand konden brengen zoals beschreven in Hoofdstuk 4. Tot onze grote verbazing bleek dit echter niet het geval! Om te kijken hoe de vork nu precies in de steel zat hebben we met behulp van *Thethered Particle Motion* (TPM) (zie Fig. 1.16 en 6.7) gekeken of de bruggende werking van Alba nu wel gemeten kon worden. Dit bleek wel het geval en bovendien konden we opnieuw het stijver worden van het DNA observeren. Uit al deze verschillende experimenten bleek dat er voor Alba eigenlijk twee modussen zijn om aan het DNA te binden. Bij lage concentratie, als er dus her en der een Alba eiwit op het DNA zit, kunnen er bruggen gevormd worden, waarschijnlijk doordat Alba twee DNA-bindende domeinen heeft. Echter, bij hoge concentratie bindt het zo snel aan het DNA dat het hele DNA 'vol loopt'. Doordat het DNA nu veel stijver is is het minder waarschijnlijk dat er bruggen worden gevormd en bovendien kan Alba niet een tweede verbinding kan maken, het DNA is immers vol! De mogelijke functie van deze hoge concentratie bindingsmodus is dat het mogelijk een beschermende laag om het DNA vormt om het zo te beschermen tegen schadelijke invloeden.

DNA condensatie

In de het voorgaande staat met name beschreven hoe DNA kan worden gecompacteerd met behulp van eiwitten. Een andere methode die in de natuur wordt toeg-

past om DNA in een compactere vorm te krijgen is door gebruik te maken van de negatieve lading die DNA van zichzelf heeft. Door deze negatieve lading te 'compenseren' met sterk positief geladen moleculen kan het DNA op zichzelf terug slaan en zo een *condensaat* vormen. De structuren die dan kunnen ontstaan zijn prachtige spoel- of donutachtige vormen waarin het DNA heel sterk gecompacteerd is (zie Fig. 1.9). Hoewel er al veel onderzoek naar deze manier van DNA compactie is gedaan is er weinig bekend over de dynamica en welke structuur er nu precies gevormd wordt. In Hoofdstuk 7 wordt beschreven hoe we met behulp van fluorescentie en optisch pincetten hebben aangetoond wat voor structuur er nu precies gevormd wordt en hoe dit gebeurt. Door een DNA molecuul, heel spaarzaam gelabeld met een fluorescent molecuul en gevangen tussen twee optisch pincetten, heel langzaam te laten condenseren in de aanwezigheid van spermine, een sterk positief geladen molecuul, zagen we *live* DNA condensatie (zie Fig 7.1). Midden in het DNA molecuul zagen we plots een sterk oplichtende spot die duidt op een sterk verhoogde concentratie DNA. Daar werd het DNA dus op zichzelf teruggeslagen. Frappant is, door de uiteinden van het DNA molecuul steeds dichter bij elkaar te brengen, dat het gevormde condensaat DNA van zowel de ene als de andere kant bleek 'in te rollen'. Dit is een eerste aanwijzing dat inderdaad een 'spoel' structuur aanwezig is. Als we hetzelfde experiment deden terwijl we heel nauwkeurig de kracht meten zagen we dat op een gegeven moment, terwijl we de uiteinden van een DNA molecuul langzaam naar elkaar toe bewogen, de kracht plotsklaps $\sim$5 picoNewton omhoog schoot. Deze plotselinge verandering markeerde blijkbaar de vorming van een DNA condensaat. Als we nu de uiteinden van het DNA weer uit elkaar trokken bleef het condensaat veel langer stabiel! Dit duidt erop dat de vorming van een condensaat pas kan plaatsvinden als er genoeg 'rek' in het DNA zit, maar dat als het eenmaal gevormd is het vrij lang stabiel blijft. Bovendien zagen we dat er minimaal twee lussen nodig zijn om een stabiel condensaat te vormen. Door het condensaat uit elkaar te trekken zagen we dat de 'spoel' niet gelijkmatig 'ontrolde' maar dat we lussen van $\sim$40 nanometer (40 miljoenste milimeter) lostrokken. Hoewel dit veel kleiner was dan in andere experiment was aangetoond, bleek het in uitstekende overeenstemming met de maat die verwacht wordt als er een DNA-spoel wordt gevormd tussen twee optisch pincetten. Hier was in de ander metingen geen sprake van. Door deze experimenten waren we ook in staat een model op te stellen voor hoe zo'n DNA-spoel nu precies gevormd wordt.

Conclusie

De experimenten en analyses beschreven in dit proefschrift zijn uniek. Met nieuw ontwikkelde methodes hebben we vragen kunnen beantwoorden over het bacterieel chromosoom die al lang openstonden. De nieuwe experimenten die mogelijk zijn

door de komst van deze methodes zullen ongetwijfeld een schat aan nieuwe informatie opleveren. De stap van één naar twee enkele moleculen geeft aan dat steeds ingewikkeldere constructen kunnen worden gevormd. Mogelijk kan ooit op deze manier *in vitro* de situatie in de cel volledig worden nagebootst. De ontwikkeling van de flow-kamer zal daar zeker in bijdragen. Op korte termijn zal het apparaat dat staat beschreven in Hoofdstuk 2 met name gebruikt worden om andere DNA-organiserende eiwitten te karakteriseren.

Dankwoord

Mijn promotie en (dus) mijn tijd op de VU zit er op. Toen ik de laatste keer als AIO naar de VU fietste bedacht ik me dat ik het nooit echt als werk heb beschouwd. Bijna meer als een soort leuke tijdsbesteding. Elke ochtend van de afgelopen 4+ jaar ben ik met plezier naar de VU gefietst. Dit kwam in grote mate doordat de Complexe Systemen vakgroep echt een fantastische plek is om te promoveren. De uitgangspositie toen ik begon als AIO was al goed, met goede vrienden Joost en Bram ook net begonnen als AIO, maar alle leden maken de groep tot wat het is. Wat ik zeker ga missen is de tijd die samen werd doorgebracht tijdens lunches en koffiepauzes. Discussiëren over van alles en nog wat en zo nu en dan over wetenschap. Maar ook de momenten buiten 'werktijd', bijvoorbeeld de filmavondjes in de koffiekamer. Zelfs de lauwe pizza deed niet af aan het plezier. To circumvent the risk of forgetting anyone, I want to thank the group as a whole for the fantastic time and all the help I received. I do however want to pick a few people out. Steph, thanks for all the cookies and what not. And thanks for all the effort for all the CoSy-movie nights. U-030 inhabitants, it was a great pleasure to be part of the ever-critical, sweatband throwing, poster-bashing but always listening and helping colleagues. Erwin, bedankt voor je immer ongezouten mening. Was iedereen maar zo recht-door-zee. En daarnaast, met wie moet ik nu mijn gadget-fetish delen? Ik hoop dat we niet altijd zinloze weddenschappen nodig hebben om met zijn vieren te eten (en drinken)... In het bijzonder wil ik Joost bedanken, voor al je hulp sta ik eeuwig bij je in het krijt. Of het nu LabVIEW was of iets anders, je was er altijd. Ik heb ook erg genoten van de laatste paar maanden toen we een bureau deelden. Elk incident om ons heen werd met een veelzeggende blik afgedaan. Ik ga het missen.

Tijdens mijn periode in de groep heb ik aan een apparaat gebouwd wat uniek is, dit betekend dat er nogal wat speciale onderdelen gemaakt moesten worden. Dit was zeker niet mogelijk geweest zonder de hulp van allerlei mensen die me ten alle tijden met raad en daad hebben bijgestaan. De fijnmechanische afdeling, met in het bijzonder Pierre en Arie, zou ik daarvoor graag willen bedanken.

Bram, dude, je bureau was akelig leeg de laatste maanden. Nooit meer een smerig duitse vloek uit die hoek. We hebben veel projecten samen gedaan en ik heb je

daarbij leren kennen als de wetenschapper 'pur sang'. Eeuwig op zoek naar (soms onbereikbare) perfectie. Soms frustrerend, maar veel vaker heel inspirerend. Tevens hebben we, soms letterlijk, gerold over de vloer van het lachen. Ofwel om de volgende briljante practical joke, of een computer die ons hilarisch verraste. Ik ben blij dat ik met je heb kunnen werken en ben vereerd dat je mij als par(a)nimf wilt bijstaan tijdens mijn verdediging.

Dat brengt me eigenlijk vanzelf op Remus. We deden, eigenlijk terloops, wat test-experimenten aan het begin van mijn promotie, niet wetende dat het de hoofdmoot van mijn proefschrift zou worden. We vormden, vond ik, de afgelopen jaren een goed team als fysicus en chemicus, waarin ik veel van je heb geleerd. Je bent een uitstekend schrijver en een gepassioneerd onderzoeker met een goede neus voor leuke projecten. Maar het ging vaak niet over wetenschap als we daar in die kelder zaten. Ik heb je leren kennen als een warm en integer persoon. En daar doet die mac-fetish niets aan af. Ik ben daarom erg blij dat je mijn paranimf wilt zijn.

Gijs, ik had me geen betere begeleider kunnen wensen. In de afgelopen vier jaar ben ik er eindelijk achtergekomen wat je nou uitvoert daar in dat kantoortje... Met bewondering heb ik gezien hoe je je eigen plek binnen de wetenschap hebt veroverd met nieuwe ideeën en een onuitputtelijk en aanstekelijk enthousiasme. Niet alleen als je een verhaal aan anderen verteld, maar ook hoe je mijn verhaal aan mijzelf verkoopt. Ik ben nog nooit je kantoor minder vrolijk uitgelopen dan dat ik erin liep. Daarnaast wil ik je bedanken voor alle kansen die je me geboden hebt. Ik heb heel wat plekken in het buitenland mogen bezoeken en zo nieuwe kennis en tevens ook vrienden opgedaan. Heel erg bedankt voor alles.

Among the people I met abroad are a couple of guys who taught me a thing or two about biochemistry, John Perona and Dave Hiller. Apart from the good time, it has been a very valuable experience and has been a solid base for the rest of my PhD-time. Thank you for your hospitality! The same goes for Paul Wiggins; I had a ton of fun when I visited Cambridge. Your mind-boggling brain never seizes to amaze me but apart from that you have been a great host and incredibly fun to work with. Thanks.

Pap en Mam, het lijkt af en toe zo normaal, maar ik realiseer me terdege dat ik door alle kansen en steun die ik heb gehad van jullie nu hier ben aangeland. Jullie onvoorwaardelijke steun en gastvrijheid is immer hartverwarmend.

Alle plezier ten spijt, soms zit het ook wel eens tegen. In beide gevallen was er altijd iemand om het mee te delen. Lieve Liselot, ik ben zo blij dat je je door de taaie kost heen hebt weten te bijten en hebt willen luisteren naar wat soms een wirwar van projecten leek. Je verfrissend nuchtere opmerkingen hebben me meer dan eens weer met beide benen op de grond gezet. Mocht het er ooit van komen dat jij kiest voor een promotie hoop ik voor jou minstens hetzelfde te kunnen betekenen.

List of publications

The work presented in this thesis is based on the following publications:

Chapter 2:
Visualizing DNA-bound proteins using DNA as a scanning probe
M.C. Noom†, B. van den Broek†, J. van Mameren, and G.J.L. Wuite
Nature Methods, **4**(12):1031-36, 2007

Chapter 3:
The architectural role of nucleoid-associated proteins in the organization of bacterial chromatin: a molecular perspective
M.C. Noom†, M.S. Luijsterburg†, G.J.L. Wuite and R.T. Dame
Journal of Structural Biology, **156**(2):262-72, 2006

Chapter 4:
Bacterial chromatin organization by H-NS protein unravelled using dual DNA manipulation
M.C. Noom†, R.T. Dame† and G.J.L. Wuite
Nature, **444**(7117):387-90, 2006

Chapter 5:
H-NS promotes looped domain formation in the bacterial chromosome
M.C. Noom, W.W. Navarre, T. Oshima, G.J.L. Wuite and R.T. Dame
Current Biology, **17**(21):R913-4, 2007

Chapter 6:
Characterization of the architectural properties of the archaeal nucleoid-associated protein Alba
M.C. Noom, F.J.H. Hol, M.F. White, R.T. Dame* and G.J.L. Wuite*
Manuscript in preparation

Chapter 7:
Toroids under tension: DNA condensation unraveled with optical tweezers
M.C. Noom†, B. van den Broek†, J. van Mameren and G.J.L. Wuite
Manuscript in preparation

†These authors contributed equally to this work.

Other publications to which the author contributed:

DNA-tension dependence of restriction enzyme activity reveals mechanochemical properties of the reaction pathway
B. van den Broek, M.C. Noom, and G.J.L. Wuite
Nucleic Acids Research, **33**(8):2676-2684, 2005

Het bacterieel chromosoom ontrafeld met een viervoudig optisch pincet
M.C. Noom, R.T. Dame and G.J.L. Wuite
Nederlands Tijdschrift voor Natuurkunde, nr. 2, 2007

Protein mediated bridging motifs: a key mechanism in biopolymer organization
P.A. Wiggins, R.T. Dame, M.C. Noom, G.J.L. Wuite
Manuscript in preparation